AFRL-RX-WP-TP-2011-4290

AN ASSESSMENT OF BINARY METALLIC GLASSES: CORRELATIONS BETWEEN STRUCTURE, GLASS FORMING ABILITY AND STABILITY (PREPRINT)

Daniel B. Miracle

Metals Branch
Metals, Ceramics, and NDE Division

Dmitri Louzguine-Luzgin, Larissa Louzguina-Luzgina, and Akihisa Inoue

Tohoku University

JULY 2011

AIR FORCE RESEARCH LABORATORY
MATERIALS AND MANUFACTURING DIRECTORATE
WRIGHT-PATTERSON AIR FORCE BASE, OH 45433-7750
AIR FORCE MATERIEL COMMAND
UNITED STATES AIR FORCE

REPORT DOCUMENTATION PAGE

Form Approved
OMB No. 0704-0188

1. REPORT DATE *(DD-MM-YY)*	2. REPORT TYPE	3. DATES COVERED *(From - To)*
July 2011	Journal Article Preprint	01 July 2011 – 01 July 2011

4. TITLE AND SUBTITLE
AN ASSESSMENT OF BINARY METALLIC GLASSES: CORRELATIONS BETWEEN STRUCTURE, GLASS FORMING ABILITY AND STABILITY (PREPRINT)

5a. CONTRACT NUMBER
In-house

5b. GRANT NUMBER

5c. PROGRAM ELEMENT NUMBER
62102F

6. AUTHOR(S)
D.B. Miracle (AFRL/RXLM)
Dmitri Louzguine-Luzgin, Larissa Louzguina-Luzgina, and Akihisa Inoue (Tohoku University)

5d. PROJECT NUMBER
4347

5e. TASK NUMBER
20

5f. WORK UNIT NUMBER
LM10512P

7. PERFORMING ORGANIZATION NAME(S) AND ADDRESS(ES)

Metals Branch (AFRL/RXLM)
Metals, Ceramics, and NDE Division
Air Force Research Laboratory, Materials and Manufacturing Directorate
Wright-Patterson Air Force Base, OH 45433-7750
Air Force Materiel Command, United States Air Force

WPI Advanced Institute of Materials Research, and the Institute of Materials Research
Tohoku University
Sendai, Japan

8. PERFORMING ORGANIZATION REPORT NUMBER
AFRL-RX-WP-TP-2011-4290

9. SPONSORING/MONITORING AGENCY NAME(S) AND ADDRESS(ES)
Air Force Research Laboratory
Materials and Manufacturing Directorate
Wright-Patterson Air Force Base, OH 45433-7750
Air Force Materiel Command
United States Air Force

10. SPONSORING/MONITORING AGENCY ACRONYM(S)
AFRL/RXLM

11. SPONSORING/MONITORING AGENCY REPORT NUMBER(S)
AFRL-RX-WP-TP-2011-4290

12. DISTRIBUTION/AVAILABILITY STATEMENT
Approved for public release; distribution unlimited.

13. SUPPLEMENTARY NOTES
PAO Case Number: 88ABW 2010-2015; Clearance Date: 13 Apr 2010. Document contains color.
Journal article submitted to the *International Materials Review*.

14. ABSTRACT
This manuscript explores the influence of atomic structure on glass-forming ability and thermal stability in binary metallic glasses. A critical assessment gives literature data for 629 alloys from 175 binary glass systems. The atomic structure is quantified for each alloy using the efficient cluster-packing model. Comparison of atomic structure with amorphous thickness and thermal stability gives the following major results. Binary glasses show a strong preference for discrete solute-to-solvent atomic radius ratios, R^*, that give efficient local atomic packing. Of fifteen possible R^* values, only five are common and only four represent the most stable glasses. The most stable binary glasses are also typically solute-rich, with enough solute atoms, α, to fill all the solute sites and roughly 113 of the solvent sites. This suggests that anti-site defects, where solutes occupy solvent atom sites, are important in the glass-forming ability of the most stable glasses. This stabilizing effect results from an increase in the number of more stable solute-solvent bonds in solute-rich glasses.

15. SUBJECT TERMS
metallic glass, atomic structure, topology, glass forming ability, stability

16. SECURITY CLASSIFICATION OF:			17. LIMITATION OF ABSTRACT:	18. NUMBER OF PAGES	19a. NAME OF RESPONSIBLE PERSON (Monitor)
a. REPORT	b. ABSTRACT	c. THIS PAGE			
Unclassified	Unclassified	Unclassified	SAR	100	Jonathan E. Spowart 19b. TELEPHONE NUMBER *(Include Area Code)* N/A

An assessment of binary metallic glasses: Correlations between structure, glass forming ability and stability

Daniel B. Miracle[a*], Dmitri Louzguine-Luzgin [b,c], Larissa Louzguina-Luzgina[b,c**] and Akihisa Inoue[b,c]

a. Air Force Research Laboratory, Materials and Manufacturing Directorate, AFRL/RX, Dayton, OH USA

b. WPI Advanced Institute of Materials Research, Tohoku University, Sendai, JAPAN

c. Institute of Materials Research, Tohoku University, Sendai, JAPAN

Abstract

This manuscript explores the influence of atomic structure on glass-forming ability and thermal stability in binary metallic glasses. A critical assessment gives literature data for 629 alloys from 175 binary glass systems. The atomic structure is quantified for each alloy using the efficient cluster-packing model. Comparison of atomic structure with amorphous thickness and thermal stability gives the following major results. Binary glasses show a strong preference for discrete solute-to-solvent atomic radius ratios, R^*, that give efficient local atomic packing. Of fifteen possible R^* values, only five are common and only four represent the most stable glasses. The most stable binary glasses are also typically solute-rich, with enough solute atoms, α, to fill all the solute sites and roughly 1/3 of the solvent sites. This suggests that anti-site defects, where solutes occupy solvent atom sites, are important in the glass-forming ability of the most stable glasses. This stabilizing effect results from an increase in the number of more stable solute-solvent bonds in solute-rich glasses. Solute-rich glasses also enable efficient global atomic packing. Together, these structural constraints represent only a narrow range of topologies and thus give a useful predictive tool for the exploration and discovery of new binary BMGs.

Keywords: metallic glass, atomic structure, topology, glass forming ability, stability

* Corresponding author, daniel.miracle@wpafb.af.mil

** part-time employee at WPI AIMR

1. Introduction

It has long been suggested that metallic glass stability and glass-forming ability (GFA) are influenced by atomic structure, but it has been difficult to systematically explore this idea until recently. The efficient cluster packing (ECP) model gives a simple approach to specify and characterize metallic glass structures [1, 2]. From this model, metallic glass structures can be constructed from topology alone (the relative sizes and numbers of constituent atoms). The ECP model shows that metallic glass structures are comprised of a solvent atom and one to three solute species of different sizes that are taken from 15 allowed atomic sizes relative to the solvent that give efficient local atomic packing. Considering the distinct number of ways that the different structural sites can be filled by the preferred atom sizes, and from the type of defect states that can exist, 276 topologically unique atomic structures have been outlined for metallic glasses [2]. Aside from the expectation that structures with higher global packing efficiency may give more stable glasses, there is no fundamental basis for predicting stability from topology alone. It is thus not known if some of these 276 structures are intrinsically more stable than others, or if all provide a roughly equal topological contribution to metallic glass stability.

Using an ECP analysis, the structural topology can be obtained from the alloy specification, which gives the constituent species (and hence atomic sizes) and their concentrations. As the alloy specification is given for essentially every glass reported in the literature, and since many thousands of distinct metallic glasses have been produced and reported in the past 48 years, an enormous amount of information is available from which structural topology can be assessed. The critical cooling rate needed to produce a fully amorphous product is a principal metric of GFA, but it is difficult to measure and is rarely reported. A more practical measure of GFA is the maximum amorphous thickness that can be produced, and this can be taken from the literature to establish correlations between structural topology and GFA. Thermal stability is represented by primary parameters such as glass transition temperature (T_g), crystallization temperature (T_x) and liquidus temperature (T_ℓ), and by derived quantities such as reduced glass transition temperature

($T_{rg} = T_g/T_\ell$), T_x/T_ℓ, the temperature interval $\Delta T_x = T_x - T_g$, and $\gamma = T_x / (T_g + T_\ell)$ [3]. These, too, can be taken from the literature and correlated with atomic structure.

The goal of this assessment is to explore the influence of metallic glass structure and topology on GFA and thermal stability. To bound the problem to a workable subset and to simplify structural determination, the present work considers only binary metallic glasses. The data needed to explore correlations between atomic structure, GFA and metallic glass stability are collected from the literature. The ECP model is used to define the structural topology and defect state for each metallic glass in this assessment. Analysis of the topological characteristics and glass stability are conducted to identify relationships between these quantities. These relationships are used to develop more quantitative insights into the role of structure on the GFA and stability of metallic glasses.

2. Approach

2.1 Data Collection

An extensive review of the literature was conducted to collect the data needed for binary metallic glasses. Only metallic glasses produced by quenching from the molten liquid are considered. Amorphous solids produced by techniques such as mechanical alloying, electro-deposition and vapor deposition are not included. Data retrieved from the literature include alloy specification, amorphous thickness and representative temperatures T_g, T_x, T_ℓ. The compositions used in the present review are usually nominal compositions given by the pre-melting weight of the elements– measured compositions are rarely reported. Measured weight loss is sometimes given, and this data supports compositional precision of 2 or 3 significant digits. Minority species picked up during processing may be present and may influence results, but such information is rarely available. Liquidus temperatures were taken from binary phase diagrams [4] where this value was not measured in the cited work. Common thermal stability parameters derived from T_g, T_x and T_ℓ were calculated, including T_{rg}, T_x/T_ℓ, ΔT_x and γ. Atomic radii used here are based on a recent assessment [2], on published values [5, 6, 7, 8] and on measured interatomic separations in

metallic glasses, and are given in Table 1. The radii of several elements have been modified slightly from earlier assessments (see Section 4.7). The assessed precision is ±6 pm. The elastic properties of the constituent elements are taken from [8] to explore the suggestion that this property may influence GFA [9], and Pauling electronegativities are taken from [8] to explore a possible correlation with GFA. Where available, additional structure-specific data such as density and partial coordination numbers are also tabulated from the literature. The collected data and citations are compiled in Table A1 of the Appendix.

2.2 Structural Assessment

The solvent (Ω) and solute (α) species produce structure-forming clusters that consist of a central α site surrounded by Ω sites. These clusters are centered at positions in space that approximate to a cubic close-packed (ccp, also commonly referred to as face-centered cubic) organization in space. Additional solute sites in the structure include β sites that are surrounded by an octahedron of these clusters and γ sites surrounded by a tetrahedron of clusters. A representative unit cell of this structure is shown schematically in Figure 1.

Figure 1 near here.

In binary glasses, there are thus two species *i* (solvent atoms Ω and solute atoms α) and four sites *j* (Ω, α, β and γ). The number of structural sites can be counted in the ECP model, where $\hat{S}_j$ is the total number of *j* sites per α site [1, 2]. By definition, $\hat{S}_\alpha = 1$. From ccp symmetry, there is 1 β site and 2 γ sites for every α site, so that $\hat{S}_\beta = 1$ and $\hat{S}_\gamma = 2$. Each α site in the structure creates $\hat{S}_\Omega$ Ω sites. The value of $\hat{S}_\Omega$ is given by the geometry of efficient local atomic packing around α sites, and depends only on the ratio $R = r_\alpha / r_\Omega$ between the solute radius, r_α, and solvent radius, r_Ω, as shown by equation 5 in [10]. The total number of structural sites is $\sum S = \sum_j \hat{S}_j = \hat{S}_\Omega + 4$ [2].

These relationships are illustrated in Table 2.

Metallic glass structures are specified by the way in which the sites are occupied. For binary alloys, eight structural site occupancies, $S(i_j)$, give the number of *j* sites that are occupied by *i*

species, normalized by the number of α sites in the structure (Table 2). Quantitative comparisons with structure-specific measurements [2] give no support for a structurally significant presence of solvent anti-site defects on solute sites, so that $S(\Omega_\alpha) = S(\Omega_\beta) = S(\Omega_\gamma) = 0$. The total number of Ω atoms per α site in the structure, $\bar{S}_\Omega$, is thus given as $S(\Omega_\Omega)$. The $S(\alpha_j)$ values can be obtained from the metallic glass constitution by determining the total number of α atoms in the structure normalized by the number of α sites, $\bar{S}_\alpha$. The atom fractions are given by

$$F_\alpha = \bar{S}_\alpha / \left(\bar{S}_\alpha + \bar{S}_\Omega\right) \quad 1a$$

$$F_\Omega = \bar{S}_\Omega / \left(\bar{S}_\alpha + \bar{S}_\Omega\right) \quad 1b$$

so that

$$F_\alpha / F_\Omega = \bar{S}_\alpha / \bar{S}_\Omega \quad 2$$

where F_i is the atom fraction of species *i* and $\bar{S}_i$ is the total number of *i* atoms in the structure normalized by the number of α sites. As a basic identity from the discussion above, and assuming that all Ω sites are occupied

$$\hat{S}_\Omega = S(\Omega_\Omega) + S(\alpha_\Omega) \quad 3$$

Substituting $\bar{S}_\Omega = S(\Omega_\Omega)$ from above gives

$$\hat{S}_\Omega = \bar{S}_\Omega + S(\alpha_\Omega) \quad 4$$

Rearranging terms and combining with Equation 2 gives the general result

$$\bar{S}_\alpha = \left(F_\alpha / F_\Omega\right)\left(\hat{S}_\Omega - S(\alpha_\Omega)\right) \quad 5$$

that depends only on metallic glass constitution (through the terms F_α and F_Ω), on geometry (through the term $\hat{S}_\Omega$) and on the number of α atoms that occupy Ω sites. Specific solutions to Equation 5 are developed below in solute-lean and solute-rich glasses.

In solute-lean glasses, the number of solute atoms is less than or equal to the number of solute sites, so that $\bar{S}_\alpha \le 4$. Since α atoms fill solute sites before Ω sites [2], there are no solute anti-site defects on Ω sites in solute-lean glasses, and $S(\alpha_\Omega) = 0$. Inserting this in Equation 5 gives the final result for solute-lean glasses

$$\bar{S}_\alpha = \left(F_\alpha / F_\Omega\right)\left(\hat{S}_\Omega\right) \quad 6$$

An important number of solute sites will be vacant when $\bar{S}_\alpha < 4$, so that $S(\alpha_\alpha)$, $S(\alpha_\beta)$and $S(\alpha_\gamma)$ may be less than the maximum values.

Solute-rich glasses have all solute sites occupied by α and enough extra α atoms to occupy some Ω sites, forming α_Ω anti-site defects. Since there are four solute sites per α site

$$\bar{S}_\alpha = S(\alpha_\Omega) + 4 \qquad 7$$

Rearranging terms and substituting in Equation 5 gives

$$\bar{S}_\alpha = \left(F_\alpha / F_\Omega\right)\left(\hat{S}_\Omega - \bar{S}_\alpha + 4\right) \qquad 8$$

Collecting $\bar{S}_\alpha$ terms and simplifying gives the final result for solute-rich glasses

$$\bar{S}_\alpha = \left(F_\alpha\right)\left(\hat{S}_\Omega + 4\right) \qquad 9$$

$\bar{S}_\alpha$ is thus given by Equation 6 if $\left(F_\alpha / F_\Omega\right)\left(\hat{S}_\Omega\right) \leq 4$, otherwise it is given by Equation 9. $S(\alpha_j)$ values are determined from $\bar{S}_\alpha$ by filling α solute sites first (to the maximum value of $S(\alpha_\alpha) = 1$), then β sites (to the maximum value of $S(\alpha_\beta) = 1$) then γ (to the maximum value of $S(\alpha_\gamma) = 2$) and finally Ω sites, until the solutes are all distributed in the structure. $S(\Omega_\Omega)$ is determined from Equation 3 once $S(\alpha_\Omega)$ is known.

In crystalline structures, solute and solvent elements are taken to be the minority and majority species, respectively, since the number of structural sites is independent of the relative size of the atomic constituents. However, this definition becomes ambiguous near the equiatomic composition of metallic glasses, where the number of structural sites depends explicitly on the relative size of the constituent atoms. For example, when $R = 0.80$, each α site is at the center of an efficiently-packed cluster with 10 Ω atoms in the first coordination shell, so that each α site in the structure produces 10 Ω sites. When all the α sites are filled by α, $F_\alpha = 1/11 = 0.091$; when all the α and β sites are filled by α the solute atom fraction is $F_\alpha = 2/12 = 0.167$; and when all the α, β and γ sites are filled by α the solute atom fraction is $F_\alpha = 4/14 = 0.286$. These structures are represented by many transition metal-metalloid binary glasses such as Co-P and Pd-Si, and also by metal-metal glasses such as Zr-Cu and Zr-Ni. Now consider a glass where α is larger than Ω. For example, $R = 1.25$ in Al-Y and Cu-Zr glasses, where each α site now produces 17 Ω sites. In this structure, all the α sites are occupied when $F_\alpha = 1/18 = 0.056$; all the α and β sites are

occupied when F_α = 2/19 = 0.105; and all the α, β and γ sites are occupied when F_α = 4/21 = 0.190. From a structural perspective, larger solutes are thus more potent, since they produce more Ω sites than do smaller solutes.

If we continue to add Cu solutes to the Zr-Cu glasses described above, and we continue to add Zr solutes to the Cu-Zr glasses, we can imagine that an iso-structural condition will eventually be produced. We define the iso-structural condition as the singular structure where the same structural description is obtained regardless of which atom is used as the solute and which is the solvent. This will occur at the equiatomic composition when the two atoms are the same size, but it will occur at a different composition in metallic glass structures with unequal atomic sizes, since different sized atoms have different structural potency.

The concept of inverse structures is introduced here to give a rigorous, structure-specific definition for solvent and solute species in binary structures with different atom sizes. Consider a glass with solute and solvent radii r_α and r_Ω. $\hat{S}_\Omega$ and other structural parameters are defined using $R = r_\alpha / r_\Omega$ and atom fractions F_α and F_Ω as described earlier. An inverse structure can also be described for the same glass, using $R^I = r_\Omega / r_\alpha$, $F_\alpha^I = F_\Omega$ and $F_\Omega^I = F_\alpha$. In this way, the solute of a normal structure is the solvent in the inverse structure. The iso-structural condition is defined when the total number of solute atoms per α site in the normal structure equals the total number of solute atoms per α site in the inverse structure, $\bar{S}_\alpha = \bar{S}_\alpha^I$. This always occurs for solute-rich glasses, so using Equation 9 and the relation $F_\alpha^I = F_\Omega = 1 - F_\alpha$ gives

$$F_\alpha\left(\hat{S}_\Omega + 4\right) = \left(1 - F_\alpha\right)\left(\hat{S}_\Omega^I + 4\right) \qquad 10$$

Rearranging terms gives the α atom fraction at which the iso-structural condition is met

$$F_\alpha^{iso} = \frac{\hat{S}_\Omega^I + 4}{\hat{S}_\Omega + \hat{S}_\Omega^I + 8} \qquad 11$$

From Equation 11, $F_\alpha^{iso} = 0.5$ only when $\hat{S}_\Omega = \hat{S}_\Omega^I$, and this occurs only when $R = R^I = 1$. When $R < 1$, $\hat{S}_\Omega < \hat{S}_\Omega^I$ and $F_\alpha^{iso} > 0.5$, and when $R > 1$, then $\hat{S}_\Omega > \hat{S}_\Omega^I$ and $F_\alpha^{iso} < 0.5$. In the present analysis, structural parameters are determined for both cases: where the α constituent is taken to be the smaller atomic species (R<1) and where the α constituent is taken to be the larger atomic

species (R>1). The solute is defined as the species that gives the smaller value of $\bar{S}_\alpha$. Throughout this work, the terms α and Ω are used to represent the solute and solvent species, respectively, as established by this criterion. When specifying a metallic glass system, the convention is used throughout the manuscript of listing the solvent species first and the solute species second.

An adjustment is made in $\hat{S}_\Omega$ to account for a change in the number of structural sites that accompanies a significant number of α_Ω defects in solute-rich glasses. For example, solutes with R=0.71 are surrounded by $\hat{S}_\Omega = 10$ Ω sites, but as more of these sites are occupied by the smaller α atoms, the number of sites can increase. Similarly, filling Ω sites by α can decrease $\hat{S}_\Omega$ when R>1. To estimate the change in $\hat{S}_\Omega$, we calculate an effective solvent radius, $\tilde{r}_\Omega$, as

$$\tilde{r}_\Omega = r_\Omega\left(S(\Omega_\Omega)/\hat{S}_\Omega\right) + r_\alpha\left(S(\alpha_\Omega)/\hat{S}_\Omega\right) \qquad 12$$

where r_i is the atom radius. Since $\hat{S}_\Omega$ depends on the effective solvent size, Equation 12 is solved iteratively. This correction applies only to solute-rich glasses, or about 40% of the alloys in this study. The average adjustment to $\hat{S}_\Omega$ is less than 5%, and is never more than 15%. Throughout this work, the term $\hat{S}_\Omega$ is understood to incorporate this correction.

This structural analysis has been applied to all of the binary metallic glass alloys in this assessment. The glass constitutions are given by solute and solvent species and solute atom fractions, F_α. The structural parameters include the nominal radius ratio R; the total number of solvent structural sites $\hat{S}_\Omega$; the total number of atoms per α site $\bar{S}_\alpha$ and $\bar{S}_\Omega$; and the $S(i_j)$ site occupancy values. These data are included in Table A1 of the Appendix.

3. Results

The elements found in binary metallic glasses are presented in Section 3.1, followed by the phenomenological correlations between the measured amorphous thickness and thermal stability parameters (Section 3.2). The remainder of the results is devoted to establishing the influence of atomic structure (Section 3.3 through Section 3.6) and physical properties of the constituent elements (Sections 3.7 and Section 3.8) on the thermal stability and thickness of binary metallic glasses.

3.1 Elements Found in Binary Metallic Glasses

A total of 629 distinct metallic glass alloy compositions are identified from 175 different binary systems (Table A1). The A-B glass system is counted separately from the B-A glass system in the present study, since they are topologically distinct and are separated by the iso-structural composition defined by Equation 11. Most metallic elements have been used to produce binary metallic glasses, including 42 solvent elements and 51 solute elements, representing a total of 60 different elements (Figure 2). Solutes or solvents are taken from alkaline earth metals, early and late transition metals, lanthanides and actinide elements. Other metal elements include Al, Ga, Sn, Tl and Pb. Nearly all of the metalloids, including B, Si, Ge, As, Sb and Te, and half of the non-metals, including C, P and Se, are constituents of binary metallic glasses. Binary metallic glasses containing alkali metals, inert gas and halogen elements were not found in this assessment. The number of binary glass systems contained in this assessment represents over 8% of the binary systems possible from the elements represented. While metallic glasses are unusual, it is no longer true that they are rare.

Figure 2 near here.

3.2 Influence of Thermal Parameters on GFA

While binary glasses generally have relatively poor GFA, sixteen binary bulk metallic glass (BMG) alloys, defined as glasses that can be produced by melt quenching to thicknesses ≥1 mm, are reported in seven binary systems (Table A2). With the exception of Ca-Al and Pd-Si, the binary BMGs are pairs of early and late transition metals. These include the inverse glass-forming pairs of Cu-Hf and Hf-Cu, and of Cu-Zr and Zr-Cu, where the BMG composition ranges span the iso-structural composition. Only single compositions are reported for Ca-Al and Hf-Cu BMGs, but the remaining four BMG systems include two or more alloys that cover F_α ranges of 0.02 to 0.11. It is not clear if binary BMGs can be produced for compositions between the Cu-Hf BMGs ($Cu_{65}Hf_{35}$ and $Cu_{60}Hf_{40}$) and the $Hf_{45}Cu_{55}$ BMG. However, three of the BMGs found in

the Cu-Zr and Zr-Cu systems ($Cu_{64}Zr_{36}$, $Zr_{50}Cu_{50}$ and $Zr_{44}Cu_{56}$) are shown to be distinct, and do not form a continuous series of BMG alloys [11]. Together, these BMGs allow analysis of relationships between the maximum reported amorphous thickness and thermal stability parameters such as T_{rg}, ΔT_x, T_x/T_ℓ and γ. Correlations between thickness and these thermal stability parameters are shown in Figure 3. Binary BMGs require minimum values of approximately 0.52 for T_{rg}; 0.55 for T_x/T_ℓ; 0.37 for γ; or 10 K for ΔT_x. Contrary to popular belief, there seems to be no systematic increase in amorphous thickness with increasing thermal stability once these minimum values are achieved. Although the number of BMGs in this comparison is rather small, the stability parameters cover similar ranges found in more complex, and more stable, metallic glasses.

Figure 3 near here.

In addition to comparison between thickness and derived thermal stability parameters, correlations may also exist between thickness and the basic thermal quantities T_ℓ, T_x and T_g. Figure 4 shows the GFA, represented by the reported amorphous thickness, and derived thermal stability parameters plotted against these three basic thermal parameters. A wide range in temperatures is reported for binary metallic glasses. Consistent with expectation, the most stable glasses tend toward the lower half of the temperature range found for T_ℓ (Figure 4a) and the upper half of the temperature range for T_g (Figure 4c).

Figure 4 near here.

3.3 Solute Atom Fraction and Solute-to-Solvent Radius Ratio in Binary Metallic Glasses

The two principal topological parameters in binary metallic glass structures are the relative size and relative number of Ω and α atoms. These parameters are plotted in Figure 5, where each open symbol represents one of the 175 binary glass systems. The relative number of atoms is given by the solute atom fraction, F_α, and the vertical bars indicate a range in reported

compositions for a given binary glass system. Radius ratios range from 0.601 to 1.436 (the value R = 0.438 for Gd-C is a singular exception that significantly extends the range of R values), and F_α ranges from 0.07 to 0.625. There are essentially no metallic glasses with R~1 (Ti-Pt and Te-Al are exceptions), in agreement with the long-held empirical observation that a radius ratio difference greater than 12% is needed for good GFA [12, 13, 14, 15, 16]. The dashed line in Figure 5 indicates the boundary between solute-lean and solute-rich glasses ($\bar{S}_\alpha = 4$). Binary BMGs are indicated by filled symbols, and it is found that binary BMGs are solute-rich (fluxed Pd-Si glasses are exceptions). Structurally, solute-rich BMGs have no vacant solute sites and have significant numbers of solute anti-site defects. A similar result is found for glasses with good thermal stability, where 29 out of 36 binary glasses with $\Delta T_x \geq 20$ K are solute-rich (Table A2). The solid line indicates the iso-structural composition as a function of R, and is the upper limit on F_α. With the exception of Ca-Al and Pd-Si, binary BMGs tend toward the iso-structural composition. The dotted line represents the values of F_α needed to satisfy the condition $\bar{S}_\alpha = 1$, proposed here as the minimum solute atom fraction needed to form a metallic glass by liquid quenching (see Section 3.5).

Figure 5 near here.

A histogram of the relative atomic sizes of Ω and α in binary metallic glass systems is shown in Figure 6. This histogram counts only the 175 binary systems, rather than the 629 distinct alloy compositions, to avoid any bias introduced by more extensive characterization of systems such as Co-B, Cu-Zr, Fe-B, Ni-B, Pd-Si and Zr-Ni resulting from practical considerations such as the extent of the glass-forming region, the ease of GFA and the availability of constituent elements. The nominal radius ratio, $R = r_\alpha / r_\Omega$, from each of the 175 binary glass systems is placed in a bin that spans an interval from R to R+0.02. The vertical bars in this figure give the total number of systems where R falls within the indicated interval. The values from all of the vertical bars in Figure 6 sum to 175. A clear preference for specific radius ratios is shown, consistent with earlier work [10]. The specific radius ratios, R^*, needed to give efficient local atomic packing of Z solvent

atoms around a central α solute (Table 3) are indicated by the vertical lines in Figure 6 [10]. Metallic glasses most commonly have a radius ratio near R^*=0.799, indicating a structure that is comprised of solute-centered atomic clusters with Z=10 and designated as a <10> glass [1]. Additional significant peaks are shown at R^*=0.710, R^*=0.902, R^*=1.116 and R^*=1.248 representing <9>, <12>, <15> and <17> structures, respectively. Far fewer glasses have radius ratios near R^*=0.617 and R^*=1.433. An insignificant number of <6>, <7>, <13>, <14>, <16>, <18> and <19> binary metallic glasses are reported. Four of the 6 binary BMG systems have R near R^*=0.799 or R^*=1.248, and the remaining 2 have R near 0.710 and 1.116. This dataset suggests that GFA is best for <9>, <10>, <12>, <15> and <17> glasses, representing about a third of the radius ratios that enable efficient local atomic packing.

Figure 6 near here.

Additional trends are highlighted by replotting the data of Figure 6 to count the number of glasses within an increment $R+\Delta R$ and an increment $F_\alpha+\Delta F_\alpha$. The Kriging gridding method [17], commonly used to convert irregularly-spaced data into contour and surface plots, was applied using an interval of 0.05 for both ΔR and ΔF_α with an overlap of 0.025. The integrated number of alloys per specified interval in R and F_α is shown in Figure 7. Glasses with $R \cong 0.799$ that span a composition interval from about $0.16 \le F_\alpha \le 0.24$ are most commonly reported. Glasses with $R \cong 0.71$ are the next most common with compositions centered near F_α =0.20 and F_α =0.30, and a lesser peak occurs near R = 1.25 and F_α near 0.10.

Figure 7 near here.

3.4 Influence of Solute-to-Solvent Radius Ratio on GFA and Stability

In the following series of plots, the GFA (represented throughout this work by the maximum reported fully amorphous thickness) and the glass stability (represented by the thermal parameters T_{rg}, T_x/T_ℓ, ΔT_x and γ) are compared with metallic glass characteristics, emphasizing

glass topology but also including physical characteristics. These parameters are plotted against R in Figure 8a. All binary BMGs, where the thickness is ≥1 mm, occur near R^* values that suggest efficiently-packed structure-forming clusters with Z of <9>, <10>, <15> and <17>. A strong correlation is also seen for ΔT_x, where values above 10 K are found only near the same four values of R^* and also near R^* = 0.902 for structures with Z = <12>. The highest reported values of ΔT_x occur near R^* = 0.799 and R^* = 1.248, reinforcing the dominance of <10> and <17> structures. The clear preference for the most stable glasses to occur at specific radius ratios, R^*, reconfirms efficient local atomic packing as a primary motivation in glass formation.

The values of T_x/T_ℓ span a range from 0.222 to 0.715, but show neither a strong correlation with discrete values of R nor a continuous variation with R. The same is true for T_{rg}, which ranges from 0.417 to 0.688, and for γ, which varies from 0.296 to 0.428. Linear regressions of the full dataset against R for these three parameters all have shallow slopes and correlation coefficients below 0.6, showing no clear, continuous dependence of GFA or thermal stability on R. This simple regression of the full dataset treats all datapoints with equal weight. Chemistry is known to exert an important stabilizing effect in metallic glasses, and this may contribute to some of the scatter in thermal stability, since glasses with equivalent structural topologies may have important chemical differences. To reduce scatter from chemical contributions, a selected number of chemically similar metallic glasses is considered. These binary systems have one element of Ti, Zr, Hf or Th, and the second element is taken from the group of Fe, Co, Ni or Cu. The first group of elements belong to the same period and have similar electronic structures and electronegativities, while the second group are all late transition metals that also have similar electronegativities. The specific binary systems selected are Zr-Fe, Zr-Co, Zr-Ni, Zr-Cu, Hf-Co, Hf-Ni, Hf-Cu, Ti-Ni, Ti-Cu and Th-Fe. These glasses all exist over an extended composition range, usually spanning the iso-structure composition, and include 4 binary BMG systems.

The data from this selected subset are shown in Figure 8b for T_{rg}, T_x/T_ℓ and γ. Although the scatter in T_{rg} and T_x/T_ℓ is still significant, a small but consistent trend of increasing stability with increasing R seems apparent. The γ dataset has the lowest scatter, and consideration of the full γ

dataset in Figure 8a further supports this correlation with R. A topological origin for the spread in thermal stability parameters at a given nominal radius ratio is shown in Figure 8c, where T_{rg} and γ are plotted against the effective solute-to-solvent radius ratio, $\tilde{R} = r_\alpha / \tilde{r}_\Omega$. (see Equation 12). For solute-rich glasses, $S(\alpha_\Omega)$ increases with increasing F_α, giving a systematic change in $\tilde{r}_\Omega$ and $\tilde{R}$. For glasses with a nominal radius ratio, R<1, $\tilde{R}$ increases with increasing F_α and approaches R^*=0.902, the value required to form icosahedra. For glasses with R>1, $\tilde{R}$ decreases with increasing F_α and approaches R^*=1.183, which is the value required to form an efficiently packed cluster with Z = 16. In both cases, the thermal stability increases systematically with increasing F_α as $\tilde{R}$ approaches 0.902 or 1.183. Thus, in addition to a clear discrete-value correlation (Figure 8a), there is also a small, systematic effect of increasing thermal stability with increasing R (Figure 8b). Further, a combined effect of F_α and R on thermal stability is shown (Figure 8c).

Figure 8 near here.

3.5 Influence of Solute Atom Fraction on GFA and Stability

There is a clear threshold influence of F_α on GFA and thermal stability (Figure 9a). With the exception of Pd-Si glasses, all binary BMGs and nearly all glasses with $\Delta T_x \geq 20$ K are solute-rich, with F_α greater than 0.33. The boundary between solute-lean and solute-rich structures varies significantly with R (Figure 5), and this is accounted for in Figure 9b, where the stability parameters are shown against the number of α atoms per α site in the structure, $\bar{S}_\alpha$. Since there is 1 β site and 2 γ sites for each α site, the α, β and γ solute sites are all filled when $\bar{S}_\alpha = 4$, which defines the boundary between solute-lean structures with solute vacancies and solute-rich glasses with α_Ω solute anti-site defects. Binary BMGs and nearly all glasses with $\Delta T_x \geq 20$ K typically have $\bar{S}_\alpha > 4$ (Figure 9b). Pd-Si BMGs have $\bar{S}_\alpha \approx 2$, so that the α and β sites are occupied by α but γ sites are vacant. The number of α_Ω defects produced when α atoms occupy Ω sites can be obtained by subtracting 4 from $\bar{S}_\alpha$ in Figure 9b. Thus, the best binary glasses most often have from about 2 to 4 α_Ω defects per α site. The GFA and stability parameters are plotted against the

fraction of Ω sites occupied by α in Figure 9c. Solute-lean glasses have a value of $S(\alpha_\Omega)/\hat{S}_\Omega = 0$ in this plot, and the best glasses typically have from about 20-40% of the Ω sites filled by α.

Another structural threshold is shown in Figure 9b. With $Fe_{91}B_9$ as the only exception, all of the glasses have $\bar{S}_\alpha \geq 1$. Since α atoms fill α sites first, this shows that it is essential to fill the α sites by α atoms in binary metallic glasses. This validates an earlier assumption of the ECP model, and underscores the dominant role of α-centered clusters in forming the structural scaffold for metallic glasses.

A significant, continuous influence of F_α and the related structural parameters $\bar{S}_\alpha$, $S(\alpha_\Omega)$ and $S(\alpha_\Omega)/\hat{S}_\Omega$ on T_{rg}, T_x/T_ℓ, ΔT_x and γ is not apparent in Figure 9. Chemical differences between glass systems discussed in Section 3.4 may overcome small trends in thermal stability with F_α. In addition, Figure 9a does not distinguish between glasses with R<1 and R>1. This is important in solute-rich glasses, since the iso-structural composition occurs in the range of $0.40 \leq F_\alpha \leq 0.47$ for glasses with R>1, while glasses with R<1 reach the iso-structural condition at the higher atom fractions of $0.53 \leq F_\alpha \leq 0.60$. Thus, a glass near the iso-structural condition with R<1 may have $F_\alpha \approx 0.57$, while a glass just on the other side of the iso-structural boundary with R>1 may have $F_\alpha \approx 0.43$. Although these two glasses are nearly identical structurally, they are separated by a significant F_α margin in Figure 9a.

Correlations between F_α and related structural parameters are shown in Figure 10 for the chemically similar subset of binary alloys used in Figure 8b,c. Comparing Figure 10a with the data from all binary glasses (Figure 9a) shows that scatter remains due to systematic differences in F_α for glasses with R<1 and R>1. A clearer association is shown by comparing thermal stability with $\bar{S}_\alpha$ (Figure 10b), since $\bar{S}_\alpha$ accounts for the magnitude of R through the $\hat{S}_\Omega$ term (Equation 6). The group of relatively stable glasses that occur in the mid-range of the dataset in Figure 10a (compositions from $0.3 \leq F_\alpha \leq 0.4$ with T_{rg} and T_x/T_ℓ greater than about 0.6 and γ near 0.4) represent glasses with R>1 near the iso-structure composition, F^{iso}. Data from these alloys occur at high values of $\bar{S}_\alpha$ in Figure 10b that are comparable to data for relatively stable glasses with R<1. Linear regression correlation coefficients are 0.88 and 0.90 for T_{rg} and γ, respectively

in Figure 10b, showing a clear, consistent connection between stability and solute atom fraction. GFA and thermal stability for the chemically similar dataset are plotted against F_α normalized by F^{iso} in Figure 10c. A good correlation is shown for T_{rg} and γ, similar to that in Figure 10b. Additionally, a threshold value of about 80% of the iso-structure composition is satisfied for the glasses with a high ΔT_x and good GFA.

Figures 9, 10 near here.

3.6 Combined Influence of Radius Ratio and Solute Atom Fraction on GFA and Stability

The best metallic glasses satisfy the criteria for relative atomic size and solute-rich concentrations simultaneously. For glass structures that satisfy the solute-rich criterion (alloys with $\bar{S}_\alpha \geq 4$ or $F_\alpha \geq 0.8F^{iso}$), poorer GFA and lower thermal stability can result when R does not give a good match with an R^* value needed for efficient local atomic packing, or when the solute-solvent atom pair gives a poorer chemical contribution to stability. For glass structures that satisfy the R^* criterion, poorer GFA and lower thermal stability can result when F_α, and hence $\bar{S}_\alpha$, is insufficient for BMG formation. It is possible to fix R and to vary F_α by considering a pair of constituent atoms that satisfy the R^* criterion and display an extended compositional range of stability. A chemical influence can be analyzed by comparing different binary systems with the same value of R. It is difficult to isolate the effect of R at a given F_α, since R cannot be systematically changed without also changing constituent elements, which changes the chemical contribution. However, a comparison between two discrete R values can be made by comparing an A-B glass system with the inverse B-A system. The two values of R may or may not both satisfy R^* criterion (see Section 4.6).

To explore comparisons for the combined influence of R, F_α and chemistry, the Cu-Zr, Zr-Cu, Ni-Zr, Zr-Ni, Cu-Hf, Hf-Cu, Zr-Be and Ni-Nb systems are considered. These systems are chosen, since they have T_{rg} and γ data over an extended range of compositions, and since T_{rg} and γ are more reliable indicators of thermal stability (see Section 4.8). The first six of these systems

are taken from the limited set of binary alloys shown in Figures 8b,c and Figure 10. Zr-Cu, Zr-Ni and Hf-Cu have radius ratios near $R^* = 0.799$ to give <10> structures; Cu-Zr, Ni-Zr and Cu-Hf have $R \approx 1.248$ for <17> structures; Ni-Nb represents <15> structures with $R \approx 1.116$ and Zr-Be has a radius ratio near $R^* = 0.710$ for a <9> structure. Four of these structures– Cu-Zr, Zr-Cu, Zr-Ni and Zr-Be– allow F_α to be varied over a significant range at a fixed R in a given binary system. Comparison of the stability of Cu-Zr, Cu-Hf and Ni-Zr allow the effect of chemistry to be observed in three different binary systems with the same value of R at structurally equivalent compositions. The effect of R can be explored by comparing stability in Cu-Zr with $R = 1.254$ and in Zr-Cu with $R = 0.797$ at structurally equivalent solute concentrations and identical chemical contributions. A similar comparison can be made in the Ni-Zr and Zr-Ni system pair.

These comparisons are shown in Figure 11. A clear effect of composition is shown by the Cu-Zr, Zr-Cu, Zr-Ni and Zr-Be systems. These systems all display the same general trend of increasing thermal stability with increasing solute concentration, represented by F_α / F^{iso}. Maximum stability is achieved at $F_\alpha = F^{iso}$. The Cu-Zr system has a slightly higher thermal stability compared to Zr-Cu, and Ni-Zr is more stable than Zr-Ni at the same values of F_α / F^{iso} when T_{rg} is the measure of thermal stability (Figure 11a). This suggests that the higher R of Cu-Zr and Ni-Zr improves the thermal stability, which is consistent with the same trend shown for a larger set of binary glasses (Figure 8b). However, these four systems all display the same thermal stability when γ is used for comparison (Figure 11b). Linear regression for the Cu-Zr and Zr-Cu systems give similar fits, with regression coefficients from 0.66 to 0.93. The limited data for Cu-Hf, Hf-Cu and Ni-Nb fit within the scatter shown for the Cu-Zr, Zr-Cu, Ni-Zr and Zr-Ni datasets and so show no significant difference from these data. This suggests that these seven glass systems all have similar chemical contributions to stability, or that the differences in chemical interactions provided by these systems do not significantly influence thermal stability. The trends for Zr-Be in Figure 11 are clearly different from the other systems. The maximum thermal stability seems to occur near $F_\alpha = 0.6F^{iso}$. Zr-Be glasses have a different R and are likely to have significantly different chemical interactions, and it is not clear which of these are responsible for

the different response of Zr-Be glasses. By contrast, the Ni-Nb system also has a different *R* than those of the Cu-Zr, Zr-Cu, Cu-Hf, Hf-Cu, Ni-Zr and Zr-Ni systems, and the chemical interaction may be different, since Nb has an electronic structure different than Zr and Hf. Nevertheless, the single datapoint for Ni-Nb seems to agree with these other systems.

Figure 11 near here.

3.7 Influence of r_Ω, T_ℓ, *and Constituent Element Elastic Properties on GFA and Stability*

Topological and thermodynamic modeling of metallic glasses predicts an increase in T_{rg} with increasing solvent atom radius, r_Ω, and/or solvent shear modulus, G_Ω; with decreasing liquidus temperature, T_ℓ; with decreasing solute bulk modulus, B_α; and with decreasing difference between Ω and α bulk moduli, $|B_\Omega - B_\alpha|$ [9]. In nominal agreement with these predictions, T_{rg} is seen to increase slightly with decreasing T_ℓ (Figure 4a), with decreasing B_α (Figure 12) and with decreasing $|B_\Omega - B_\alpha|$ (Figure 13). The magnitude of the change in T_{rg} with the indicated parameters is small. There is no apparent systematic influence of r_Ω (Figure 14) or G_Ω (Figure 15) on T_{rg}. These parameters similarly show no meaningful effect on T_x/T_ℓ and γ (Figures 12-15). Since these two parameters are inversely proportional to T_ℓ, decreasing T_ℓ leads to a slight increase in T_x/T_ℓ and γ, as expected (Figure 4a).

These same physical characteristics exert distinct influences on ΔT_x and GFA. A clear threshold dependence is shown in Figure 13, where all of the most stable glasses have $|B_\Omega - B_\alpha|$ less than ~90 GPa. This is a new result that validates a prediction from earlier thermodynamic modeling [9]. Although less clear, a similar trend is suggested for T_ℓ (Figure 4a) and B_α (Figure 12), where the most stable binary glasses are found only for the lower half of the ranges in T_ℓ and B_α values. There seems to be no influence of r_Ω (Figure 14) or G_Ω (Figure 15) on ΔT_x and GFA.

Figures 12-15 near here.

3.8 Influence of Electronegativity on GFA and Stability

A comparison is made between electronegativity, χ, of the constituent elements and the GFA and stability. The absolute value of the difference in Pauling electronegativity of the solvent and solute constituents is used here, $|\chi_\Omega - \chi_\alpha|$. Binary glasses with the best GFA have discrete electronegativity differences of either ~0.3 or ~0.6 (Figure 16a). The smoothed contour plot in Figure 16b exhibits several clear peaks, showing that the electronegativity difference $|\chi_\Omega - \chi_\alpha|$ also correlates with nominal radius ratio. These small differences in electronegativity suggest a component of covalent bonding with a slightly polar nature between Ω and α, similar to the bonding in intermetallic systems. The preference shown here for specific differences in electronegativities may be an artifact of the small number of binary BMG systems- only 5 distinct pairs of atom species are found in this assessment. More complicated electronegativity functions were also considered, including an averaged electronegativity weighted by the constituent atom fractions [18]. No correlations were found with these other electronegativity functions.

4. Discussion

4.1 Binary Metallic Glasses are Simple Proxies for the Expansive Family of Metallic Glasses

Binary metallic glasses represent a diverse category of relatively simple metallic glasses. They cover a wide range of elements that include most of the element types in the periodic table. A small number of relatively stable glasses is also found, whether measured by an amorphous thickness of more than 1 mm or by thermal stability parameters. These characteristics qualify binary metallic glasses as a simple proxy for the more expansive field of metallic glasses. As structural complexity is a hallmark of disordered solids, the relative simplicity of binary metallic glass structures and the relative ease of measuring structure-specific properties such as partial pair distribution functions favor binary metallic glasses for more extensive characterization. There are surprisingly few studies that measure the influence of glass composition on structure-specific properties. The influence of systematic changes in binary composition on density, partial

coordination numbers and free volume (via indentation, relaxation or positron annihilation) are expected to significantly clarify structural descriptions. Further insights may be available by coupling new experimental data with the structural analysis techniques developed here. Additional structural studies in binary glasses using techniques such as scanning tunneling microscopy and 3D atom probe are suggested for future work.

4.2 Thermal Stability Parameters Give Post-Mortem Correlations with GFA

Relationships between thermal stability parameters and GFA are satisfying from a scientific standpoint, as they validate insights into the physics underlying glass formation. However, they lack practical appeal since they do not give a predictive capability. The glass must first be produced to measure the GFA and thermal stability, so that correlations between thermal stability and GFA are all post-mortem relationships. The present analysis shows that GFA is maximized once threshold values are achieved for T_{rg}, T_x/T_ℓ, ΔT_x or γ, but the data show no further correlation (Figure 3). For example, a binary BMG is produced with a thickness of 2 mm when T_{rg} = 0.556, but increasing T_{rg} to 0.638 does not increase the maximum thickness produced. Further, thicknesses less than 2 mm and as low as 100 μm are also produced over roughly the same range in T_{rg}. Reported thicknesses are typically not the maximum thickness possible in the binary glasses assessed here, and this may contribute to the lack of correlation. The majority of the literature data come from studies to discover new glass-forming compositions or to measure some property of the metallic glass. Processing techniques such as melt spinning and suction casting are often used, since they enable rapid production and require only a small amount of material. Thermal stability can be evaluated in glasses found in these studies, but significant extra material and effort is needed to define the maximum fully amorphous thickness possible. This extra work involves the systematic variation of process variables such as wheel speed in melt-spinning or mold size in casting. Such efforts are rarely undertaken for binary glasses that are not BMGs. Given the possibility that glasses with a large ΔT_x may also be binary BMGs, studies to establish the maximum fully amorphous thickness of the glasses with large ΔT_x but

small reported thicknesses are suggested. Also contributing to the lack of a systematic variation in GFA with thermal stability parameters may be the limited number of relatively stable binary BMGs. A critical evaluation similar to the analysis provided here of more complex metallic glasses, where BMGs are more common, may give additional insight and is suggested for future work.

The data in Figure 4 support the suggestion that the amorphous thickness in binary metallic glasses is maximized when threshold values of T_ℓ and T_g are satisfied. The temperatures proposed from these figures (T_g > 600 K and T_ℓ < 1500 K) are broadly consistent with the expectation that T_{rg} is maximized for BMGs.

4.3 Atomic Structure Gives Predictive Correlation with GFA and Thermal Stability: Radius Ratios

The present results show clear correlations between GFA and structural parameters. These correlations give an important predictive capability, since the structure can be described before a glass is made from only atom sizes and concentrations. The nominal solute-to-solvent radius ratio, *R*, is one of single best structural parameters to predict the occurrence, GFA and thermal stability of binary metallic glasses. The physical motivation for satisfying specific radius ratios is that efficient local atomic packing is enabled when *R* is close to a value of R^* [10]. Of the 15 R^* values available for efficient local atomic packing (Table 3), only 5 are commonly observed in metallic glasses (Figure 6), and only 4 produce the most stable glasses (Figure 8a). Metallic glasses with *R* required for <9>, <10>, <12>, <15> and <17> structures are commonly reported; <8> and <20> structures are uncommon; and <6>, <7>, <13>, <14>, <16>, <18> and <19> structures are rare or not reported. The best GFA is achieved for <9> structures with $R\cong0.710$, for <10> structures with $R\cong0.799$, for <15> structures with $R\cong1.116$ and for <17> structures with $R\cong1.248$. It seems unusual that no BMGs are found with $R\cong0.902$ for icosahedral clusters. Essentially no <13> or <14> glasses were found in this assessment, confirming the empirical rule that a significant size difference is needed between solute and solvent species to form metallic glasses. A mechanistic understanding is given by the elastic strain [14] or strain energy [19] needed to

destabilize competing crystalline structures. There is no explanation at present for the rarity of <6>, <7>, <16>, <18> and <19> glasses. <11> glasses are topologically degenerate with icosahedra [20]and are not expected to be structurally significant.

The thermal stability parameter ΔT_x is similarly influenced by this discrete value correlation with the same five preferred values of R^*. All binary glasses with $\Delta T_x \geq 20$ K have specific values of R that enable efficient local atomic packing with <9>, <10>, <12>, <15> or <17> structures. A more subtle influence is seen in T_{rg}, T_x/T_ℓ and γ, which increase with increasing R up to $R \cong 1.248$ (Figure 8b).

The more closely the nominal R matches a discrete value of R^*, the better is the GFA and thermal stability. Of the 43 most stable alloys listed in Table A2, 35 have a nominal R within ±0.01 of the nearest R^*. Thus, an assessed practical tolerance of ±0.01 is assigned to preferred values of R (Table 3). It is perhaps surprising that GFA and thermal stability show such a good correlation with the nominal value of R, especially for solute-rich glasses. The values of R^* are determined from the efficient packing of solute-centered clusters with solvent atoms only in the first coordination shell [10]. However, both solute and solvent atoms occupy the first coordination shell of solute-rich glasses, so that the effective radius ratio, $\tilde{R}$, will be different than the nominal value. The effect of mixed occupancy in the first shell of these clusters on the values of R that give efficient local atomic packing has not been evaluated and is suggested for future work.

4.4 Atomic Structure Gives Predictive Correlation with GFA and Thermal Stability: Atom Fraction

The structural perspective developed here gives minimum and maximum values of F_α required for metallic glass formation by melt quenching (Figure 5). With only one exception, all of the 629 binary metallic glasses fall within these bounds. This composition range is quite broad, and so these bounds do not give a useful aid in the exploration and development of metallic glasses. However, the observation that the most stable binary metallic glasses are typically solute-rich and generally approach the iso-structural condition is a major insight that

gives a useful predictive tool for the development of binary BMGs. This correlation shows that the most stable glasses have solute atom fractions high enough to fill all of the solute sites and up to 40% of the solvent sites. As a predictive guide to alloy exploration, specific solute concentrations can be proposed using the structural requirements $\overline{S}_\alpha \geq 4$ or $F_\alpha \geq 0.8F^{iso}$ (Figure 10c) as a lower bound, and F^{iso} as an upper bound. Together with the discrete value correlation for five values of R^*±0.01, this gives a restricted range in constitutions that should be useful in exploring and developing binary metallic glasses (Table 3).

Three physical motivations for the high solute atom fraction associated with the most stable glasses are discussed in the following sub-sections.

4.4.1 Global packing efficiency

The maximum global atomic packing fraction is expected to be a key topological parameter in the stability of metallic glass structures, but there are very few analytical approaches to determine the packing fraction in binary systems of spheres. Developed for the packing of ceramic particles, and based on the filling of interstices between larger particles by much smaller particles, the Furnas model [21, 22, 23] has been extended empirically to the packing in binary systems of spheres with R ranging from 0.1 to 0.5 [24]. This model shows a shallow maximum in the packing fraction of these systems at a volume fraction of smaller particles, X_f, of 0.37±0.10. Although the applicability of the concept of smaller spheres filling the interstices of larger spheres diminishes with decreasing difference in size, the efficient packing of larger spheres around a smaller sphere, directed by volume minimization and by chemical interactions, suggests that this approach may give useful insights into atomic packing in metallic glasses. Converting X_f to F_α for glasses with $0.6 \leq R \leq 0.9$, and truncating F_α at the iso-structure composition, F^{iso}, the F_α range over which maximal global packing is expected is shown as a function of R by the hatched regions in Figure 5. The compositions predicted from this analysis are all solute rich and reach the iso-structural composition over the full range of R studied. The compositions predicted from the Furnas model for efficient global packing at $R \cong 0.799$ match surprisingly well the

actual compositions for binary BMGs with <10> structures. Maximal global packing efficiency is also predicted for $0.6 \lesssim R \lesssim 0.9$ when $F_\alpha > F^{iso}$. In these cases, the inverse structure is the appropriate description of the glass structure. Applying the appropriate conversion for R and F_α (see Section 2.2), the current prediction shows that maximal global packing efficiency can also be achieved for $1.11 \lesssim R \lesssim 1.46$. Reasonable agreement is shown between the predicted and observed values of R and F_α for binary BMGs with $R > 1$. The trend of achieving maximal global packing efficiency with solute-rich compositions and the general agreement with selected BMG compositions is encouraging, but additional work is needed to develop more accurate models for predicting global packing efficiency in systems of binary spheres.

4.4.2 Bond enthalpy

The preference for solute-rich glasses suggests a stabilizing influence of solutes on β, γ and Ω sites. β and γ sites are surrounded by Ω atoms from the 1st shells of the bounding α clusters, so that roughly $\hat{S}_\Omega$ new Ω–α bonds are formed for every α atom that occupies a β or γ site (α_β and α_γ defects). Although the actual magnitudes of atomic bond energies are not known in condensed solids, the negative heats of mixing commonly observed for metallic glasses suggest that α–Ω bonds are more stable than the weighted average of α–α and Ω–Ω bonds, so that solute occupancy of β and γ sites increases metallic glass stability through an enthalpic bond energy contribution. The term, "glue atoms" [25, 26] has been used to describe the influence of solutes at β and γ sites in binding the structure-forming solute-centered clusters and in stabilizing the metallic glass.

A qualitative thermodynamic argument gives a simple basis for the observation shown here that the most stable glasses have roughly between 20-40% of the Ω sites filled by α. Each α_Ω defect replaces an Ω atom with an α atom in the 1st shell of an α-centered cluster. Considering only bonds within this cluster, removing the Ω atom breaks one α–Ω bond of energy $\varepsilon_{\Omega-\alpha}$ and q Ω–Ω bonds of energy $\varepsilon_{\Omega-\Omega}$, where q is the number of Ω atoms in the first shell that contact an Ω

atom that is also in the first shell [10]. Placing an α atom on this site forms one α–α bond of energy $\varepsilon_{\alpha-\alpha}$ and q α–Ω bonds. An α_Ω defect will be energetically favored if

$$(q-1)\varepsilon_{\alpha-\Omega} < (q)\varepsilon_{\Omega-\Omega} - \varepsilon_{\alpha-\alpha} \quad 13$$

Values of the bond energies ε_{i-j} are not available for condensed solids, and so it is not currently possible to evaluate this prediction. However, given the expectation that $\varepsilon_{\Omega-\alpha}$ is more negative than the weighted average of $\varepsilon_{\alpha-\alpha}$ and $\varepsilon_{\Omega-\Omega}$, it is suggested here that this condition may be satisfied in selected systems. Considering efficiently-packed clusters with coordination numbers $8 \le Z \le 20$ [20], it can be shown empirically that roughly 1/4 to 1/3 of the Ω sites in the 1st coordination shell can be replaced by α before α–α contacts are introduced in the 1st shell. Beyond this fraction, the number of new α–α contacts increases rapidly and the number of new α–Ω bonds decreases. The finding in this assessment that roughly 20-40% of the Ω sites are occupied by α in the most stable glasses (Figure 9c) agrees with this qualitative observation. It is quite likely that α_Ω defects thus give an enthalpic bond energy term that helps stabilize metallic glasses. Of course, α_Ω defects are also likely to give an entropic term that may also stabilize solute-rich glasses.

4.4.3 Defects and free volume

The finding that the most stable glasses are solute-rich has direct structural implications that include the suggestion that metallic glass stability is diminished by solvent anti-site defects on solute sites, Ω_{solute}, and by solute vacancies, V_{solute}. Ω_{solute} defects are most likely to occur in solute-lean glasses (*ie*, solvent-rich glasses), where there are insufficient solute atoms to fill solute sites. However, a significant concentration of these defects would enable metallic glasses with $\bar{S}_\alpha < 1$, which is essentially not observed. Further, these defects give inefficient local atomic packing that is inconsistent with the principle of the efficient filling of space that dominates metallic glass formation. While Ω_{solute} defects are not expected to be structurally significant, they may nevertheless occur as thermally-induced defects in small concentrations.

Although metallic glasses are often produced with V_{solute} defects (all solute-lean glasses have constitutional V_{solute} defects), they do not exist in any binary BMG (Pd-Si BMGs are an exception) and they occur only rarely in glasses with ΔT_x larger than 20 K (Figure 9b). Qualitatively, the reason that the most stable glasses do not have V_{solute} defects can be understood from the energy penalty (the PdV term of Gibbs free energy, where P is pressure and V is volume) paid by a condensed solid for free volume – 'free' volume isn't free. Even though vacancy defects in metallic glasses consist of many unoccupied spaces that are small fractions of an atomic volume which are locally distributed about a vacancy site [2], the energy penalty is nevertheless expected to be important. The free volume provided by vacancies also increases atom mobility, which further degrades the stability of metallic glasses.

4.5 Atomic Structure Gives Predictive Correlation with GFA and Thermal Stability: Combined Radius Ratio and Atom Fraction

The present work shows that the most stable glasses simultaneously satisfy the R^* and F_α criteria. Satisfying the R^* criterion gives efficient *local* atomic packing [10], which is a necessary condition for efficient *global* atomic packing. Thermal stability (T_{rg}, T_x/T_ℓ and γ) increases continuously with F_α in glasses that satisfy the R^* criterion (Figure 8c, Figure 10b). For F_α values that give $\bar{S}_\alpha \leq 4$, increasing thermal stability results from increased bonding enthalpy (Section 4.4.2) and reduced free volume (Section 4.4.3) as β and γ sites are filled with α atoms. For F_α values that give $\bar{S}_\alpha > 4$, increasing thermal stability comes from increased bonding enthalpy and increased configurational entropy as Ω sites become filled with α atoms (Section 4.4.2). Although T_{rg}, T_x/T_ℓ and γ increase continuously with F_α, ΔT_x and GFA do not improve until $F_\alpha > 0.8\,F^{iso}$, which seems to be a threshold beyond which good GFA is achieved but a systematic change is not apparent. This threshold behavior suggests a structural change that is not yet understood. Increased global packing efficiency is easily conceptualized by the filling of β and γ sites when $\bar{S}_\alpha \leq 4$, but it is not yet clear why global packing efficiency continues to

increase when $\bar{S}_\alpha > 4$ and as F_α approaches F^{iso}, as suggested by the Furnas model (Section 4.4.1).

The preferred structural topologies defined by the R^* and F_α criteria give a rather restricted set of conditions, which may be useful in the exploration and development of metallic glasses. Preferred relative atomic sizes include R values near 0.71, 0.80, 0.90, 1.12 and 1.25. An assessed precision in R from the present work is ±0.01, and the bounds on F_α are taken to be from $0.8F^{iso}$ to F^{iso}. These preferred structural topologies are listed in Table 3 for glass systems that are most likely to provide binary BMGs.

4.6 Complementary Inverse Glass Systems

Complementary inverse glass systems are companion structures where the solute-to-solvent radius ratio, R, and the solvent-to-solute radius ratio, $1/R$, both match R^* values required for efficient local atomic packing. The <10> and <17> structures are complementary inverse systems, since $R^*_{10} = 0.799$ and $R^*_{17} = 1.248$ match almost exactly the values $1/R^*_{10} = 1.252$ and $1/R^*_{17} = 0.801$. Only one other pair of structures, <12> glasses with $R^*_{12} = 0.902$ and <15> glasses with $R^*_{15} = 1.116$, match nearly as closely, since $1/R^*_{12} = 1.109$ and $1/R^*_{15} = 0.896$. None of the other structures have a topologically matched inverse system. For example, the inverse of a <16> glass has $1/R^*_{16} = 0.845$, which neither matches $R^*_{10} = 0.799$ nor $R^*_{12} = 0.902$ (R^*_{11} glasses are topologically unstable [1, 2]). Thus, while other structures may form inverse systems, they are not complementary, as efficient local atomic packing is not achieved on both sides of the iso-structure composition. Since BMGs tend toward the iso-structure composition, and since BMGs are likely to have structures with maximal global packing efficiency (Section 4.4.1), then complementary inverse structures may play an important consideration in BMG stability. This supports the observed preference for <10>, <12>, <15> and <17> glass structures.

BMGs are obtained in the complementary inverse glass systems Zr-Cu and Cu-Zr, as well as for Hf-Cu and Cu-Hf systems. Not only do these represent the companion structure pair with the best fit (<10> and <17>), but the actual radius ratios most closely match the ideal radius ratios

needed for efficient local atomic packing. Specifically, the actual R values for these systems (R = 0.797 and R = 1.254, Table A2) vary by less than 0.5% from the ideal R^* values for <10> and <17> structures. Ni-Nb binary BMGs are <15> glasses and could conceivably have a companion Nb-Ni complementary inverse structure. However, the actual R values for these glasses (R = 1.135 for Ni-Nb and R = 0.881 for Nb-Ni, Table A2) deviate from the ideal values of $R_{15}^* = 1.116$ and $R_{12}^* = 0.902$ by about 2%, and this may be a factor in the lack of a Nb-Ni binary BMG. Ca-Al glasses are not expected to have a companion inverse glass system, since $1/R_9^* = 1.408$, which is midway between the R needed for <19> and <20> glasses. However, the actual R for Ca-Al is 0.723, so that R for Al-Ca is 1.383 (Table A1). These are within about 1.3% of the ideal R values for <9> and <19> glasses. Although Al-Ca glasses exist, they are not reported to be BMGs (Table A1).

Using the binary Zr-Cu alloy system as an example, the relationships between inverse glasses that span the iso-structure composition are illustrated in Figure 17. The Zr-Cu and Cu-Zr systems are separated by the iso-structure composition. The iso-structure composition is bounded by solute-rich glasses on each side. Cu-rich Zr-Cu BMGs approach the iso-structure composition on one side, while Zr-rich Cu-Zr BMGs approach the iso-structure composition from the other. These inverse glass systems are structurally distinct– one is best described as a Zr-based glass with a <10> structure, and the other is best described as a Cu-based glass with a <17> structure. Only at the iso-structure composition can the glass be described equally well as either a Cu-based or a Zr-based glass. The R^* criterion is satisfied for these inverse glasses across the full range of F_α. Both packing fraction (Section 4.4.1) and enthalpic (Section 4.4.2) contributions stabilize solute-rich glasses near the iso-structural composition. The composition of the boundary between solute-lean and solute rich glasses depends on R (Equation 11 and Figure 5) and varies from F_α = 0.33 for R = 0.617 to F_α = 0.25 for R = 0.902. For glasses with R > 1, F_α varies from 0.21 for R = 1.116 to 0.17 for R = 1.433. As shown in Figure 5, the iso-structure composition varies from 0.53 for R = 0.902 to 0.63 for R = 0.617. The compositions shown in Figure 17 for the

boundaries between solute-lean and solute-rich glasses and for the iso-structural composition are for glasses in the Zr-Cu binary system with $R = 0.797$.

Twelve sets of binary metallic glass systems in the present assessment approach or span the iso-structure composition (Figure 18). The values of F_α and R are plotted for each of the reported alloys in these systems, and the iso-structure composition is shown for each set of glasses. The iso-structure composition is just approached or marginally crossed by the Ca-Cu, Ca-Zn, Zr-Co, Ni-Ta and Nb-Rh systems. The remaining systems extend by atom fractions of at least 0.10 on both sides of the iso-structure composition. A simple analysis was conducted to explore the influence of R on these complementary inverse systems. The difference between the actual R for the given binary system and the nearest value of R^* was normalized by R^* and summed with a similar normalized difference between the actual $1/R$ and the nearest value of R^* (Table 4) Five of the seven largest sums, representing the poorest match for efficient local atomic packing, are given by the five systems that only approach or marginally cross the iso-structure composition. The lowest sums, representing the best match for efficient local atomic packing, are found for the Hf-Cu, Hf-Ni, Zr-Cu and Zr-Ni systems, which all extend by significant compositions on both sides of the iso-structure boundary. Additionally, four of the seven binary BMGs occur in these systems. Eight of the thirteen most stable binary glass systems in Table A2 span the iso-structure composition. This simple argument provides a topological basis for the occurrence and stability of complementary inverse glasses that span the iso-structure composition. Chemical considerations are also likely to be important, but there are presently no approaches for exploring this effect. Although some systems show gaps in reported atom fractions of over 0.10 that may require verification of the proposed continuity of the amorphous phase, this does not change the ranking of systems that span the iso-structure composition.

Figure 17, 18 near here.

4.7 Reassessment of Atomic Radii

The good alignment of the present radius ratios with R^* values required for efficient local atomic packing (Figure 6) improves on earlier results from a more limited dataset [10]. The improved agreement here is achieved in part by a more detailed assessment of atomic radii. The radii used here represent a small increase in the radius of B, r_B, (from 85 pm to 88 pm) and corresponding decreases in r_{Fe} and r_{Co} (from 128 pm to 125 pm) and r_{Ni} (from 128 pm to 126 pm) relative to earlier assessments. Previous values of r_{Fe}, r_{Co} and r_{Ni} were obtained from pure elements, and r_B was derived by difference from the respective Fe–B, Co–B and Ni–B separations measured in transition metal-boron binary metallic glasses. However, it is well known that bonding between unlike metals can be shortened by 5-15%, especially if some degree of covalent bonding is present. The approach used earlier assigned all of the shortening in the transition metal-boron bond to the boron atom, giving an r_B value that is likely to be too low. Supporting this expectation, the earlier value of r_B gave a solute-to-solvent radius ratio of $R = 0.664$ for transition metal-boron glasses, which is smaller than the value of 0.710 required by geometry to allow nine transition metal atoms to occupy the first coordination shell as measured experimentally [27]. The present approach uses a slightly smaller value of r_{Ni}, which gives a slightly larger value of r_B when determined by difference from the Ni–B separation. The new values used here give $R = 0.698$, in better agreement with the value of 0.710 required for consistency with measured coordination numbers. Radii used here for Rh, Ti, Nb, Au and Hf are reduced by 2 pm each, and r_{Ta} is reduced by 3 pm relative to earlier assessed values. Small adjustments were also made to radii for Ba, Ca, Cu, Gd, Pt, Zn, Y and Th. The value of r_{Nd} used here is 182 pm, correcting an earlier typographic error [2].

The assessed atomic radii are given in Table 1 and are plotted as a function of atomic number in Figure 19, where they are compared with atomic radii from earlier assessments [5, 6, 7, 8]. With Ca as the only exception, all of the assessed radii fall within the range of values from previous assessments. In general, the assessed values are at the upper end of the radii range for elements with empty *p*, *d* and *f* orbitals, and are near the middle or lower end of the range for elements as

the *p*, *d* and *f* shells become filled. Within experimental error, the assessed radii generally agree very well with interatomic separations measured by diffraction in metallic glasses [28, 29, 30, 27, 31, 32, 33, 34, 35, 36, 37, 38, 39, 40].

Figure 19 near here.

4.8 Variance in GFA and Thermal Stability

Apparent scatter (variance) in thermal stability data is shown in the present assessment, and may arise from chemical and topological influences. The present work shows that the most stable glasses satisfy both R^* and F_α criteria simultaneously. A glass that satisfies one but not the other may thus have poorer stability, which may be reflected in lower values of T_{rg}, T_x/T_ℓ, ΔT_x or γ. The variance in thermal stability is reduced and systematic trends become apparent when one of these parameters is fixed and the second parameter is systematically changed. For example, fixing R (by selecting data from a single binary system with an extended composition range) and varying F_α shows a clear link between thermal stability and F_α (Figure 11). A simple physical basis for this dependence is highlighted by the influence of $S(\alpha_\Omega)$, and hence F_α, on the effective solute-to-solvent radius ratio, $\tilde{R}$ (Equation 12). Explicit consideration of $\tilde{R}$ replaces an apparent variance in thermal stability with a systematic trend (compare Figure 8b with Figure 8c). Analysis using simple solute atom fraction, F_α, also gives significant variance. Comparisons made with F_α normalized by the iso-structure composition, F^{iso}, show improved correspondence, as does use of the structural parameter, $\bar{S}_\alpha$ (compare Figure 11a with Figure 11b,c). Both of these terms account for the different structural potency of different solute sizes.

Even if the R^* and F_α topological criteria are satisfied and properly represented, differences in GFA and thermal stability can still result. Cu-Zr, Cu-Hf and Ni-Zr glasses all satisfy the R^* and F_α criteria, but Cu-Zr and Cu-Hf form BMGs and Ni-Zr does not. The same is true for comparison of Zr-Cu, Hf-Cu and Zr-Ni glasses. Different chemical contributions to stability are proposed to cause this distinction. There is presently no clear approach for quantifying chemical

contributions to metallic glass stability, so that this proposition cannot be explored in detail. A chemical influence is also expected from impurities introduced in the melting process. Melt cleanliness and the type and amount of impurity elements present are generally not well documented or controlled, contributing to possible scatter in GFA and thermal stability. This may have the largest influence on T_x, since impurities strongly influence crystallization in metallic glasses. In agreement with this suggestion, the present work shows significant variance in GFA as indicated by the maximum reported thickness, on ΔT_x, and on values of T_x/T_ℓ. Although γ depends on T_x, it nevertheless shows the smallest variance of any of the thermal stability parameters. T_{rg} also shows relatively little variance. Many of the comparisons in the present work favor T_{rg} and γ as indicators of thermal stability based on this reduced variance.

5. Summary

Binary glasses are a large and diverse subset of metallic glasses, representing 60 different elements and most element types in the periodic table. Six hundred and twenty nine binary alloys are identified from 175 different binary systems. These 175 binary systems represent over 8% of the possible binary systems that can be produced from the constituent elements, so that binary metallic glasses, although uncommon, are not rare. Sixteen binary bulk metallic glass (BMG) alloys, being produced in the fully amorphous condition at thicknesses ≥1 mm, are found in 7 systems: Ca-Al, Cu-Hf, Cu-Zr, Hf-Cu, Ni-Nb, Pd-Si and Zr-Cu. The constitutional breadth, relative structural simplicity and availability of relatively stable alloys recommend binary glasses as convenient proxies for the broader family of more complex metallic glasses.

Metallic glasses are analyzed using the efficient cluster packing (ECP) model, which shows that binary structures consist of 2 species (solvent Ω and solute α) and 4 sites (Ω, α, and additional solute sites β and γ). An approach is developed for determining the 8 resulting site occupancy values, $S(i_j)$, that define the structural topology, using as input only the relative atomic sizes and atom fractions of the constituents. Other extensions of the ECP model developed here include definition of solute-lean glasses as structures with insufficient α atoms to fill all the α, β

and γ solute sites, and definition of solute-rich glasses as structures with enough α to fill all available solute sites and to form constitutional α_Ω anti-site defects comprised of α atoms on Ω sites. Unlike crystalline structures, the number of structural sites in metallic glasses is defined by the relative size of the atoms– larger solutes have a higher structural potency and produce more Ω structural sites than smaller solutes at an equivalent atom fraction. An iso-structure atom fraction, F^{iso}, is defined as the compositional boundary where the solute and solvent species exchange structural roles. F^{iso} depends explicitly on R– it is >0.5 when R<1 and it is <0.5 when R>1. F^{iso} gives an unambiguous structure-based definition of solute and solvent species that is important for solute-rich glasses near the equiatomic composition.

Binary metallic glasses include nominal solute-to-solvent radius ratios, R, from $0.438 \leq R \leq 1.436$, giving structure-forming, solute-centered clusters with coordination numbers from $6 \leq Z \leq 20$. Consistent with earlier work, a strong preference is shown for discrete radius ratios, R^*, that give efficient local atomic packing in the 1st coordination shell. This work shows that not all R^* values are equally effective in producing metallic glasses. Binary glasses are most commonly produced with a nominal radius ratio near $R^* \cong 0.799$ that gives <10> structures, where efficiently packed clusters consisting of a central solute atom surrounded by ~10 solvent atom sites form the structural scaffold. Other commonly observed structures include <9>, <12>, <15> and <17> glasses with R near 0.710, 0.902, 1.116 and 1.248, respectively. Binary glasses are formed less frequently with <8>, <18> and <20> structures, while glasses with R that give <6>, <7>, <13>, <14>, <16> and <19> structures are rare or not reported. <11> structures are unstable and are not observed. Thus, only five of the fifteen radius ratios that give efficient local atomic packing in metallic glasses are common. The best stability is achieved when R is within ±0.01 to the nearest R^* value.

Solute atom fractions in binary metallic glasses range from $0.07 \leq F_\alpha \leq 0.625$. A structural origin for the lower bound on F_α is given by the condition that all α sites must be filled by α solutes. The minimum F_α values decrease with increasing R due to the increased structural potency of larger solutes. The upper compositional bound on α is given by F^{iso}. With only one

exception, all of the 629 binary alloys cited here fall within the compositional bounds derived from these structural considerations. α sites are always occupied in binary glasses, but only by α atoms (the single exception is $Fe_{91}B_9$). Ω sites are always filled, either by Ω atoms or by α atoms, which form α_Ω anti-site constitutional defects. β and γ sites may be vacant or can be filled by α, but not by Ω. A significant number of solute-lean glasses (with constitutional vacancies on β and/or γ sites) and a significant number of solute-rich glasses (with α_Ω anti-site defects) are shown in this analysis.

The criteria outlined above for R and F_α define the broad topological requirements for glass formation by liquid metal quenching. However, the most stable glasses have outstanding glass-forming ability (GFA, represented by a maximum amorphous thickness ≥1 mm) and thermal stability (measured by T_{rg}, T_x / T_ℓ, ΔT_x or γ), and satisfy a more restrictive set of conditions. These most stable glasses represent only 4 values of R^*, including 0.710 for <9> structures; 0.799 for <10> structures; 1.116 for <15> structures and 1.248 for <17> structures. Further, the most stable glasses usually have solute-rich compositions that range from $F_\alpha > 0.34$ for $R = 1.248$ to $F_\alpha > 0.48$ for $R = 0.710$ (Table 3). From a structural perspective, these glasses have $\bar{S}_\alpha > 4$, so that all of the solute sites are occupied by α and a significant number of constitutional α_Ω defects exist. The stabilizing influence of α_Ω defects results from a bond enthalpy contribution, where the number of more stable Ω–α bonds in the structure is increased relative to the number of less stable α–α and Ω–Ω bonds. Reported solute-rich compositions are consistent with a structural argument that predicts that this bond enthalpy contribution will be maximized when about 1/3 of the Ω sites are occupied by α. The R^* criterion enables efficient *local* atomic packing, while models for maximal *global* packing efficiency suggest that the R^* and solute-rich criteria must be met simultaneously. In agreement with this, all of the most stable glasses satisfy both the R^* and F_α topological constraints simultaneously. The thermal stability (T_{rg}, T_x/T_ℓ and γ)) of a glass that satisfies the R^* criterion increases continuously with F_α, while ΔT_x and GFA (critical thickness) only improve once a critical value of $0.8F^{iso}$ is reached. Contrary to popular belief, there seems to be no systematic increase in amorphous thickness with increasing thermal stability once the

threshold value is met. These findings show a significant structural influence on GFA and thermal stability that gives a practically important predictive capability, since the most stable binary metallic glasses are typically restricted to a narrow range of preferred structural topologies defined by 4 values of R^*±0.01 and a relatively narrow range in F_α. (Table 3).

A description of inverse structures is developed, where the solute and solvent species of a normal structure are interchanged. Complementary inverse glasses have structures that satisfy the R^* criterion and thus have efficient local atomic packing on both sides of the iso-structure composition. This is best satisfied for <10> glasses with relative atomic sizes near R^* = 0.799 and their inverse structures, <17> glasses, with R^* near 1.248. The complementary pair of <12> and <15> glass structures, with R^* near 0.902 and 0.116, respectively, are nearly as well matched. Glasses with extensive compositional ranges that span the iso-structure composition are most often complementary inverse structures, and include some of the most stable binary glasses. This gives a rationale for the preference for <10>, <12>, <15> and <17> glass structures.

In addition to the influence of topological parameters, the present work also shows an influence of physical characteristics on GFA and thermal stability. The most stable glasses all have an absolute difference in constituent element bulk moduli of $\left|B_\Omega - B_\alpha\right|$ <80 GPa. The absolute difference in Pauling electronegativity of Ω and α atoms, $\left|\chi_\Omega - \chi_\alpha\right|$, also shows a good correlation with amorphous thickness and the thermal stability parameter, ΔT_x. All of the most stable glasses have $\left|\chi_\Omega - \chi_\alpha\right|$ equal to either ~0.3 or ~0.6. Like structure, these relationships provide a predictive capability, as these features can be established before a glass is made.

Additional work is suggested to solidify and extend the structural insights developed here. Very few studies of binary metallic glasses measure critical thickness, and this information is expected to improve the statistical validity of the correlations explored here. The measurement of structure-specific properties such as density and partial coordination numbers would also enhance structural understanding, especially if carried out in glasses where the constitution and structure are varied systematically. From the structural and analytical foundation provided here, a

similar critical assessment of more complex glasses is recommended, since the number of ternary and higher-order BMGs is significantly larger than for binary systems.

Acknowledgements

DBM thanks the Air Force Research Laboratory, Air Force Office of Scientific Research for funding during a sabbatical to the Institute of Materials Research, Tohoku University, Sendai, Japan. DL and LL acknowledge the Air Force Office of Scientific Research (Tokyo Office, Dr. J.P. Singh, Program Manager) for funding this effort under agreement number AOARD-07-4041. This work was also supported by the Research and Development Project on Advanced Metallic Glasses, Inorganic Materials and Joining Technology from MEXT, Japan. Helpful comments from K. Laws are appreciated.

References

1. D. B. Miracle: *Nature Materials*, 2004, **3**, 697-702.
2. D. B. Miracle: *Acta Mater.*, 2006, **54**, 4317-4336.
3. Z. P. Lu and C. T. Liu: *Acta Mater.*, 2002, **50**, 3501-3512.
4. H. Okamoto, P. R. Subramanian, and L. Kacprzak: in 'Binary Alloy Phase Diagrams', (ed. T. B. Massalski), Vol. 1990, Materials Park, OH USA, ASM, International.
5. C. H. MacGillavry and G. Reick: in 'Interatomic Distances in Metallic Crystals', (ed. K. Lonsdale), Vol. III Physical and Chemical Tables, 277-285; 1985, Dordrecht, Holland, Kluwer Academic Publishers.
6. J. C. Slater: *J. Chem. Phys.*, 1964, **41**, 3199-3204.
7. E. Teatum, J. K. Gschneidner, and J. Waber: 'Compilation of calculated data useful in predicting metallurgical behavior of the elements in binary alloy systems', LA-2345, Los Alamos National Laboratory, University of California, Los Alamos, New Mexico, 1960.
8. M. Winter: 'WebElements: the periodic table on the WWW', The University of Sheffield and WebElements Ltd, UK, Accessed on 2 Dec 2007.
9. O. N. Senkov, D. B. Miracle, and H. M. Mullens: *J. Appl. Phys.*, 2005, **97**, 103502.
10. D. B. Miracle, W. S. Sanders, and O. N. Senkov: *Phil. Mag. A*, 2003, **83**, 2409-2428.
11. Y. Li, Q. Guo, J. A. Kalb, and C. V. Thompson: *Science*, 2008, **322**, 1816-1819.
12. L. Battezzati and M. Baricco: *J. Less Common Metals*, 1988, **145**, 31-38.
13. R. W. Cahn: 'Metallic Glasses', in 'Materials Science and Technology', (ed. J. Zarzycki), edn, 493-548; 1991, Cambridge, UK, VCH.
14. T. Egami and Y. Waseda: *J. Non-Cryst. Sol.*, 1984, **64**, 113-134.
15. A. Inoue: *Mat. Sci. Eng.*, 1997, **A226-228**, 357-363.
16. D. E. Polk and B. C. Giesen: 'Metallic Glasses', 1-36.
17. G. Matheron: *Economic Geology*, 1963, **58**, 1246-1266.
18. Z. P. Lu, C. T. Liu, and Y. D. Dong: *J. Non-Cryst. Sol.*, 2004, **341**, 93-100.
19. D. B. Miracle and O. N. Senkov: *Mat. Sci. Eng.*, 2003, **A347**, 50-58.
20. D. B. Miracle, E. A. Lord, and S. Ranganathan: *Mater. Trans. JIM*, 2006, **47**, 1737-1742.
21. F. O. Anderegg: *Industrial and Engr. Chem.*, 1931, **23**, 1058-1064.
22. C. C. Furnas: *Report of Investigations*, 1928, **No. 2894**.
23. C. C. Furnas: *Industrial and Engr. Chem.*, 1931, **23**, 1052-1058.
24. J. Zheng, W. B. Carlson, and J. S. Reed: *J. European Cer. Soc.*, 1995, **15**, 479-483.
25. Q. Wang, Y. M. Wang, J. B. Qiang, X. F. Zhang, C. H. Shek, and C. Dong: *Intermetallic*, 2004, **12**, 1229-1232.
26. J. H. Xia, J. B. Qiang, Y. M. Wang, Q. Wang, and C. Dong: *Appl. Phys. Lett.*, 2006, **88**, 101907-101914.
27. P. Lamparter, W. Sperl, S. Steeb, and J. Bletry: *Z. Naturforsch.*, 1982, **37a**, 1223-1234.

28. K. Ahn, D. Louca, S. J. Poon, and G. J. Shiflet: *Phys. Rev. B*, 2004, **70**, 224103.

29. N. Cowlam, W. Guoan, P. P. Gargner, and H. A. Davies: *J. Non-Cryst. Sol.*, 1984, **61 & 62**, 337-342.

30. A. Hirata, Y. Hirotsu, T. Ohkubo, N. Tanaka, and T. G. Nieh: *Intermetallics*, 2006, **14**, 903-907.

31. A. Lee, G. Etherington, and C. N. J. Wagner: *J. Non-Cryst. Sol.*, 1984, **61-62**, 349-354.

32. M. Maret, A. Soper, G. Etherington, and C. N. J. Wagner: *J. Non-Cryst. Sol.*, 1984, **61-62**, 313-318.

33. E. Matsubara and Y. Waseda: *Mater. Trans. JIM*, 1995, **36**, 883-889.

34. E. Matsubara, Y. Waseda, A. Inoue, H. Ohtera, and T. Masumoto: *Z. Naturforsch.*, 1989, **44a**, 814-820.

35. T. Nakamura, E. Matsubara, M. Sakurai, M. Kasai, A. Inoue, and Y. Waseda: *J. Non-Cryst. Sol.*, 2002, **312-314**, 517-521.

36. E. Nold, P. Lamparter, H. Olbrich, G. Rainer-Harbach, and S. Steeb: *Z. Naturforsch.*, 1981, **36a**, 1032-1044.

37. T. Ohkubo and Y. Hirotsu: *Phys. Rev. B*, 2003, **67**, 094201.

38. J. F. Sadoc and J. Dixmier: *Mat. Sci. Eng.*, 1976, **23**, 187-192.

39. S. Steeb and P. Lamparter: *J. Non-Cryst. Sol.*, 1993, **156-158**, 24-33.

40. C. N. J. Wagner: *J. Non-Cryst. Sol.*, 1992, **150**, 1-9.

41. A. Inoue, N. Nishiyama, K. Hatakeyama, and T. Masumoto: *Mater. Trans. JIM*, 1994, **35**, 282-285.

42. A. Inoue, K. Ohtera, A. P. Tsai, H. Kimura, and T. Masumoto: *Japanese Journal of Applied Physics*, 1988, **27**, L1579-L1582.

43. H. A. Davies and J. B. Hull: *J. Mat. Sci.*, 1974, **9**, 707-717.

44. A. Inoue, T. Zhang, K. Kita, and T. Masumoto: *Mater. Trans. JIM*, 1989, **30**, 870-877.

45. A. Inoue and T. Masumoto: *Mat. Sci. Eng.*, 1991, **A134**, 1125-1128.

46. A. Inoue, H. Yamaguchi, T. Zhang, and T. Masumoto: *Mater. Trans. JIM*, 1990, **31**, 104-109.

47. A. Inoue, T. Ochiai, Y. Horio, and T. Masumoto: *Mat. Sci. Eng.*, 1994, **A179/A 180**, 649-653.

48. J. H. Perepezko, R. J. Hebert, and G. Wilde: *Mat. Sci. Eng.*, 2004, **A 375-377**, 171-177.

49. P. Predecki, B. C. Giessen, and N. J. Grant: *Trans. Metall. Soc. AIME*, 1965, **233**, 1438-1439.

50. H. S. Chen and K. A. Jackson: 'The Influence of Alloy Composition on Glass Formation and Properties', Metallic Glasses, Metals Park, OH USA, 74-96.

51. W. Klement, R. H. Willens, and P. Duwez: *Nature*, 1960, **187**, 869, 870.

52. F. Sommer, G. Duddek, and B. Predel: *Z. Metallkde.*, 1978, **69**, 587-590.

53. R. St.Amand and B. C. Geissen: 'Easy glass formation in simple metal alloys: amorphous metals containing calcium and strontium', Scripta Metall., 1021-1026.

54. B. C. Giessen, J. Hong, L. Kabecoff, D. E. Polk, R. Raman, and R. St.Amand: 'Compositional dependence of the thermal stability and related properties of metallic

glasses I: T(g) for $Ca_{0.65}M_{0.35}$ and $Zr_{0.475}Cu_{0.475}M_{0.05}$ glasses', Rapidly Quenched Metals III, Proc. 3rd International Conference on Rapidly Quenched Metals, Brighton, England, 249-260.

55. F. Q. Guo, S. J. Poon, and G. J. Shiflet: *Appl. Phys. Lett*, 2004, **84**, 37-39.
56. Z. Diao, Y. Yamada, T. Fukunaga, T. Matsuda, and U. Mizutani: *Mat. Sci. Eng.*, 1994, **A181/A182**, 1047-1050.
57. U. Mizutani, M. Sasaura, V. L. Moruzzi, and T. Matsuda: *Mat. Sci. Eng.*, 1988, **99**, 295-299.
58. A. Berrada, J. Durand, N. Hassanain, and B. Loegel: *J. Appl. Phys.*, 1979, **50**, 7621-7623.
59. Y. Obi, H. Morita, and H. Fujimori: *IEEE Trans Magnetics*, 1980, **16**, 1132-1134.
60. K. Shirikawa, Y. Waseda, and T. Masumoto: *Sci. Rep. Res. Inst. Tohoku University (Sendai)*, 1981, **29A**, 229-239.
61. Y. Waseda and H. S. Chen: *phys. stat. sol. (a)*, 1978, **49**, 387 - 392.
62. A. Inoue, T. Masumoto, M. Kikuchi, and T. Minemura: *Sci. Rep. Res. Inst. Tohoku University (Sendai)*, 1979, **27A**, 127-146.
63. A. Inoue, A. Kitamura, and T. Masumoto: *J. Mat. Sci.*, 1981, **16**, 1895-1908.
64. F.-X. Li, F. Li, G.-H. Tu, and W.-R. Chen: *Mat. Sci. Eng.*, 1988, **99**, 227-229.
65. G. Steinbrink, B. Punge-Witteler, and U. Koester: *Mat. Sci. Eng.*, 1991, **133**, 624-629.
66. A. Inoue, A. Kitamura, and T. Masumoto: *Mater. Trans. JIM*, 1979, **47**, 404-407.
67. R. Ray, R. Hasegawa, C.-P. Chou, and L. A. Davis: *Scripta Metall.*, 1977, **11**, 973-978.
68. F. Spaepen: 'Structure and flow of amorphous alloys', Rapidly Quenched Metals III, Proc. 3rd International Conference on Rapidly Quenched Metals, Brighton, England, 253-268.
69. A. Inoue, K. Kobayashi, C. Suryanarayana, and T. Masumoto: *Scripta Metall.*, 1980, **14**, 119-123.
70. M. Nose and T. Masumoto: *Sci. Rep. Res. Inst. Tohoku University (Sendai)*, 1980, **28A**, 222-236.
71. K. H. J. Buschow and N. M. Beekmans: *Phys. Rev. B*, 1979, **19**, 3843- 3846.
72. K. Shirakawa, K. Fukamichi, J. Kanehira, and T. Masumoto: 'Spontaneous hall effect and magnetostriction of Co-Cr-Zr amorphous alloys', Rapidly Quenched Metals, Proc. 4th International Conference on Rapidly Quenched Metals, Sendai, Japan, 861-864.
73. J.-C. Chen, Z.-X. Wang, W.-S. Zhan, J.-G. Zhao, B.-G. Shen, X. N. Zheng, and Q.-H. Chen: *Mat. Sci. Eng.*, 1988, **99**, 215-217.
74. K. Osamura, R. Suzuki, and Y. Murakami: 'SAXS study on the structure of amorphous metallic alloys', Rapidly Quenched Metals, Proc. 4th International Conference on Rapidly Quenched Metals, Sendai, Japan, 431-434.
75. L. Tanner and R. Ray: *Acta metall.*, 1979, **27**, 1727-1747.
76. T. Zhang, A. Inoue, and T. Masumoto: *Mat. Sci. Eng.*, 1994, **A181/A182**, 1423-1426.
77. L. Xia, D. Ding, S. T. Shan, and Y. D. Dong: *J. Phys.: Condens. Matter*, 2006, **18**, 3543-3548.
78. A. Inoue, W. Zhang, and J. Saida: *Mater. Trans. JIM*, 2004, **45**, 1153-1162.
79. A. J. Brunner, P. Oelhafen, and H.-J. Guntherodt: *Mat. Sci. Eng.*, 1988, **99**, 277-280.

80. K. Aoki and T. Masumoto: *Advanced Materials*, 1989, **3**, 393-398.

81. S. Whang and B. C. Giessen: 'Wear properties of some Ti alloy glasses', Rapidly Quenched Metals, Proc. 4th International Conference on Rapidly Quenched Metals, Sendai, Japan, 1403-1406.

82. R. Ray, B. C. Giessen, and N. Grant: *Scripta Metall.*, 1968, **2**, 357-359.

83. M. Sakata, N. Cowlan, and H. A. Davies: 'Relations between chemical short range order and stability in CuTi glasses', Rapidly Quenched Metals, Proc. 4th International Conference on Rapidly Quenched Metals, Sendai, Japan, 327-330.

84. L. A. Davis, C.-P. Chou, L. E. Tanner, and R. Ray: *Scripta Metall.*, 1976, **10**, 937-940.

85. A. Inoue, C. Suryanarayana, and T. Masumoto: *J. Mat. Sci.*, 1981, **16**, 1391-1401.

86. K. Suzuki, H. Fujimori, and K. Hashimoto: in 'Amorphous Metals', (ed. T. Masumoto), Vol. 291 (in Japanese); 1982, Tokyo, Japan, Ohmsha, Ltd.

87. K. H. J. Buschow: *J. Appl. Phys.*, 1981, **52**, 3319-3323.

88. R. C. Budhani, T. C. Goel, and K. L. Chopra: 'Formation and stability of Cu-Zr glasses prepared by melt-spinning and gun-quenching', Rapidly Quenched Metals, Proc. 4th International Conference on Rapidly Quenched Metals, Sendai, Japan, 615-618.

89. F. Spaepen and D. Turnbull: 'Formation of Metallic Glasses', Rapidly Quenched Metals II, Proc. 2nd International Conference on Rapidly Quenched Metals, Cambridge, MA, 205-229.

90. D. Xu, B. Lohwongwatana, G. Duan, W. L. Johnson, and C. Garland: *Acta Mater.*, 2004, **52**, 2621-2624.

91. P. G. Zielinski, J. Ostatek, M. Kijek, and H. Matyja: 'Formation and stability of metallic glasses containing zirconium', Rapidly Quenched Metals III, Proc. 3rd International Conference on Rapidly Quenched Metals, Brighton, England, 337-346.

92. D. Wang, Y. Lia, B. B. Sun, M. L. Sui, K. Lu, and E. Ma: *Appl. Phys. Lett*, 2004, **84**, 4029-4031.

93. A. S. Argon and H. Y. Kuo: *J. Non-Cryst. Sol.*, 1980, **37**, 241-266.

94. K. Fukamichi, S. Suzuki, and K. Sato: *Sci. Rep. Res. Inst. Tohoku University (Sendai)*, 1991, **36A**, 48-58.

95. M. Nuding, P. Lamparter, S. Steeb, and R. Bellissent: *J. Non-Cryst. Sol.*, 1993, **156-158**, 169-172.

96. K. Fukamichi, M. Kikuchi, S. Arakawa, and T. Masumoto: *Solid State Comm.*, 1977, **23**, 955-958.

97. R. Hasegawa and R. Ray: *J. Appl. Phys.*, 1978, **49**, 4174-4178.

98. H. S. Chen: *Scripta Metall.*, 1977, **11**, 367-369.

99. U. Gonser, M. Ghafari, M. Ackermann, H. P. Klein, J. Bauer, and H. G. Wagner: 'Crystallization of Fe(B,Si) amorphous alloys observed by Mossbauer spectroscopy and calorimetry', Rapidly Quenched Metals, Proc. 4th International Conference on Rapidly Quenched Metals, Sendai, Japan, 639-642.

100. Y. Waseda and H. S. Chen: *Sci. Rep. Res. Inst. Tohoku University (Sendai)*, 1980, **28A**, 143-155.

101. T. Zingg, T. Richmond, G. Leemann, H. Jenny, H. Bretscher, and H.-J. Guntherodt: *Mat. Sci. Eng.*, 1988, **99**, 179-182.

102. K. H. J. Buschow and A. M. v. d. Kraan: *phys. stat. sol. (a)*, 1979, **53**, 665-669.

103. K. Buschow and N. Beekmans: *phys. stat. sol. (a)*, 1979, **56**, 505-511.

104. H. Kobayashi, H. Onodera, and H. Yamamoto: *J. Phys. Soc. Japan*, 1986, **55**, 331-340.

105. J. Horvath, J.Ott, K. Pfahler, and W. Ulfert: *Mat. Sci. Eng.*, 1988, **97**, 409-413.

106. H. U. Krebs, W. Biegel, A. Bienenstock, D. J. Webb, and T. H. Geballe: *Mat. Sci. Eng.*, 1988, **97**, 163-167.

107. K. Buschow: *Solid State Comm.*, 1978, **27**, 275-278.

108. K. H. J. Buschow and N. M. Beekmans: 'Magnetic and electrical properties of amorphous alloys of Gd and C, Al, Ga, Ni, Cu, Rh or Pd', Rapidly Quenched Metals III, Proc. 3rd International Conference on Rapidly Quenched Metals, Brighton, England, 133-136.

109. K. H. J. Buschow, H. A. Algra, and R. A. Henskens: *J. Appl. Phys.*, 1980, **51**, 561-566.

110. D. Sellmyer, G. Hadjipanayis, and S. G. Cornelison: *J. Non-Cryst. Sol.*, 1980, **40**, 437-445.

111. K. Fukamichi, M. Kikuchi, T. Masumoto, and M. Matsuura: *Phys. Lett.*, 1979, **73A**, 436-438.

112. D. Louzguine and A. Inoue: *Mat. Sci. Eng.*, 2004, **A357-377**, 346-350.

113. K. H. J. Buschow and N. M. Beekmans: *J. Appl. Phys.*, 1979, **50**, 6348-6352.

114. K. Jansson and M. Nygren: *Mat. Sci. Eng.*, 1991, **A133**, 462-467.

115. A. Inoue, H. S. Chen, J. T. Krause, and T. Masumoto: *J. Non-Cryst. Sol.*, 1984, **68**, 63-73.

116. A. Inoue, Y. Takahashi, C. Suryanarayana, and T. Masumoto: *J. Mat. Sci.*, 1982, **17**, 1753-1764.

117. A. Apostolov, C. Christov, M. Mikhov, H. Sassik, and V. Skumriev: 'Magnetic properties of bulk amorphous alloy Ho_4Co_3 obtained by rapid quenching', Rapidly Quenched Metals, Proc. 5th International Conference on Rapidly Quenched Metals, Wurzburg, Germany, 1161-1164.

118. N. I. Varich, A. A. Y. Yakunin, and A. B. Lysenko: *Sov. Phys. Solid State*, 1975, **17**, 1194,1195.

119. P. M. Nast, K. Samwer, and G. v. Minnigerode: *Z. Physik B Condensed Matter*, 1980, **38**, 89-92.

120. K. Agyeman, R. Muller, and C. C. Tsuei: *Phys. Rev. B*, 1979, **19**, 193-195.

121. W. L. Jonson, S. J. Poon, and P. Duwez: *Phys. Rev. B*, 1975, **11**, 150-153.

122. W. L. Johnson and S. J. Poon: *J. Appl. Phys.*, 1975, **46**, 1787-1791.

123. Y. Kawazoe, J.-Z. Yu, A.-P. Tsai, and T. Masumoto: in 'Phase Diagrams and Physical Properties of Non-Equilibrium Alloys', (ed. W. Martienssen), Vol. 295; 1997, Berlin, Germany, Springer-Verlag.

124. W. H. Shull, D. G. Naugle, S. J. Poon, and W. L. Johnson: *Phys. Rev. B*, 1978, **18**, 3263-3270.

125. S. Kim, A. Inoue, and T. Masumoto: *Mater. Trans. JIM*, 1990, **31**, 929-934.

126. R. Richter, D. Baxter, and J. Strom-Olsen: *Mat. Sci. Eng.*, 1988, **99**, 183-186.

127. B. Predel and K. Hulse: *J. Less Common Metals*, 1979, **63**, 245-256.

128. A. Inoue, M. Kohinata, A.-P. Tsai, and T. Masumoto: *Mater. Trans. JIM*, 1989, **30**, 5-12.

129. H. Horikiri, A. Kato, A. Inoue, and T. Masumoto: *Mat. Sci. Eng.*, 1994, **A179/A180**, 702-706.

130. A. Niikura, P. Tsai, N. Nishiyama, A. Inoue, and T. Masumoto: *Mat. Sci. Eng.*, 1994, **A181/A182**, 1387-1391.

131. N. Shiotani, H. Narumi, H. Arai, K. Wakatsuki, Y. Sasa, and T. Mizoguchi: 'Crystallization progress of amorphous Mg-Zn alloys', Rapidly Quenched Metals, Proc. 4th International Conference on Rapidly Quenched Metals, Sendai, Japan, 667-670.

132. Z. P. Lu, Y. Li, S. C. Ng, and Y. P. Feng: *Thermochimica Acta*, 2000, **357-358**, 65-69.

133. M. Nose: 'PhD. Thesis', PhD thesis, Tohoku University, Sendai, Japan, 1988.

134. K. Togano, H. Kumakura, and K. Tachikawa: 'Liquid quenching on hot substrate', Rapidly Quenched Metals, Proc. 4th International Conference on Rapidly Quenched Metals, Sendai, Japan, 225-228.

135. S. Davis, M. Fischer, B. C. Giessen, and D. E. Polk: 'Formation and properties of refractory metallic glasses: T5-T9 glasses (T5=Nb,Ta T9=Rh,Ir)', Rapidly Quenched Metals III, Proc. 3rd International Conference on Rapidly Quenched Metals, Brighton, England, 425-430.

136. T. Masumoto, A. Inoue, S. Sakai, H. Kimura, and A. Hoshi: *Mater. Trans. JIM*, 1980, **21**, 115-122.

137. K. Tanaka, M. Yamada, T. Okamoto, Y. Narita, and H. Takaki: *Mat. Sci. Eng.*, 1991, **A181/A182**, 932-936.

138. A. Inoue, T. Nakamura, and T. Masumoto: *J. Mat. Sci. Lett.*, 1986, **5**, 1178-1180.

139. B. Punge-Witteler and U. Koster: *Mat. Sci. Eng.*, 1997, **97**, 343-346.

140. L. Xia, W. H. Li, S. S. Fang, B. C. Wei, and Y. D. Dong: *J. Appl. Phys.*, 2006, **99**, 026103.

141. Z. P. Lu, H. Bei, and C. T. Liu: *Intermetallics*, 2007, **15**, 618-624.

142. M. H. Lee, W. T. Kim, D. H. Kim, and Y. B. Kim: *Mat. Sci. Eng.*, 2004, **A375-377**, 336-340.

143. A. Kawashima, K. Asami, and K. Hashimoto: *J. Non-Cryst. Sol.*, 1985, **70**, 69-83.

144. B. P. Zhang, E. Akiyama, H. Habazaki, A. Kawashima, K. Asami, and H. Hashimoto: *Mat. Sci. Eng.*, 1994, **A181/A182**, 1111-1118.

145. K. Lu and J. T. Wang: *Mat. Sci. Eng.*, 1988, **97**, 399-402.

146. K. Asami, A. Kawashima, and K. Hashimoto: *Mat. Sci. Eng.*, 1988, **99**, 475-481.

147. H. Fenglai, P. P. Gardner, N. Cowlam, and H. A. Davies: *J. Phys. F: Metal Phys.*, 1987, **17**, 545-557.

148. K. Aoki, M. Kamachi, and T. Masumoto: *Sci. Rep. Res. Inst. Tohoku University (Sendai)*, 1983, **31A**, 191-199.

149. D. Louzguine-Luzgin, L. Louzguina-Luzgina, G. Xie, S. Li, W. Zhang, and A. Inoue: *J. Alloys Cmpds.*, 2007, **460**, 409-413.

150. A. Inoue, T. Zhang, and T. Masumoto: *Mater. Trans. JIM*, 1990, **31**, 177-183.

151. R. O. Elliott and B. C. Geissen: *Acta metall.*, 1982, **30**, 785-789.

152. N. Hayachi, T. Fukunaga, M. Ueno, and K. Suzuki: 'Nearest neighbor short range structure of Pd- Ge alloys glasses by pulsed neutron total scattering', Rapidly Quenched Metals, Proc. 4th International Conference on Rapidly Quenched Metals, Sendai, Japan, 355-358.

153. K. Suzuki, K. Shibata, and H. Mizuseki: *J. Non-Cryst. Sol.*, 1993, **156-158**, 58-62.

154. M. Hara, K. Hashimoto, and T. Masumoto: *Electrochim. Acta*, 1980, **25**, 1215-1220.

155. M. Ellner, M. El-Boragy, and B. Predel: 'Glass-forming ability in binary and ternary systems containing palladium', Rapidly Quenched Metals, Proc. 5th International Conference on Rapidly Quenched Metals, Wurzburg, Germany, 183-186.

156. H. S. Chen and D. Turnbull: *Acta metall.*, 1969, **17**, 1021-1031.

157. P. Duwez, R. Willens, and R. Crewdson: *J. Appl. Phys.*, 1965, **36**, 2267-2269.

158. C.-P. Chou and D. Turnbull: *J. Non-Cryst. Sol.*, 1975, **17**, 169-188.

159. P. Ramachandrarao, B. Cantor, and R. W. Cahn: *J. Mat. Sci.*, 1977, **12**, 2488-2502.

160. K. F. Yao and N. Chen: *Sci China Ser G-Phys Mech Astron* 2008, **51**, 414-420.

161. H. S. Chen, Y. Waseda, and K. T. Aust: *phys. stat. sol. (a)*, 1981, **65**, 695-699.

162. G. Marchal, P. Mangin, M. Piecuch, B. Rodmacq, and C. Janot: 'Electrical resistivity of amorphous Fe_xSn_{1-x} alloys', Rapidly Quenched Metals III, Proc. 3rd International Conference on Rapidly Quenched Metals, Brighton, England, 73-78.

163. H. Uhlig, L. Rohr, H.-J. Güntherodt, P. Fischer, and P. Lamparter: *J. Non-Cryst. Sol.*, 1993, **156-158**, 165-168.

164. B. Boucher, M. Sanquer, R. Tourbot, P. Chieux, P. Convert, M. Maret, and J. Bigot: *Mat. Sci. Eng.*, 1988, **99**, 161-164.

165. S. Hatta, T. Mizoguchi, and N. Watanabe: 'Structure and local anisotropy of amorphous Tb-Fe alloys', Rapidly Quenched Metals, Proc. 5th International Conference on Rapidly Quenched Metals, Wurzburg, Germany, 589-592.

166. E. S. R. Gopal and G. Parthasarathy: 'Double glass transition phenomena and fractional crystallization in $Ge_{20}Te_{80}$ and $Al_{23}Te_{77}$ glasses', Rapidly Quenched Metals, Proc. 5th International Conference on Rapidly Quenched Metals, Wurzburg, Germany, 373-375.

167. M. R. Anseau: *J. Appl. Phys.*, 1973, **44**, 3357-3359.

168. L. E. Tanner: *Scripta Metall.*, 1978, **12**, 703-708.

169. A. E. Lee, G. Etherington, and C. N. J. Wagner: 'The structure of $Be_{37.5}Ti_{62.5}$ metallic glass', Rapidly Quenched Metals, Proc. 5th International Conference on Rapidly Quenched Metals, Wurzburg, Germany, 491-494.

170. L. E. Tanner and R. Ray: *Scripta Metall.*, 1980, **14**, 657-662.

171. D. Polk, A. Calka, and B. Giessen: *Acta metall.*, 1978, **26**, 1097-1103.

172. T. Fukunaga, K. Kai, M. Naka, N. Watanabe, and K. Suzuki: 'High resolution short-range structure of Ni-Ti and Cu-Ti alloy glasses by pulsed neutron total scattering', Rapidly Quenched Metals, Proc. 4th International Conference on Rapidly Quenched Metals, Sendai, Japan, 347-350.

173. C. Seeger and P. L. Ryder: *Mat. Sci. Eng.*, 1994, **A179/A180**, 641-644.

174. A. Inoue, Y. Takahashi, C. Suryanarayana, A. Hoshi, and T. Masumoto: *J. Mat. Sci.*, 1981, **16**, 3077-3086.

175. B. C. Giessen and R. D. Elliott: 'Properties of metallic glasses containing actinide metals: I Thermal properties of U-M glasses (M=V, Cr, Mn, Fe, Co and Ni)', Rapidly Quenched Metals III, Proc. 3rd International Conference on Rapidly Quenched Metals, Brighton, England, 406-411.

176. R. O. Elliott, D. A. Koss, and B. C. Geissen: *Scripta Metall.*, 1980, **14**, 1061-1065.

177. U. Mizutani, H. Sugiura, Y. Yamada, Y. Sugiura, and T. Matsuda: *Mat. Sci. Eng.*, 1994, **A179/A180**, 132-136.

178. U. Mizutani, K. Tanaka, T. Matsuda, N. Suzuki, T. Fukunaga, Y. Ozaki, Y. Yamada, and K. Nakayama: *J. Non-Cryst. Sol.*, 1993, **156-158**, 297-301.

179. L. Jastrow, U. Köster, and M. Meuris: *Mat. Sci. Eng.*, 2004, **A375-377**, 440-443.

180. R. Hasegawa and L. E. Tanner: *J. Appl. Phys.*, 1978, **49**, 1196-1200.

181. H. Riesemeier, K. Lüders, H. C. Freyhardt, and J. Reichelt: *J. Non-Cryst. Sol.*, 1984, **61-62**, 991-996.

182. M. ElAmrani, J. Destry, and R. W. Cochrane: *Mat. Sci. Eng.*, 1988, **99**, 309-311.

183. I. Kokanovic, B. Leontic, J. Lukatela, and A. Tonejc: *Mat. Sci. Eng.*, 2004, **A375-377**, 688-692.

184. M. L. Trudeau, R. W. Cochrane, and J. Destry: *Mat. Sci. Eng.*, 1988, **99**, 187-190.

185. Y. Waseda and H. Chen: 'The structure of amorphous metal-metal alloys', Rapidly Quenched Metals III, Proc. 3rd International Conference on Rapidly Quenched Metals, Brighton, England, 415-418.

186. W. H. Wang, J. J. Lewandowski, and A. L. Greer: *J. Mater. Res.*, 2005, **20**, 2307-2313.

187. T. Mizoguchi, T. Kudo, T. Irisawa, N. Watanabe, N. Niimura, M. Misawa, and K. Suzuki: 'The structure of a metal-metal amorphous alloy, $Cu_{0.57}Zr_{0.43}$, determined by neutron diffraction', Rapidly Quenched Metals III, Proc. 3rd International Conference on Rapidly Quenched Metals, Brighton, England, 384-389.

188. W. Biegel, H. U. Krebs, C. Michaelsen, H. C. Freyhardt, and E. Heustern: *Mat. Sci. Eng.*, 1988, **97**, 59-62.

189. J. C. deLima, D. Raoux, J. M. Tonnerre, D. Udron, K. D. Machado, T. A. Grandi, C. E. M. deCampos, and T. I. Morrison: *Phys. Rev. B*, 2003, **67**, 094210.

190. T. Mizoguchi, S. Yoda, N. Akutsu, S. Yamada, J. Nishioka, T. Suemasa, and N. Watanabe: 'Structural study of an amorphous $Ni_{36}Zr_{64}$ alloy', Rapidly Quenched Metals, Proc. 5th International Conference on Rapidly Quenched Metals, Wurzburg, Germany, 483-486.

191. J. R.C. Bowman, M. J. Rosker, and W. L. Johnson: *J. Non-Cryst. Sol.*, 1982, **53**, 105-122.

192. K. Togano and K. Tachikawa: *J. Appl. Phys.*, 1975, **46**, 3609-3613.

193. A. Inoue, Y. Takahashi, and T. Masumoto: *Sci. Rep. Res. Inst. Tohoku University (Sendai)*, 1981, **29A**, 296-303.

194. A. Inoue, R. Toyota, T. Fukase, T. Masumoto, and Y. Takahashi: *J. Mat. Sci.*, 1983, **18**, 114-126.

195. M. B. Tang, D. Q. Zhao, M. X. Pan, and W. H. Wang: *Chinese Phys. Lett.*, 2004, **21**, 901-903.

Table 1. Assessed radii of atoms in metallic glass structures.

Element	At #	Radius (pm)	Element	At #	Radius (pm)	Element	At #	Radius (pm)
Li	3	152	**Se**	34	118	**Tb**	65	176
Be	4	112	**Rb**	37	244	**Dy**	66	175
B	5	88	**Sr**	38	212	**Ho**	67	177
C	6	77	**Y**	39	179	**Er**	68	175
N	7	72	**Zr**	40	158	**Tm**	69	175
O	8	64	**Nb**	41	143	**Yb**	70	190
Na	11	180	**Mo**	42	139	**Lu**	71	175
Mg	12	160	**Tc**	43	136	**Hf**	72	158
Al	13	141	**Ru**	44	134	**Ta**	73	145
Si	14	110	**Rh**	45	132	**W**	74	135
P	15	102	**Pd**	46	142	**Re**	75	137
S	16	103	**Ag**	47	144	**Os**	76	135
K	19	230	**Cd**	48	157	**Ir**	77	136
Ca	20	201	**In**	49	155	**Pt**	78	139
Sc	21	162	**Sn**	50	155	**Au**	79	143
Ti	22	142	**Sb**	51	155	**Hg**	80	152
V	23	134	**Te**	52	140	**Tl**	81	172
Cr	24	130	**Cs**	55	264	**Pb**	82	174
Mn	25	132	**Ba**	56	223	**Bi**	83	162
Fe	26	125	**La**	57	187	**Po**	84	168
Co	27	125	**Ce**	58	182	**Th**	90	178
Ni	28	126	**Pr**	59	183	**Pa**	91	165
Cu	29	126	**Nd**	60	182	**U**	92	158
Zn	30	140	**Pm**	61	185	**Np**	93	175
Ga	31	134	**Sm**	62	185	**Pu**	94	175
Ge	32	114	**Eu**	63	196			
As	33	115	**Gd**	64	176			

Table 2. **Structural sites and site occupancies per α site, $S(i_j)$, for binary structures.**

		Species (*i*)		
		Ω	**α**	**Site Sum**
Site (*j*)	**Ω**	$S(\Omega_\Omega)$	$S(\alpha_\Omega)$	$\hat{S}_\Omega$
	α	$S(\Omega_\alpha) = 0$	$S(\alpha_\alpha) \leq 1$	$\hat{S}_\alpha = 1$
	β	$S(\Omega_\beta) = 0$	$S(\alpha_\beta) \leq 1$	$\hat{S}_\beta = 1$
	γ	$S(\Omega_\gamma) = 0$	$S(\alpha_\gamma) \leq 2$	$\hat{S}_\gamma = 2$
Species Sum		$\bar{S}_\Omega = S(\Omega_\Omega)$	$\bar{S}_\alpha$	$\sum S = \hat{S}_\Omega + 4$

Table 3. **Preferred structural topologies and occurrence.**

R* (±0.01)	**<Z>**	**F^{iso}**	**Occurrence**	**Known BMGs**	**Preferred F_α**
0.414	<6>	0.733	Rare		
0.518	<7>	0.680	None		
0.617	<8>	0.637	Uncommon		
0.710	<9>	0.601	Common	Ca-Al	0.48 – 0.60
0.799	<10>	0.571	Common	Hf-Cu, Zr-Cu, Pd-Si	0.46 – 0.57
0.884	<11>	0.532	Unstable [2]		
0.902	<12>	0.527	Common		0.42 – 0.53
0.976	<13>	0.506	Rare		
1.047	<14>	0.488	None		
1.116	<15>	0.471	Common	Ni-Nb	0.38 – 0.47
1.183	<16>	0.443	Rare		
1.248	<17>	0.430	Common	Cu-Hf, Cu-Zr	0.34 – 0.43
1.311	<18>	0.417	Uncommon		
1.373	<19>	0.405	None		
1.433	<20>	0.394	Uncommon		

Table 4. **Topological analysis of inverse glass systems.**

System	R	Nearest R^*	$\frac{\lvert R-R^* \rvert}{R^*}$	(1/R)	Nearest R^*	$\frac{\lvert (1/R)-R^* \rvert}{R^*}$	SUM
Hf-Cu	0.797	0.799	0.0025	1.255	1.248	0.0054	0.0079
Hf-Ni	0.797	0.799	0.0025	1.255	1.248	0.0054	0.0079
Zr-Cu	0.797	0.799	0.0025	1.255	1.248	0.0054	0.0079
Zr-Ni	0.797	0.799	0.0025	1.255	1.248	0.0054	0.0079
Th-Fe	0.702	0.71	0.0113	1.425	1.433	0.0059	0.0172
Ca-Zn	0.697	0.71	0.0183	1.435	1.433	0.0012	0.0195
Ca-Cu	0.627	0.617	0.0162	1.595	1.6044	0.0059	0.0221
Zr-Co	0.791	0.799	0.0100	1.264	1.248	0.0130	0.0230
Ti-Cu	0.887	0.902	0.0166	1.127	1.116	0.0102	0.0268
Nb-Ni	0.881	0.902	0.0233	1.135	1.116	0.0171	0.0404
Nb-Rh	0.923	0.902	0.0233	1.083	1.116	0.0292	0.0525
Ta-Ni	0.869	0.902	0.0366	1.151	1.116	0.0311	0.0677

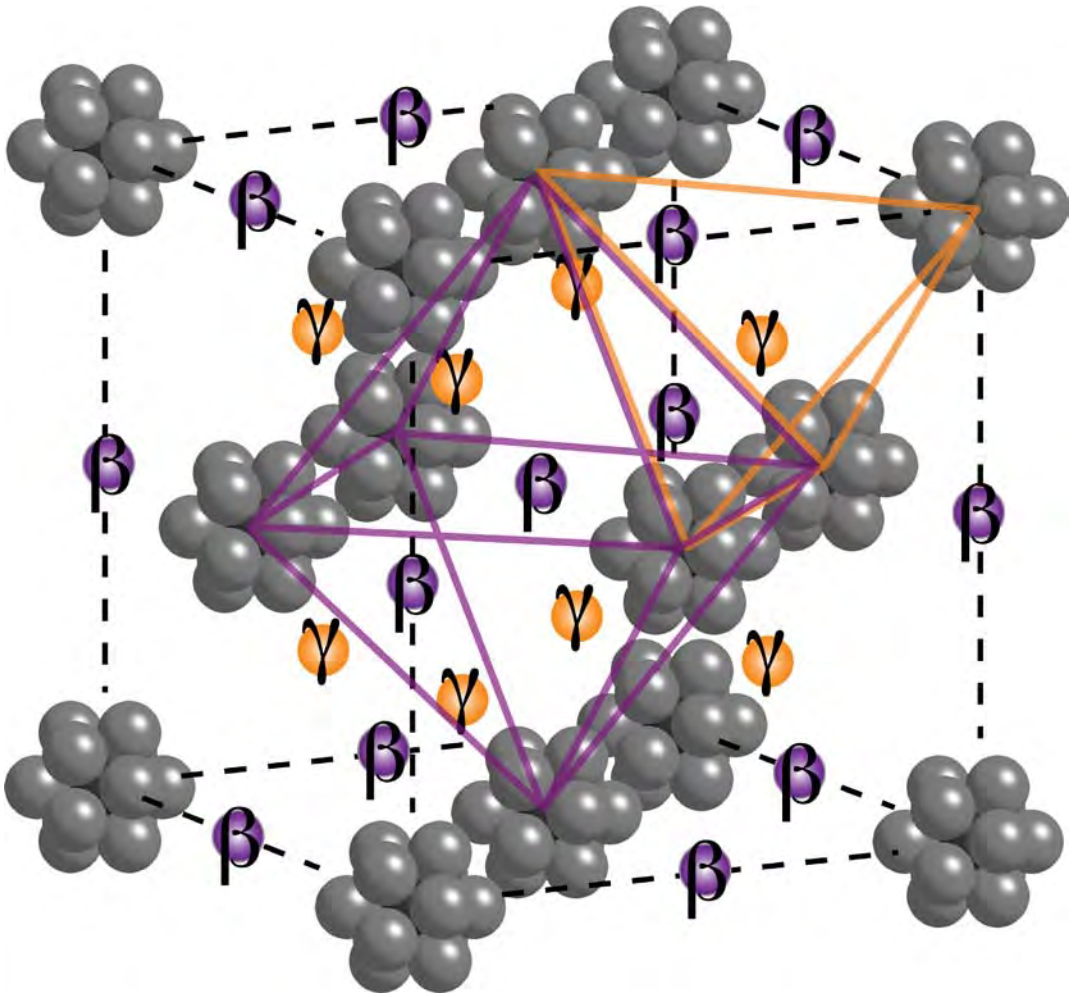

Figure 1 A representative unit cell of the efficient cluster packing structure for metallic glasses [1, 2]. The atomic clusters have an α site at the center and Ω sites in the first coordination shell, and approximate to a cubic close-packed arrangement that efficiently fills space . β sites are surrounded by an octahedron of these clusters and γ sites are enclosed by a tetrahedron of clusters. Distances between atoms are exaggerated to better illustrate the locations of atom sites.

Figure 2 Periodic table showing the solute and solvent atoms found in binary metallic glasses.

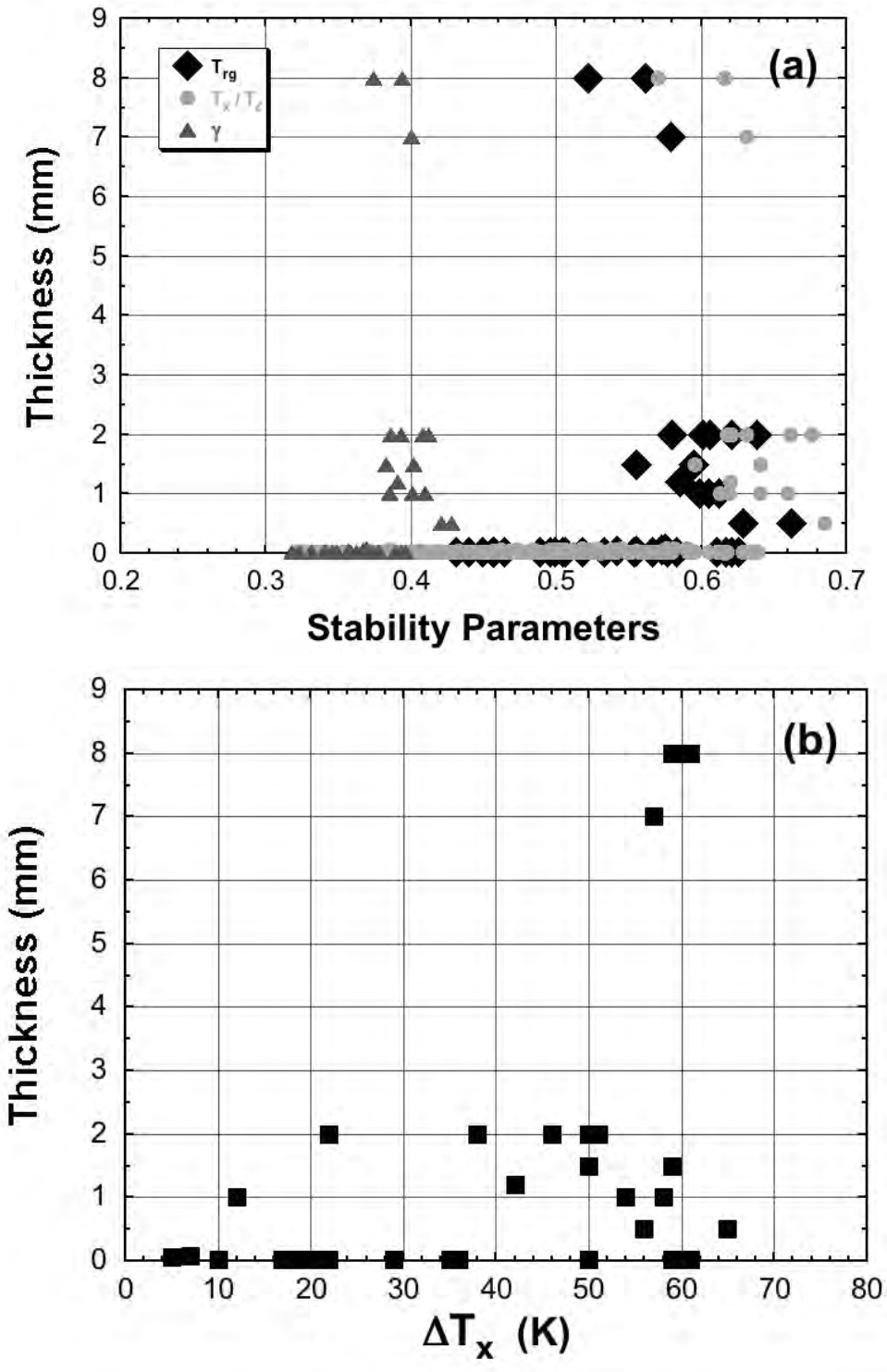

Figure 3 Influence of thermal stability parameters (a) T_{rg}, T_x/T_ℓ and γ, and (b) ΔT_x on reported amorphous thickness. Binary BMGs require minimum values of about 0.52 for T_{rg}; about 0.55 for T_x/T_ℓ, 0.36 for γ; or about 10 K for ΔT_x.

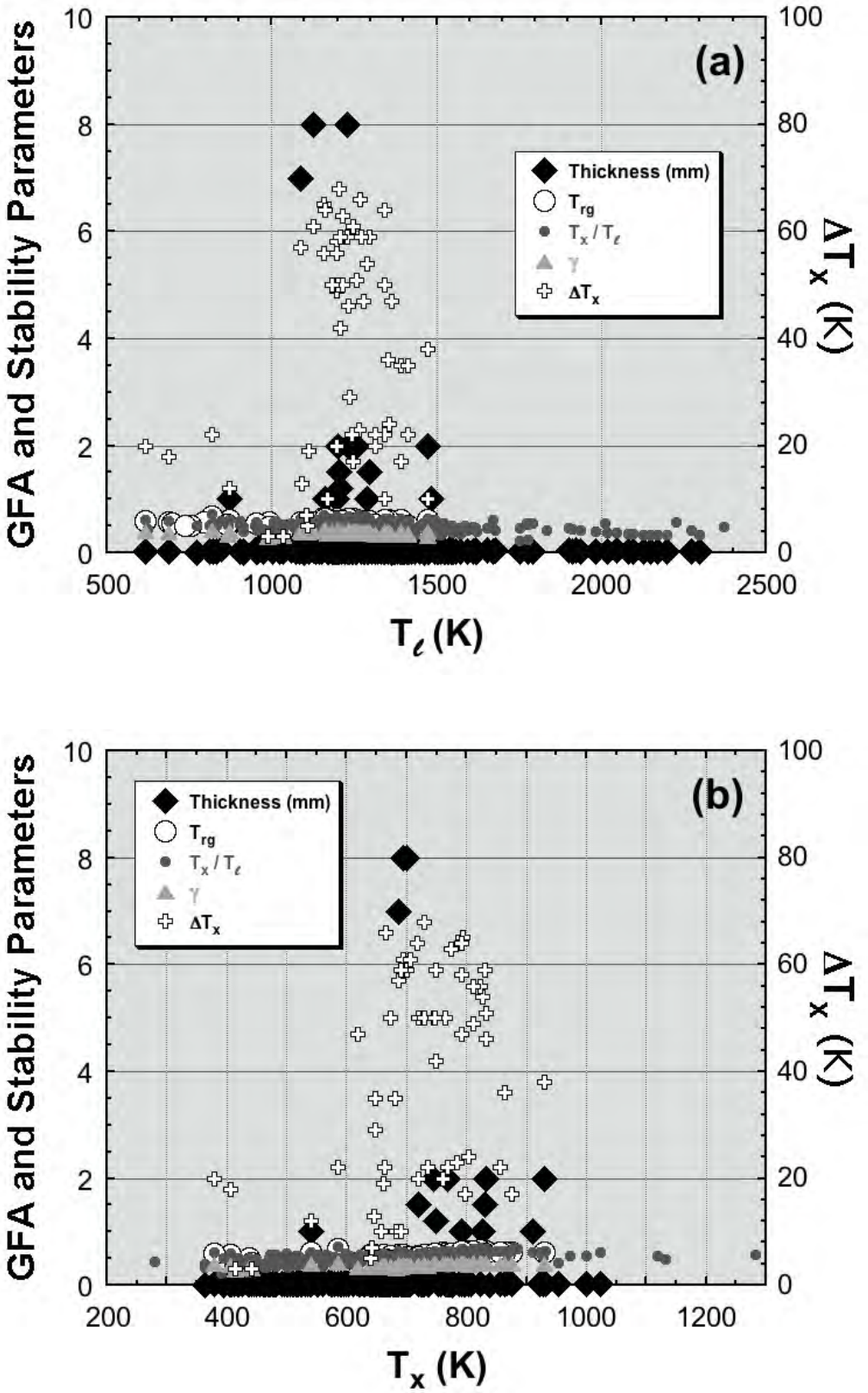

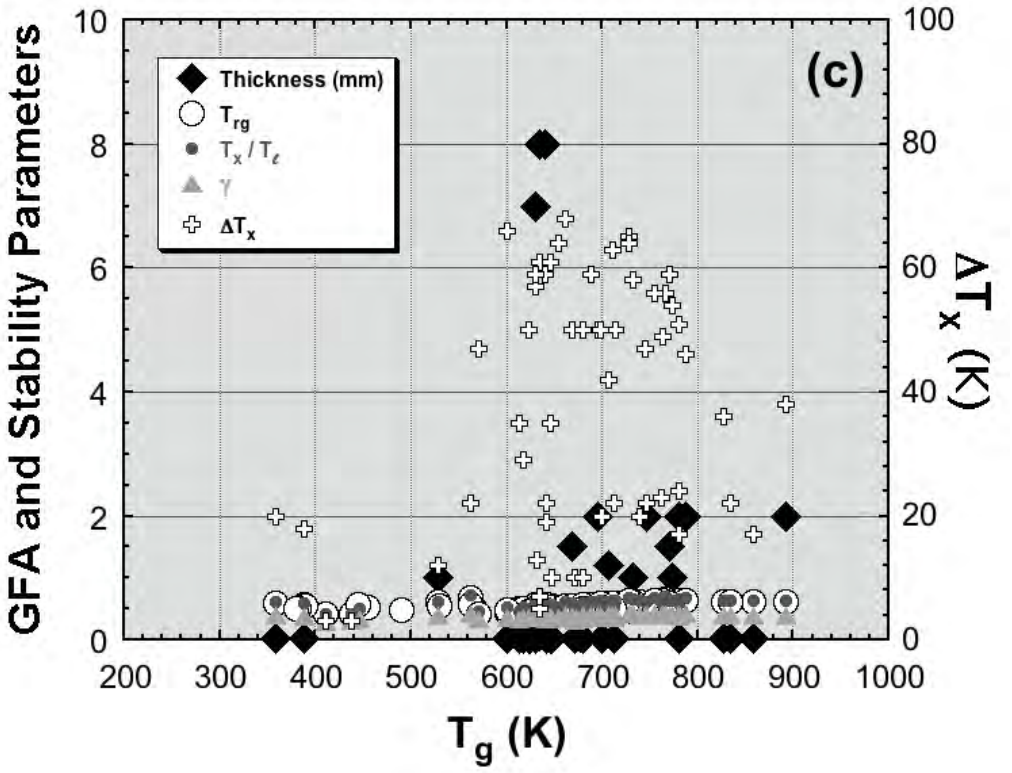

Figure 4 Dependence of the glass forming ability, as measured by the maximum reported amorphous thickness, and derived thermal stability parameters on the primary thermal stability parameters (a) liquidus temperature, T_ℓ; (b) crystallization temperature T_x; and (c) glass transition temperature, T_g.

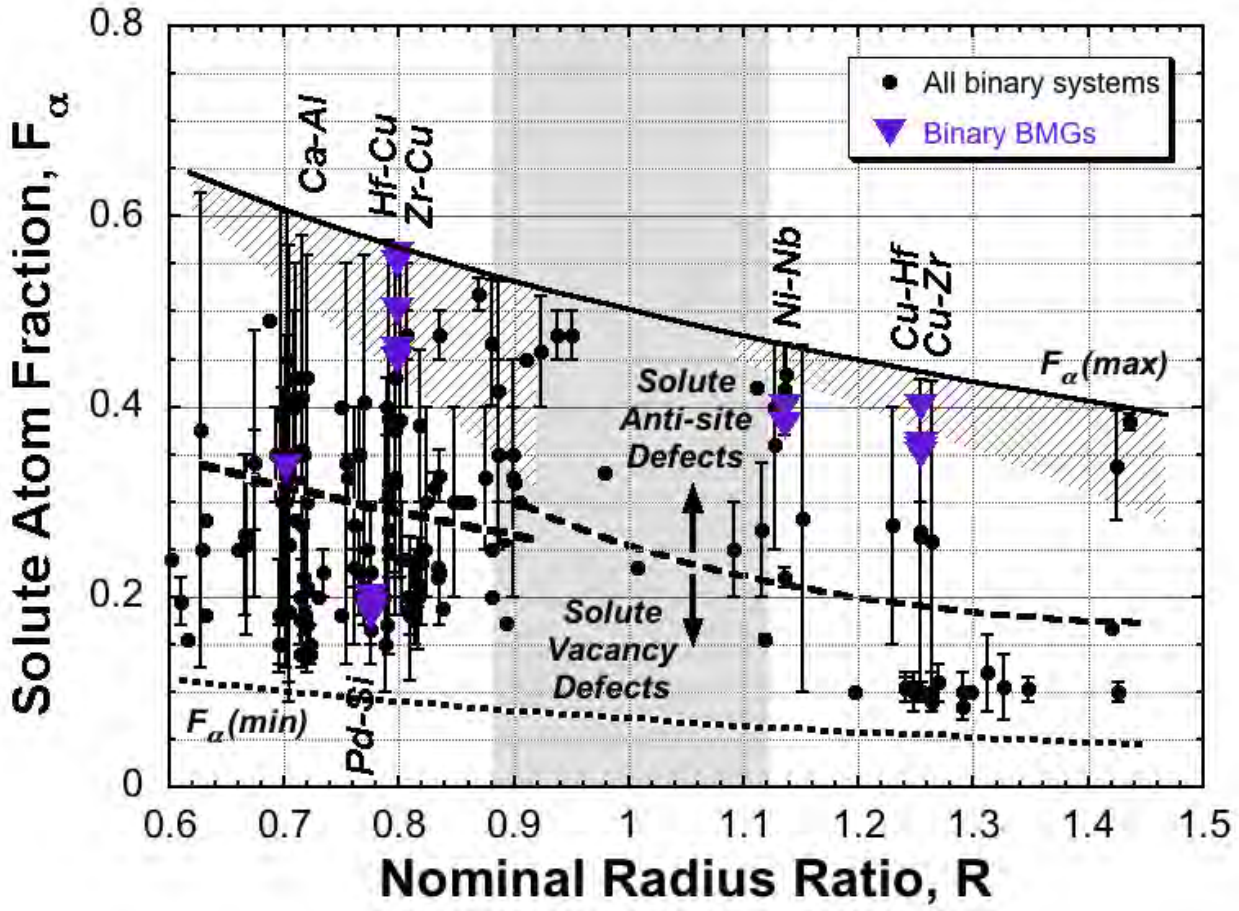

Figure 5 Solute atom fraction vs. nominal radius ratio for all binary metallic glass systems (filled circles) and binary BMGs (filled triangles). The BMG systems are labelled. The solid line is the maximum value of F_α at the iso-structure condition from Equation 11. The dashed line represents the boundary at $\overline{S}_\alpha = 4$ between solute-lean glasses with solute vacancy defects (below) and solute-rich glasses with solute anti-site defects (above). The dotted line is the minimum solute atom fraction at $\overline{S}_\alpha = 1$, where all α sites are just filled by α. The gray band is the region of poor GFA from the empirical rule that the preferred difference in solvent and solute radii is greater than ±12%. The hatched areas represent regions of maximal global packing efficiency derived in Section 4.4.1.

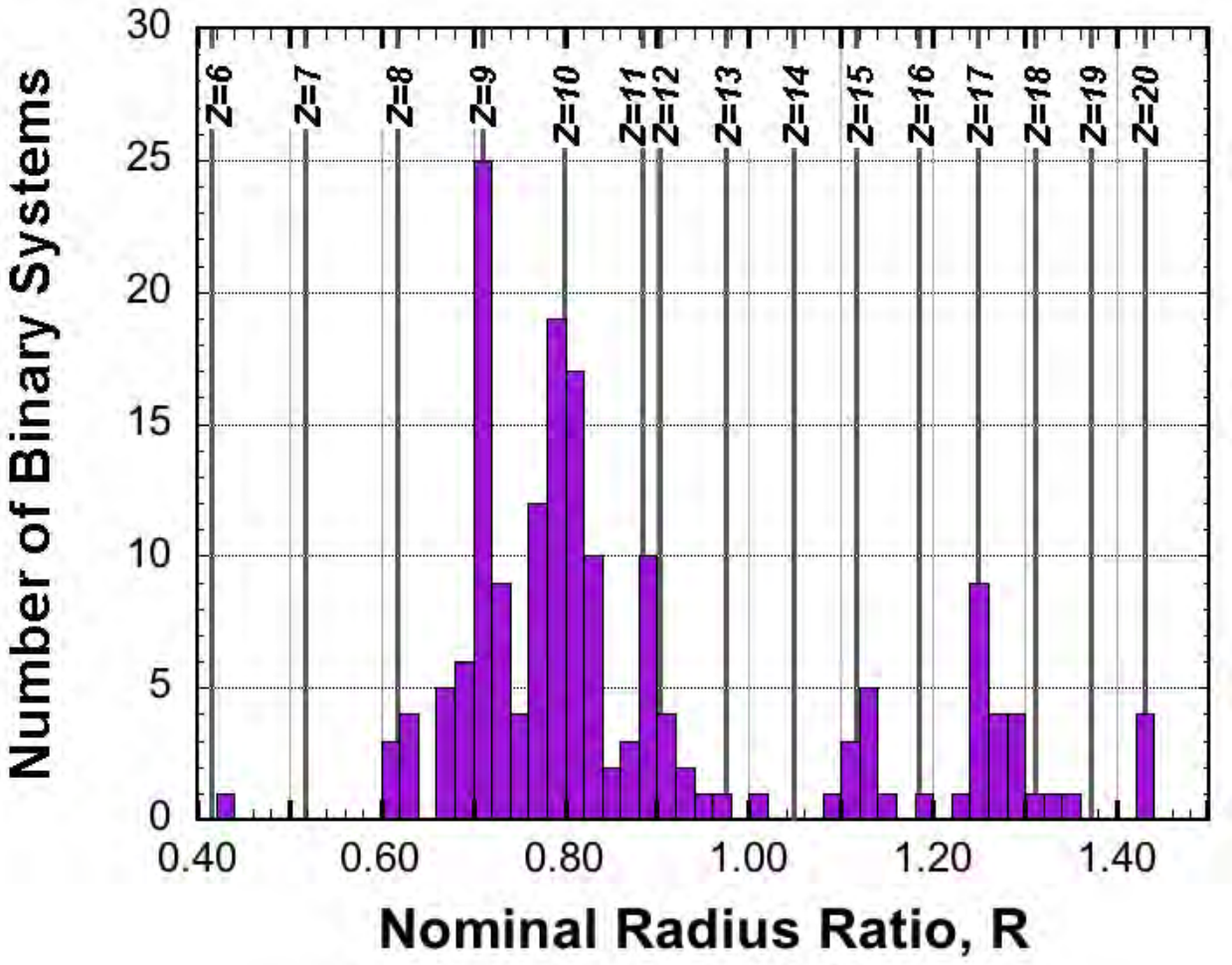

Figure 6 Histogram of the nominal solute-to-solvent radius ratios, $R = r_\alpha / r_\Omega$, in binary metallic glass systems. The vertical bars represent the number of glass systems with R values in the interval between R and R+0.02 as a function of R. The bold vertical lines indicate special radius ratios, R^*, that give efficient local atomic packing of Z solvent atoms around a central α solute.

Figure 7 Contour plot of the number of reported alloys within increments R+0.05R and F_α+0.05F_α as a function of R and F_α. The dashed line represents the maximum solute atom fraction at the iso-structural condition from Equation 11.

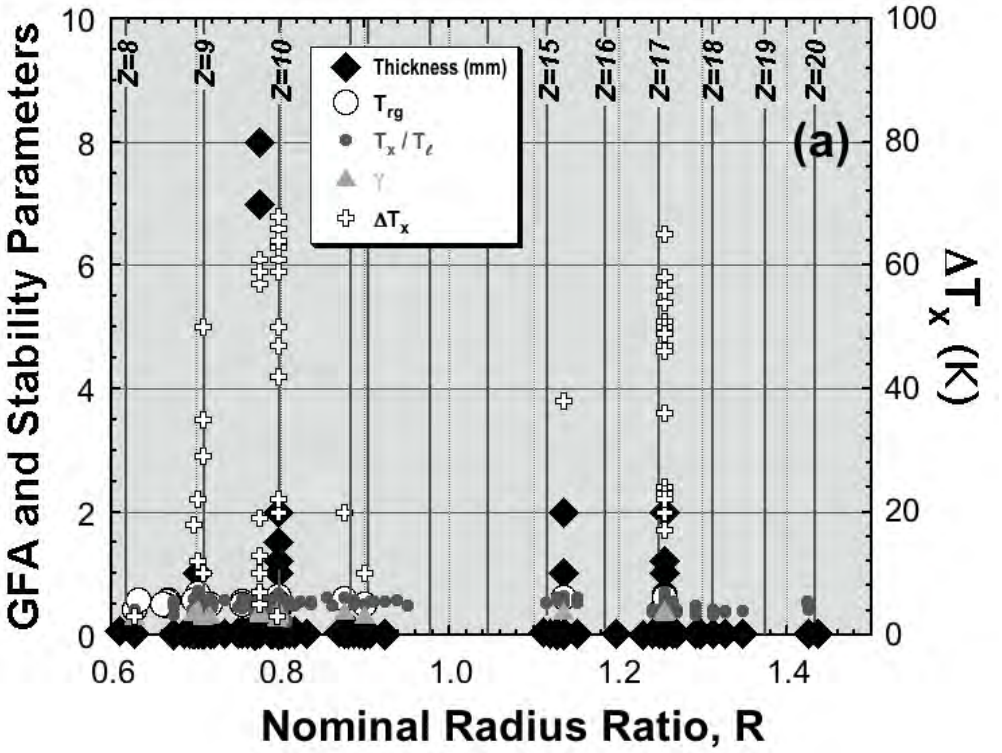

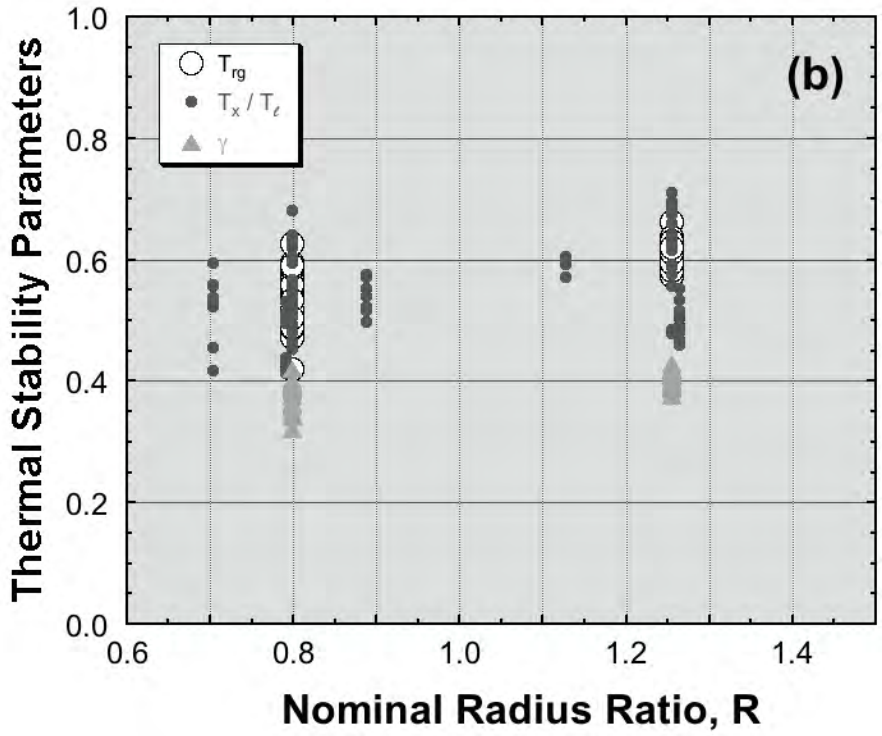

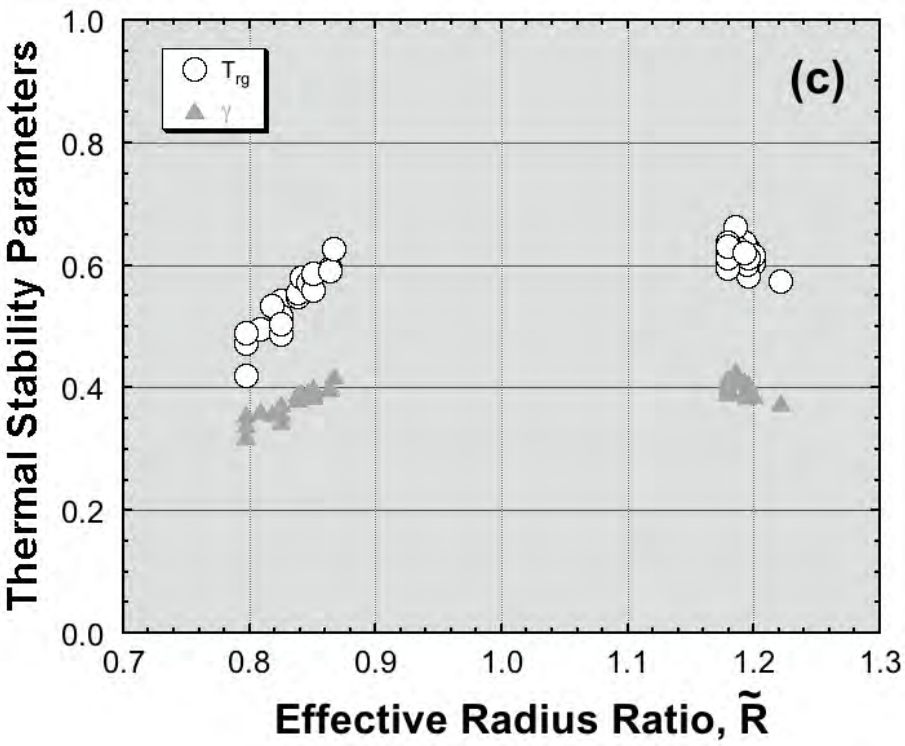

Figure 8 Effect of nominal radius ratio on (a) GFA and thermal stability parameters for the full dataset and (b) thermal stability parameters for a partial dataset of chemically similar alloys (Zr-Fe, Zr-Co, Zr-Ni, Zr-Cu, Hf-Co, Hf-Ni, Hf-Cu, Ti-Ni, Ti-Cu and Th-Fe). Values of T_{rg} and γ are shown in (c) as a function of the effective solute-to-solvent radius ratio, $\tilde{R}$, for the same limited set of alloys. Values of R^* are shown by the vertical lines in (a).

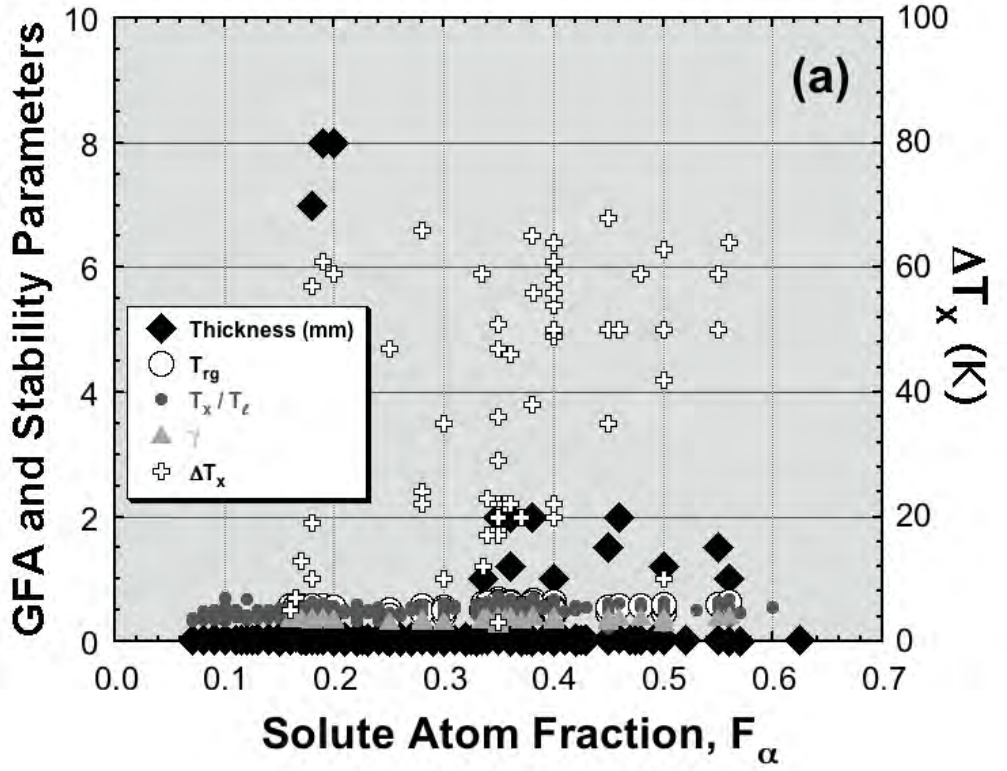

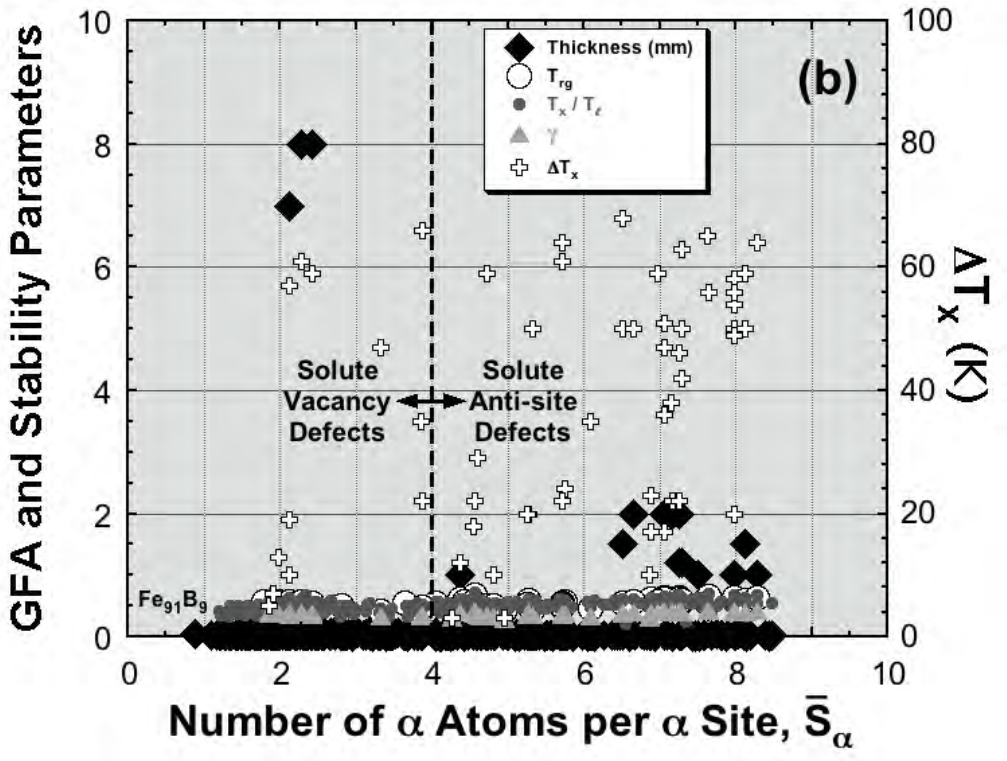

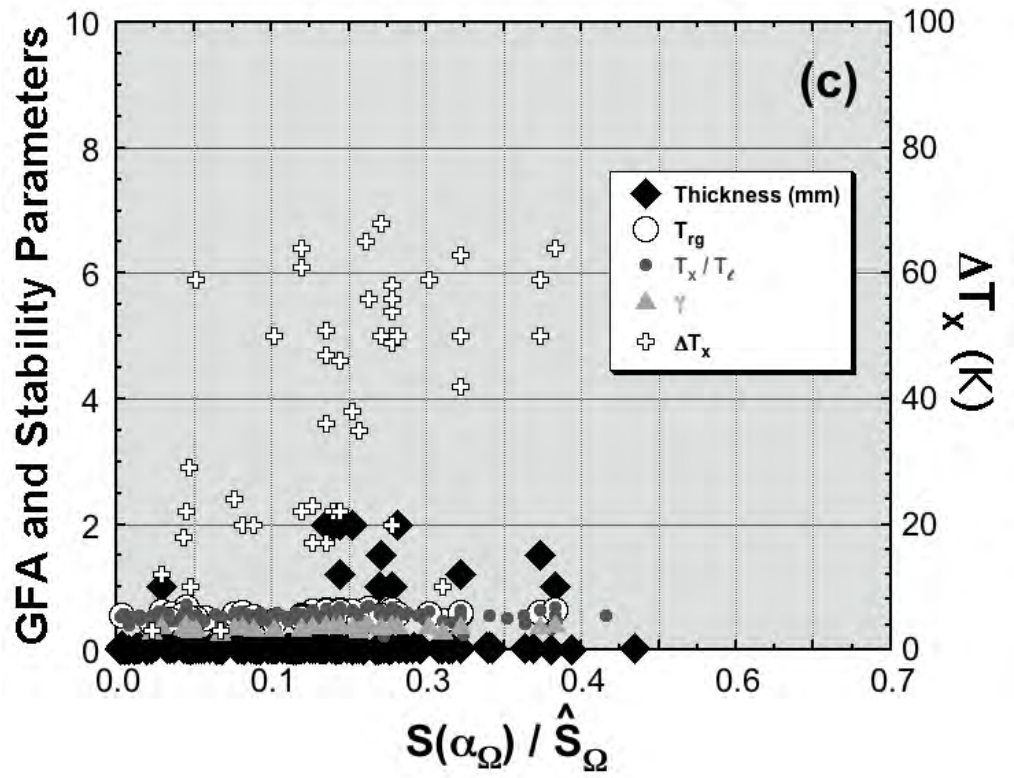

Figure 9 GFA and thermal stability parameters v. (a) F_α, (b) the number of α atoms in the structure per α site, $\bar{S}_\alpha$. and (c) the fraction of Ω sites in the structure that are occupied by α atoms. All solute sites are filled when $\bar{S}_\alpha = 4$ in (b), which defines the boundary between solute-lean and solute-rich structures.

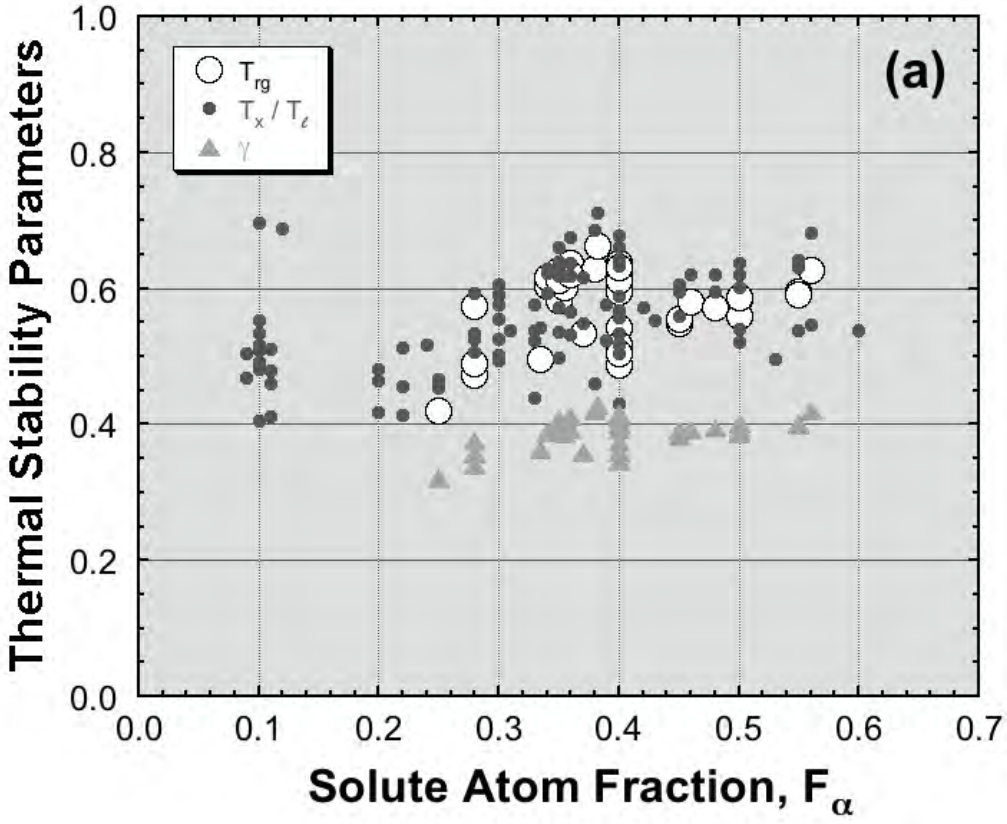

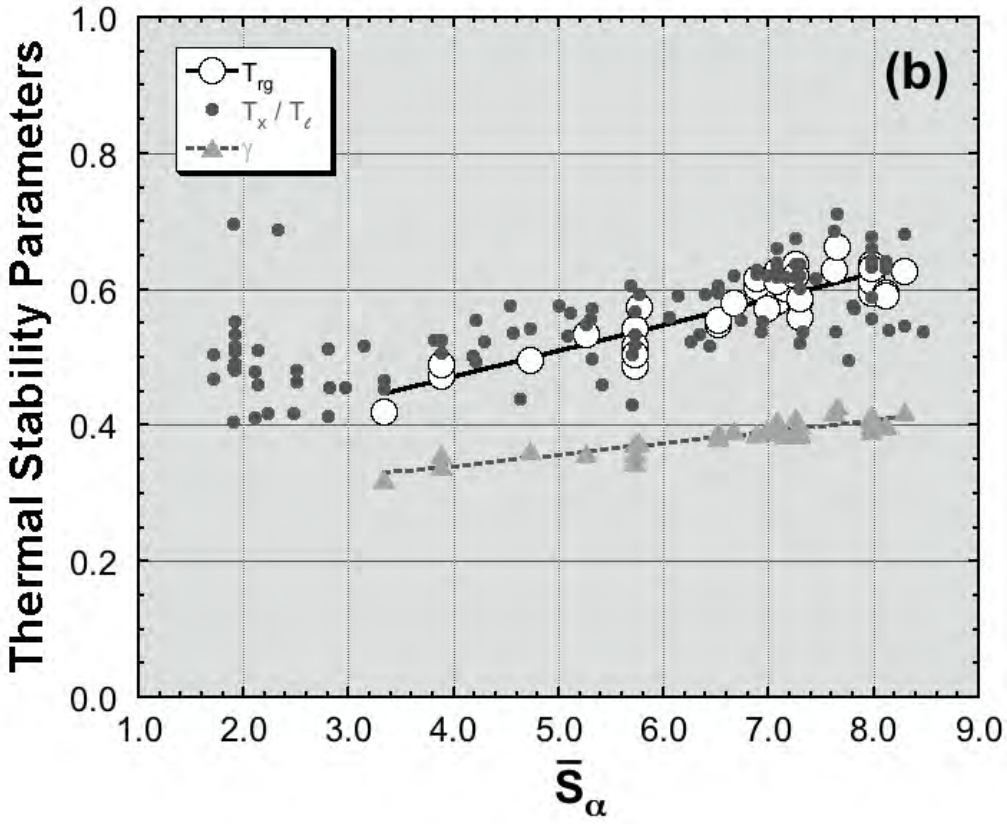

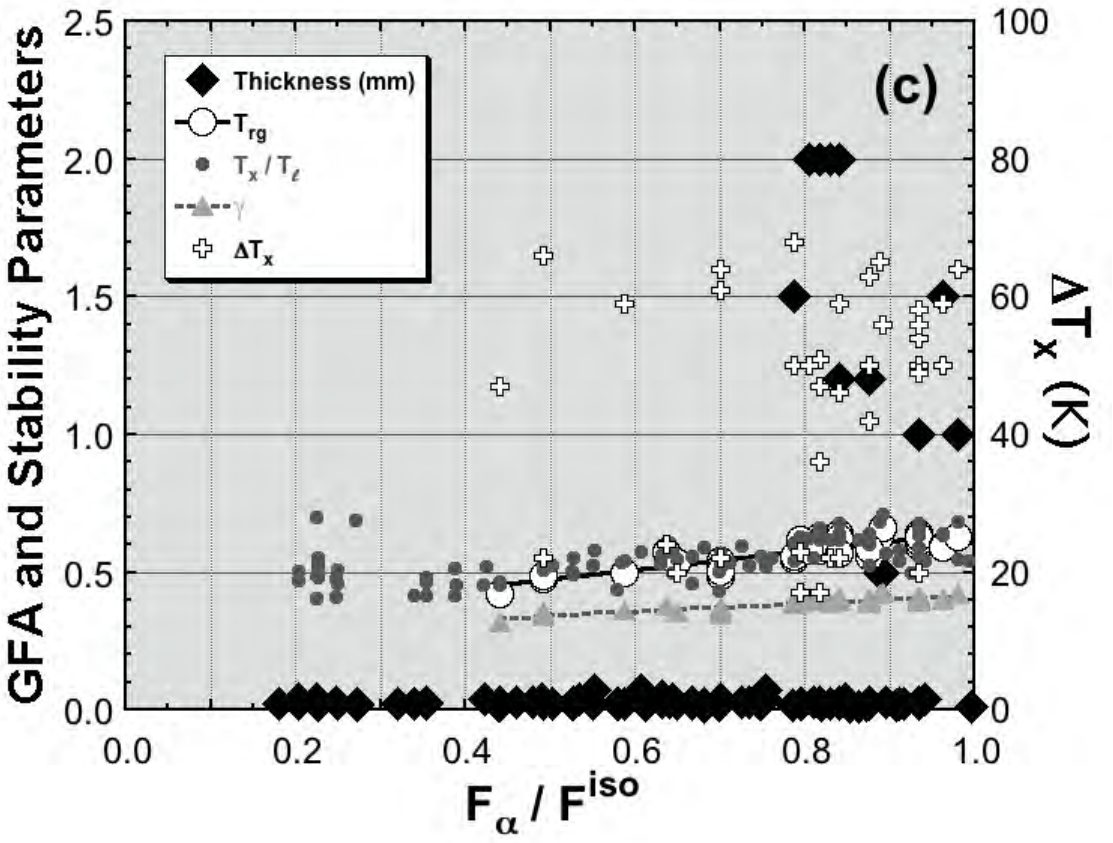

Figure 10 Thermal stability and GFA for alloys in a selected set of chemically similar metallic glasses (Zr-Fe, Zr-Co, Zr-Ni, Zr-Cu, Hf-Co, Hf-Ni, Hf-Cu, Ti-Ni, Ti-Cu and Th-Fe). Thermal stability parameters are shown v. (a) the solute atom fraction, F_α, and (b) the number of α atoms in the structure per α site, $\overline{S}_\alpha$. Thermal stability and GFA are shown in (c) as a function of F_α normalized by the iso-structure composition of each alloy, F^{iso}. Linear regressions are shown for T_{rg} and γ in (b) and (c).

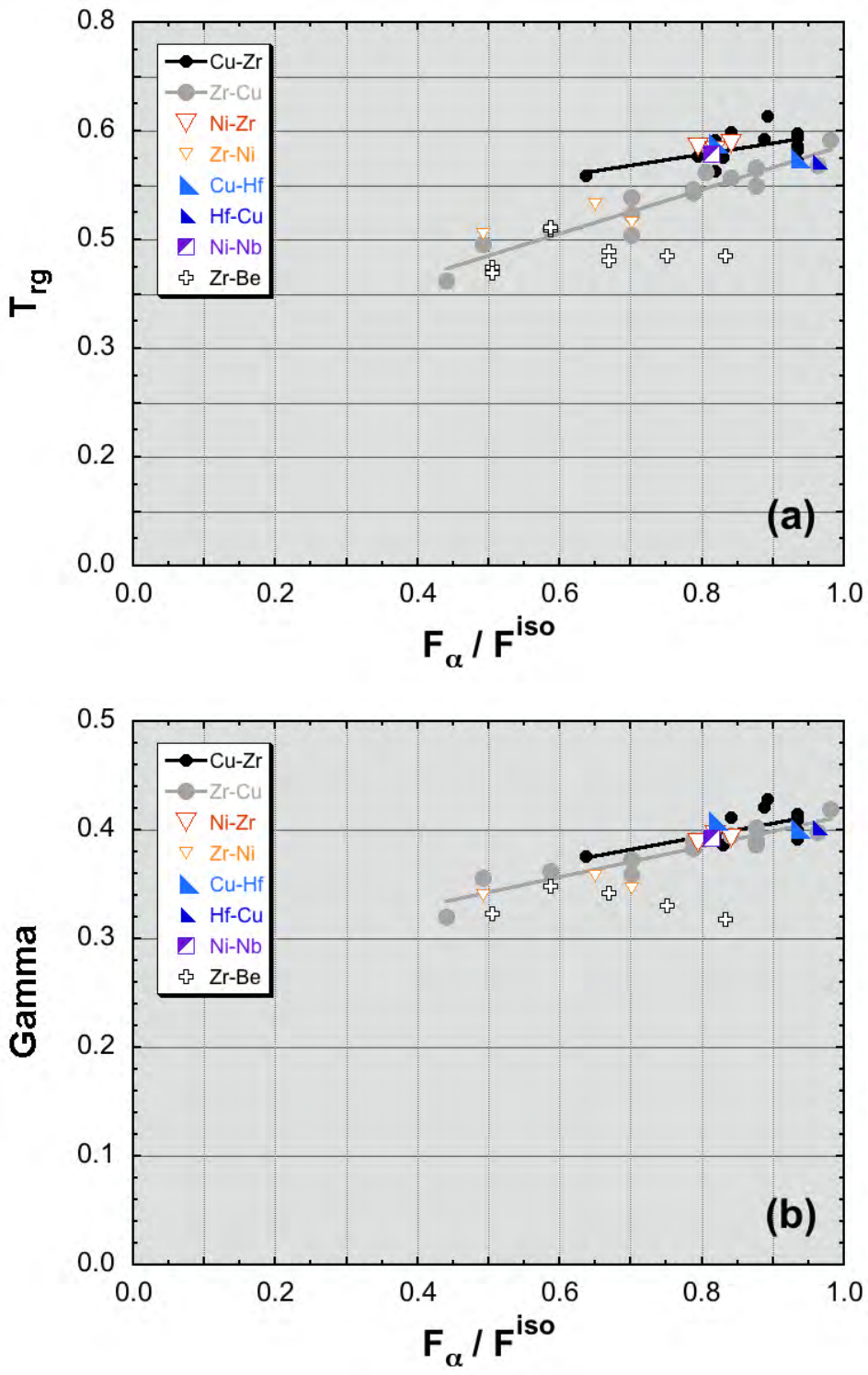

Figure 11 Comparisons of thermal stability via (a) T_{rg} and (b) γ as a function of solute concentration, represented by F_α / F^{iso}. The binary systems selected here enable separation of contributions from radius ratio, solute concentration and chemical interaction between the constituent elements.

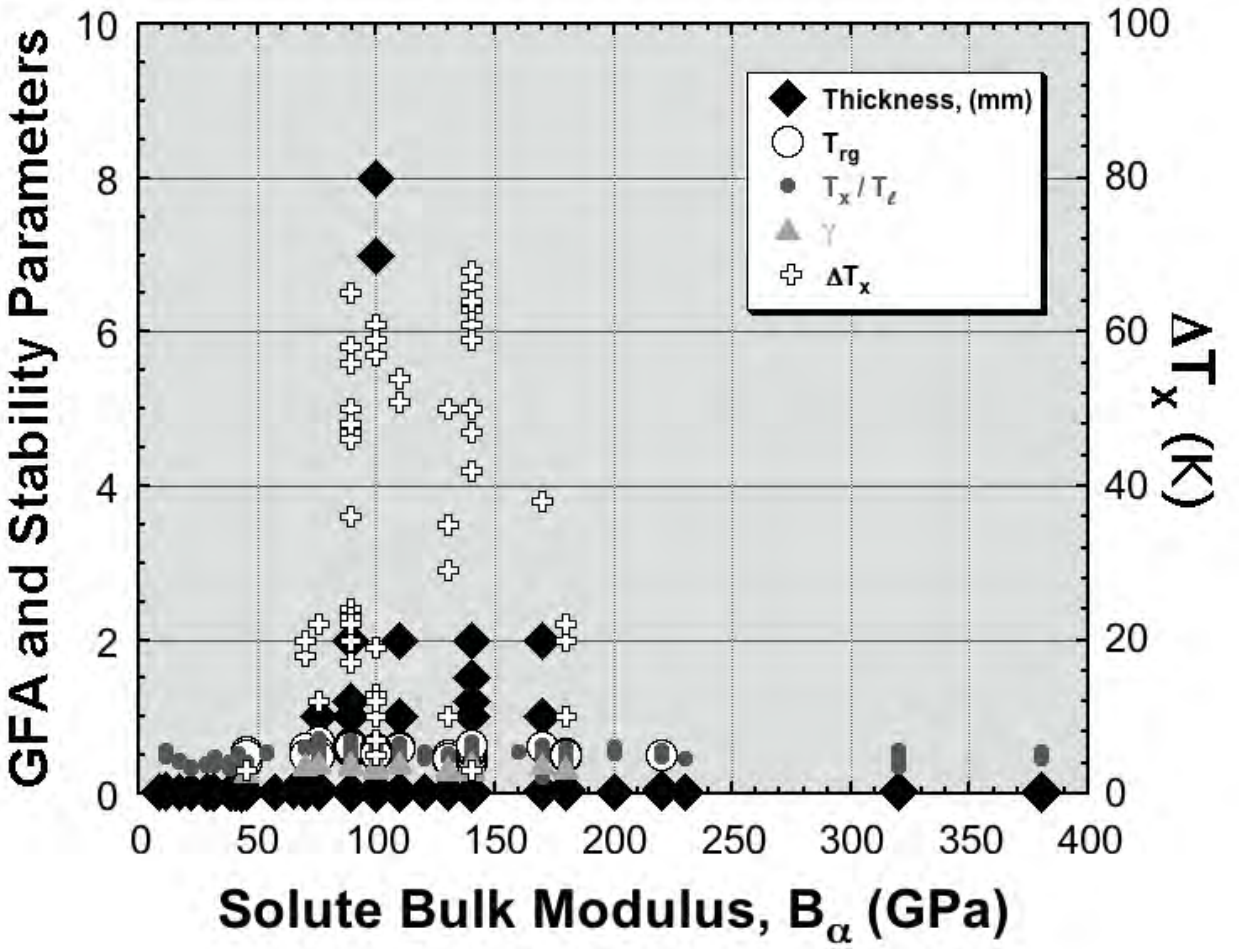

Figure 12 GFA and thermal stability parameters v. the solute bulk modulus, B_α.

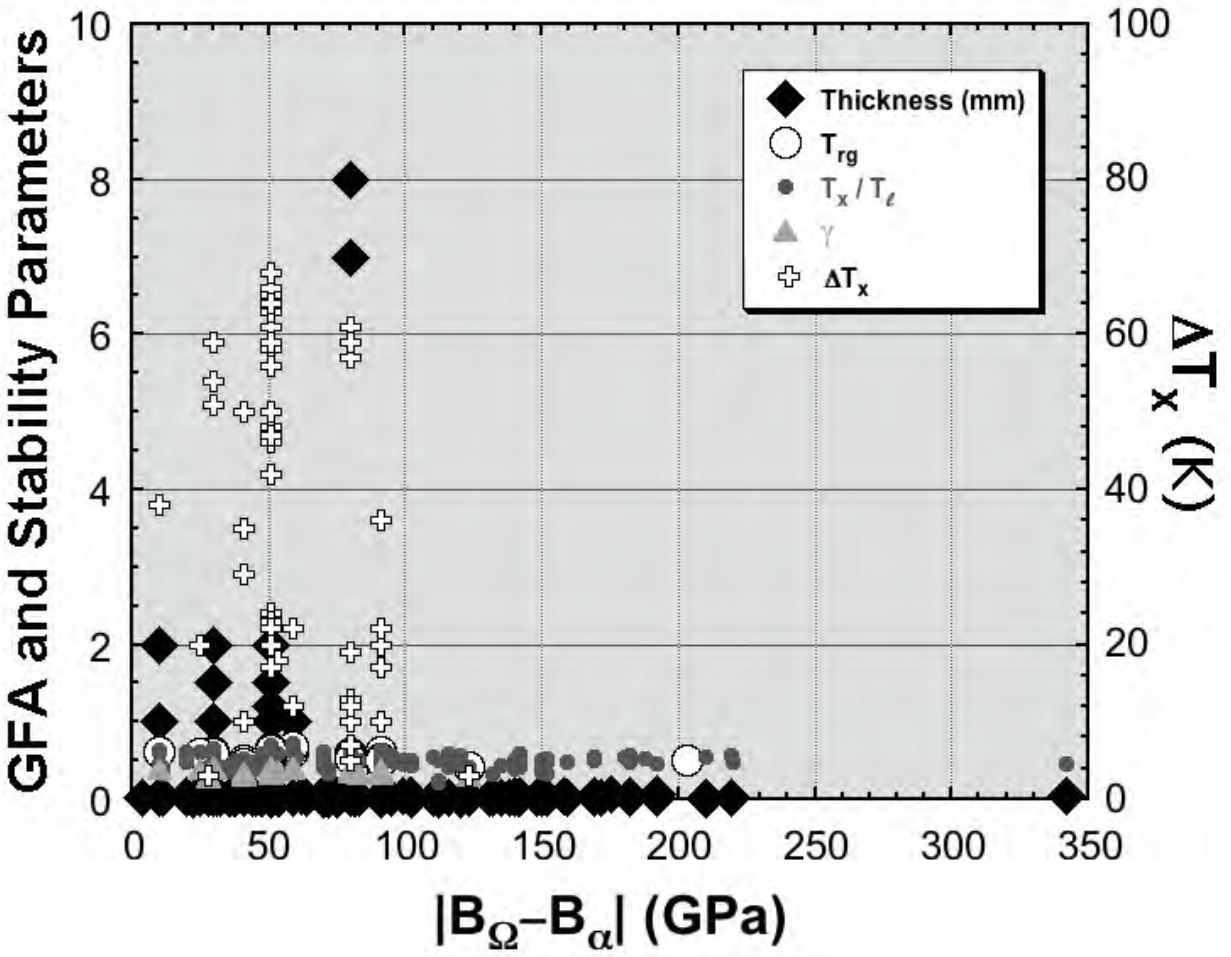

Figure 13 GFA and thermal stability parameters v. the absolute difference in solvent and solute bulk moduli.

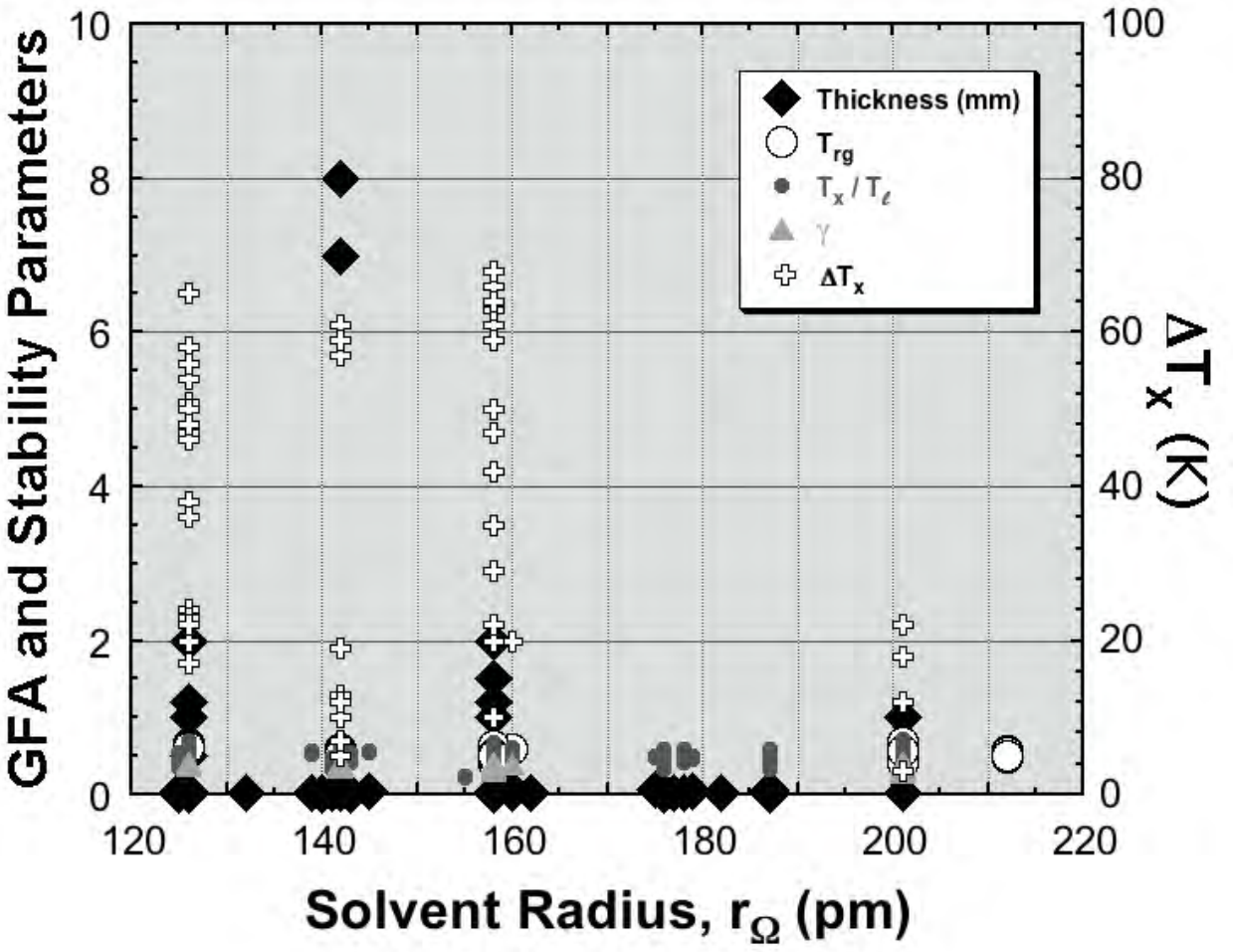

Figure 14 GFA and thermal stability parameters v. the solvent atom radius, r_Ω.

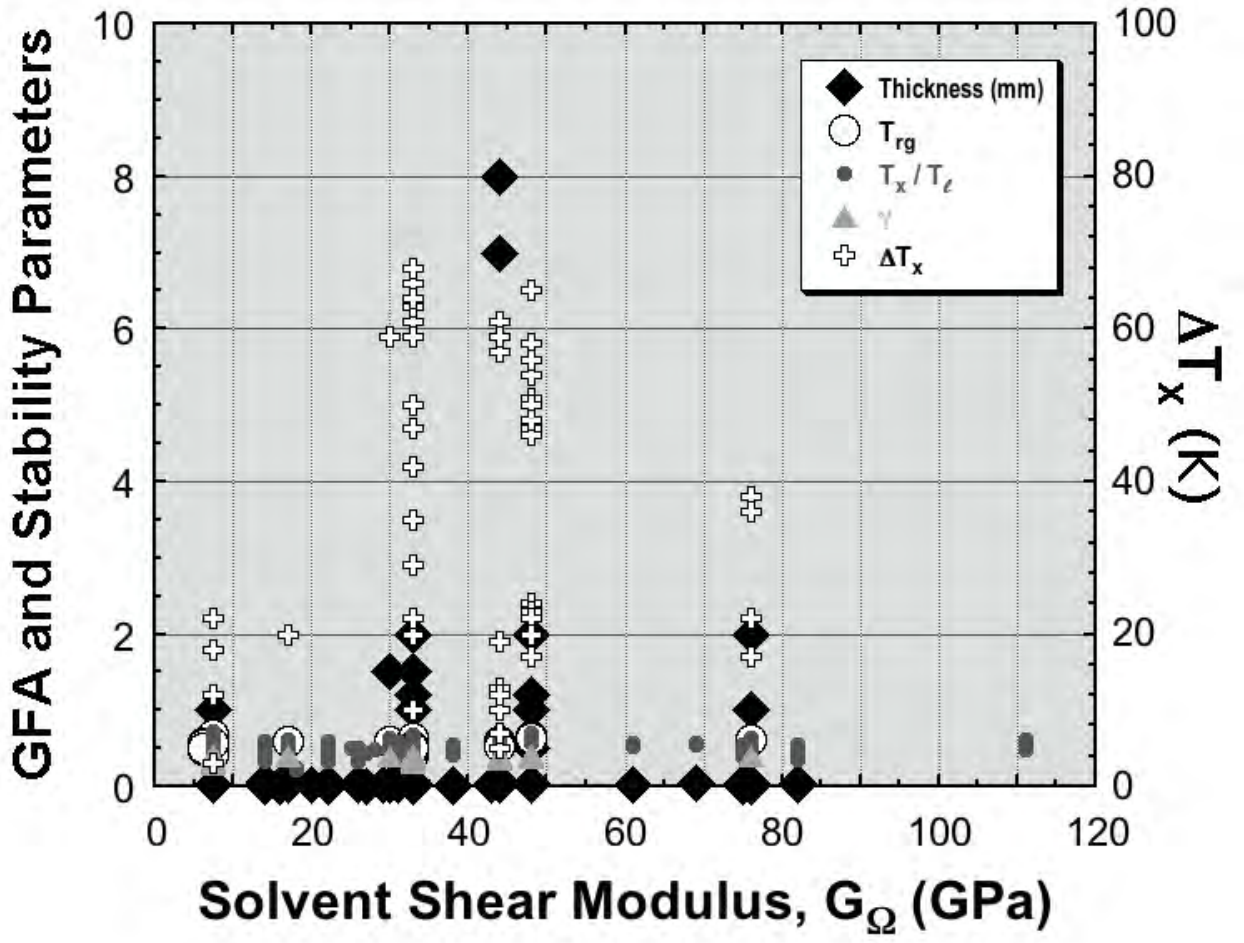

Figure 15 GFA and thermal stability parameters v. the solvent shear modulus, G_{Ω}.

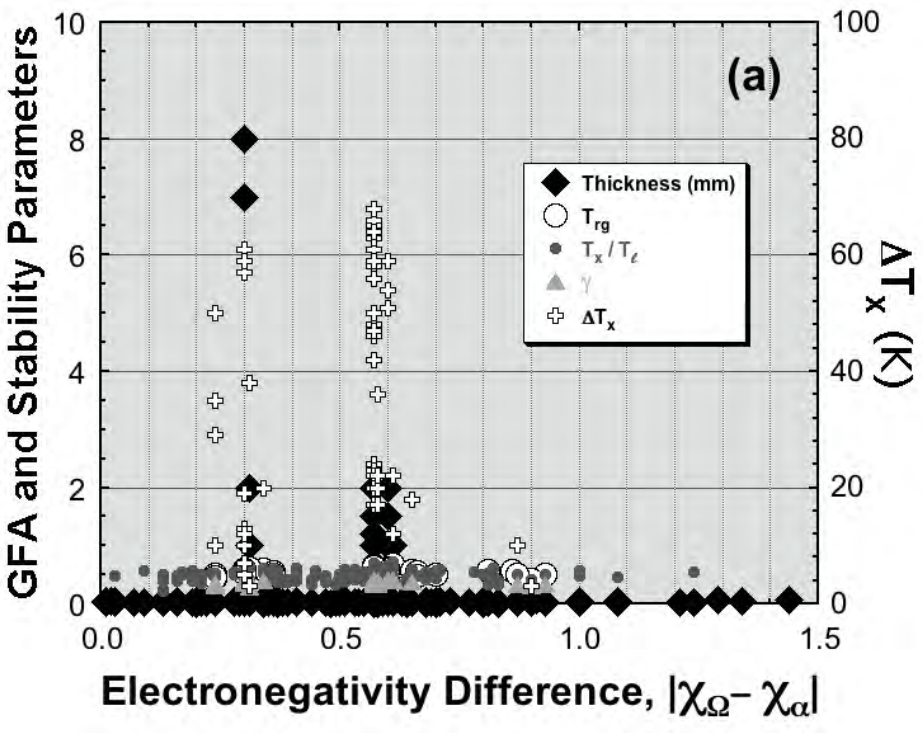

Figure 16 (a) GFA and thermal stability parameters v. the absolute difference in solute and solvent Pauling electronegativities. (b) A smoothed contour plot showing the number of glasses of a given electronegativity difference (within a range of ±0.05) as a function of radius ratio (within a range of ±0.05). The smoothing algorithm was taken from [17].

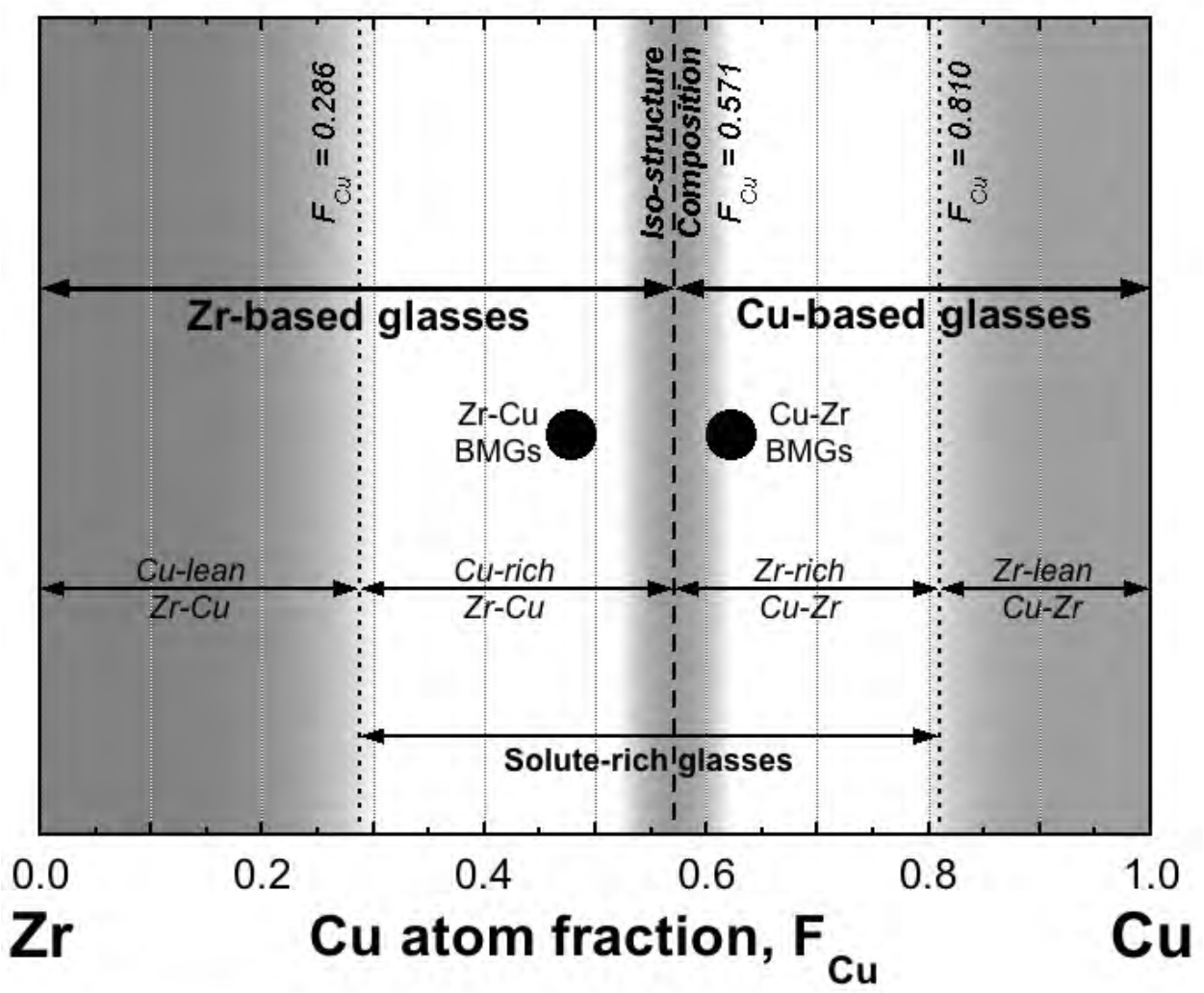

Figure 17 Illustration of composition ranges for complementary, inverse Zr-Cu and Cu-Zr binary systems. Solute-rich Zr-Cu BMGs and solute-rich Cu-Zr BMGs both approach the iso-structural composition. The iso-structural composition and the compositions of the boundaries between solute-rich and solute lean structures depend explicitly on the radius ratio of the glass system and are given here for R = 0.797.

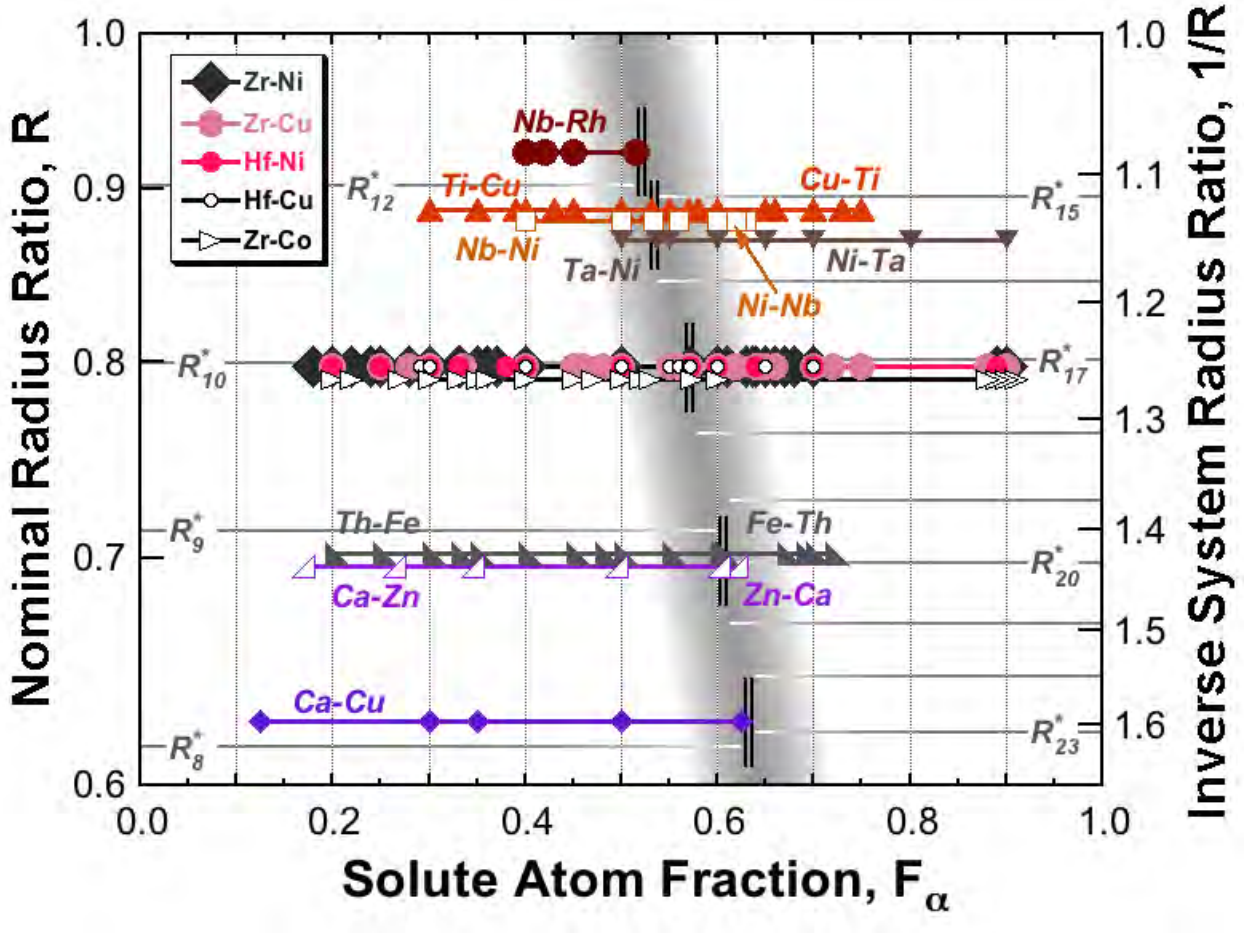

Figure 18 Radius ratios and composition ranges of binary systems that approach or span the iso-structure composition, indicated by the vertical double lines. Systems with $R<1$ are on the left of the iso-structure composition and the companion inverse systems with $R>1$ are on the right. To maintain continuity of F_α across the iso-structure composition, α is taken to be the smaller atom in each system. The values of R^* required for efficient local atomic packing are given by the gray horizontal lines, and are labeled for values nearest the observed glasses.

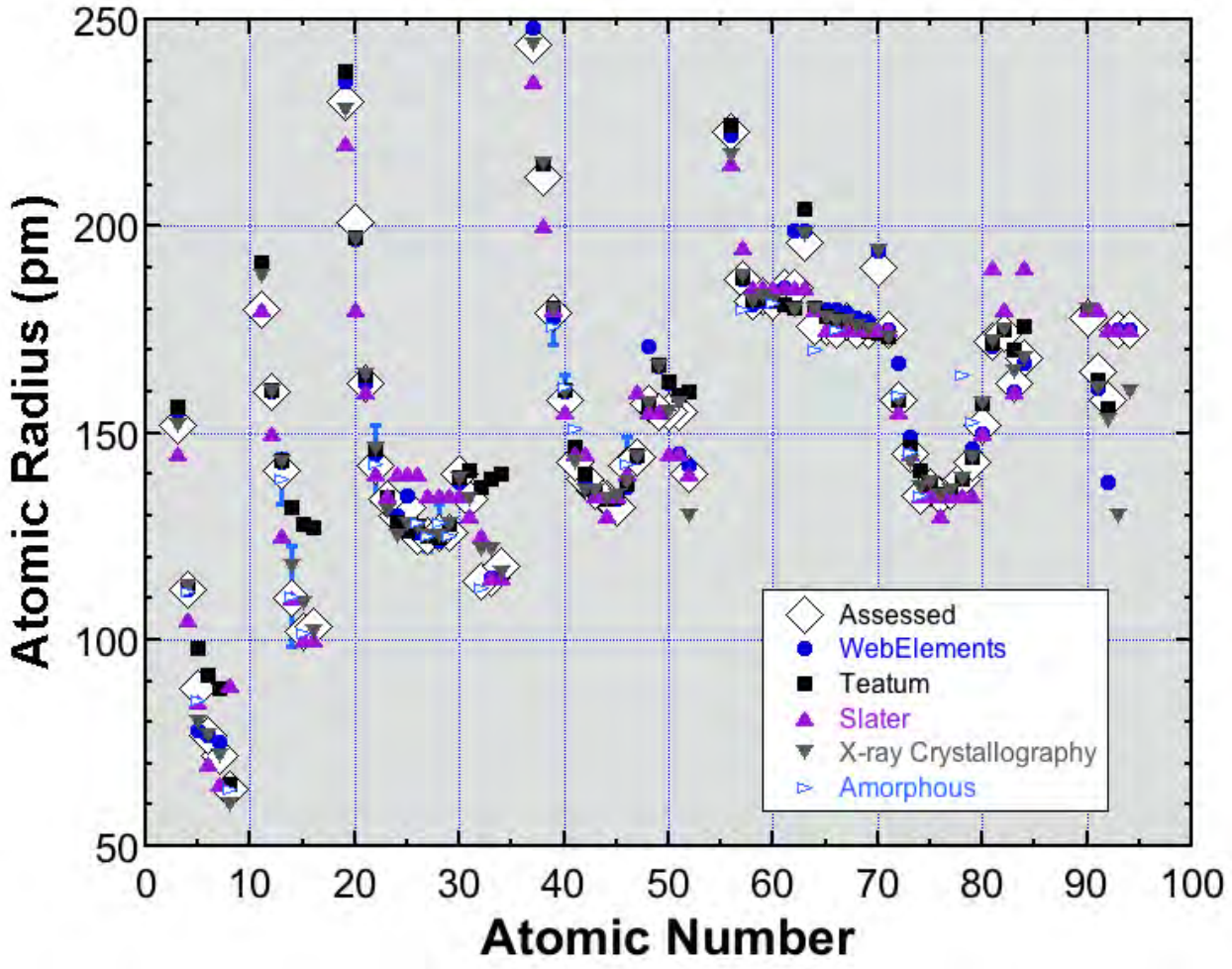

Figure 19 Assessed atomic radii from the present work (◇), from previous assessments [5, 6, 7, 8], and from diffraction measurements in metallic glass systems (▷) [28, 29, 30, 27, 31, 32, 33, 34, 35, 36, 37, 38, 39, 40]. An error bar gives the range in reported values from these experimental measurements.

Appendix

Table A1. Binary metallic glass constitutions, densities, characteristic temperatures and structural parameters.

Ω	α	F_α	R	ρ, g cm^{-3}	T_g, K	T_x, K	T_l, K	T_{rg}	T_x / T_ℓ	ΔT_x, K	γ	$\overline{S_\Omega}$	$\overline{S_\alpha}$	$\overline{S_\Omega}$	$S(\alpha_\alpha)$	$S(\alpha_\beta)$	$S(\alpha_\gamma)$	$S(\alpha_\Omega)$	$S(\Omega_\Omega)$	$Z_{\alpha\alpha}$	$Z_{\alpha\Omega}$	$Z_{\Omega\alpha}$	$Z_{\Omega\Omega}$	Citations
Al	Ca	0.09	1.426			408	955		0.427			19.9	1.97	19.9	1	0.97	0	0	19.9					[41]
Al	Ca	0.10	1.426			419	973		0.431			19.9	2.21	19.9	1	1	0.21	0	19.9					[41]
Al	Ca	0.11	1.426			425	1003		0.424			19.9	2.46	19.9	1	1	0.46	0	19.9					[41]
Al	Ce	0.07	1.291			437	1360		0.321			17.7	1.33	17.7	1	0.33	0	0	17.7					[42]
Al	Ce	0.08	1.291			468	1370		0.342			17.7	1.54	17.7	1	0.54	0	0	17.7					[42]
Al	Ce	0.09	1.291			483	1390		0.347			17.7	1.75	17.7	1	0.75	0	0	17.7					[42]
Al	Ce	0.10	1.291			463	1410		0.328			17.7	1.96	17.7	1	0.96	0	0	17.7					[42]
Al	Cu	0.173	0.894									11.1	2.33	11.1	1	1	0.33	0	11.1					[43]
Al	Dy	0.09	1.241			478	1278		0.374			16.9	1.67	16.9	1	0.67	0	0	16.9					[44]
Al	Dy	0.10	1.241			520	1353		0.384			16.9	1.88	16.9	1	0.88	0	0	16.9					[44]
Al	Dy	0.11	1.241			530	1363		0.389			16.9	2.09	16.9	1	1	0.09	0	16.9					[44]
Al	Dy	0.12	1.241			515	1393		0.370			16.9	2.30	16.9	1	1	0.3	0	16.9					[44]
Al	Er	0.09	1.241			435	1183		0.368			16.9	1.67	16.9	1	0.67	0	0	16.9					[44]
Al	Er	0.10	1.241			460	1193		0.386			16.9	1.88	16.9	1	0.88	0	0	16.9					[44]
Al	Er	0.115	1.241			505	1233		0.410			16.9	2.19	16.9	1	1	0.19	0	16.9					[44]
Al	Gd	0.08	1.248			470	1133		0.415			17.0	1.48	17.0	1	0.48	0	0	17					[44]
Al	Gd	0.10	1.248			505	1223		0.413			17.0	1.89	17.0	1	0.89	0	0	17					[44]
Al	Gd	0.12	1.248			510	1273		0.401			17.0	2.32	17.0	1	1	0.32	0	17					[44]
Al	Ho	0.09	1.255			445	1192		0.373			17.1	1.69	17.1	1	0.69	0	0	17.1					[44]
Al	Ho	0.10	1.255			495	1223		0.405			17.1	1.90	17.1	1	0.90	0	0	17.1					[44]
Al	Ho	0.11	1.255			530	1253		0.423			17.1	2.12	17.1	1	1	0.12	0	17.1					[44]

Al	La	0.07	1.326			442	1153		0.383			18.2	1.37	18.2	1	0.37	0	0	18.2						[45, 44]
Al	La	0.08	1.326			472	1188		0.397			18.2	1.59	18.2	1	0.59	0	0	18.2						[44]
Al	La	0.09	1.326			480	1233		0.389			18.2	1.80	18.2	1	0.8	0	0	18.2						[44]
Al	La	0.10	1.326			477	1273		0.375			18.2	2.03	18.2	1	1	0.03	0	18.2						[46, 44]
Al	La	0.14	1.326			540	1418		0.381			18.2	2.97	18.2	1	1	0.97	0	18.2						[45]
Al	Nd	0.08	1.291			450	913		0.493			17.7	1.54	17.7	1	0.54	0	0	17.7						[47, 44]
Al	Nd	0.10	1.291			500	1223		0.409			17.7	1.96	17.7	1	0.96	0	0	17.7						[47, 44]
Al	Nd	0.12	1.291			511	1373		0.372			17.7	2.41	17.7	1	1	0.41	0	17.7						[47, 44]
Al	Pr	0.10	1.298									17.8	1.98	17.8	1	0.98	0	0	17.8						[44]
Al	Sm	0.08	1.312			455	1133		0.402			18.0	1.57	18.0	1	0.57	0	0	18.0						[44, 48]
Al	Sm	0.10	1.312			493	1200		0.411			18.0	2.00	18.0	1	1	0	0	18.0						[44]
Al	Sm	0.12	1.312			505	1253		0.403			18.0	2.46	18.0	1	1	0.46	0	18.0						[44]
Al	Sm	0.14	1.312			509	1313		0.388			18.0	2.93	18.0	1	1	0.93	0	18.0						[44]
Al	Sm	0.16	1.312			502	1513		0.332			18.0	3.43	18.0	1	1	1.43	0	180.						[44]
Al	Tb	0.09	1.248			468	1203		0.389			17.0	1.68	17.0	1	0.68	0	0	17.0						[44]
Al	Tb	0.10	1.248			502	1243		0.404			17.0	1.89	17.0	1	0.89	0	0	17.0						[44]
Al	Tb	0.11	1.248			535	1273		0.420			17.0	2.10	17.0	1	1	0.10	0	17.0						[44]
Al	Tb	0.12	1.248			505	1293		0.391			17.0	2.32	17.0	1	1	0.32	0	17.0						[44]
Al	Y	0.09	1.270			437	1153		0.379			17.3	1.71	17.3	1	0.71	0	0	17.3						[42]
Al	Y	0.10	1.270			496	1174		0.422			17.3	1.93	17.3	1	0.93	0	0	17.3	1.1	14.1	1.6	10.7		[42, 34]
Al	Y	0.11	1.270			502	1213		0.414			17.3	2.14	17.3	1	1	0.14	0	17.3						[42]
Al	Y	0.12	1.270			526	1243		0.423			17.3	2.36	17.3	1	1	0.36	0	17.3						[42]
Al	Y	0.130	1.270			518	1283		0.404			17.3	2.59	17.3	1	1	0.59	0	17.3						[42]
Al	Yb	0.09	1.348			450	1133		0.397			18.6	1.84	18.6	1	0.84	0	0	18.6						[44]
Al	Yb	0.10	1.348			455	1153		0.395			18.6	2.07	18.6	1	1	0.07	0	18.6						[44]
Al	Yb	0.115	1.348			480	1198		0.401			18.6	2.42	18.6	1	1	0.42	0	18.6						[44]
Au	Si	0.17	0.769									9.66	1.98	9.66	1	0.98	0	0	9.66						[49]
Au	Si	0.186	0.769			280	623		0.449			9.66	2.21	9.66	1	1	0.21	0	9.66						[50]
Au	Si	0.20	0.769									9.66	2.42	9.66	1	1	0.42	0	9.66						[49]
Au	Si	0.25	0.769									9.66	3.22	9.66	1	1	1.22	0	9.66						[51]
Ba	Al	0.28	0.632									8.17	3.18	8.17	1	1	1.18	0	8.17						[52]
Ba	Ga	0.240	0.601									7.84	2.48	7.84	1	1	0.48	0	7.84						[52]

Ba	Mg	0.35	0.717									9.24	4.63	8.61	1	1	2	0.63	8.61					[52]
Ba	Zn	0.250	0.628									8.12	2.71	8.12	1	1	0.71	0	8.12					[52]
Ca	Ag	0.125	0.716									9.07	1.30	9.07	1	0.30	0	0	9.07					[53]
Ca	Ag	0.35	0.716		447	437	868	0.515	0.503		0.332	9.23	4.63	8.60	1	1	2	0.63	8.60					[54, 53]
Ca	Ag	0.425	0.716									9.51	5.74	7.77	1	1	2	1.74	7.77					[53]
Ca	Al	0.125	0.701									8.91	1.27	8.91	1	0.27	0	0	8.91					[53]
Ca	Al	0.336	0.701		528	540	873	0.605	0.619	12	0.385	9.00	4.37	8.63	1	1	2	0.37	8.63					[55]
Ca	Al	0.35	0.701		563	585	818	0.688	0.715	22	0.424	9.05	4.57	8.49	1	1	2	0.57	8.49					[52, 53]
Ca	Al	0.40	0.701	1.96								9.25	5.30	7.95	1	1	2	1.30	7.95					[56]
Ca	Al	0.475	0.701									9.55	6.44	7.11	1	1	2	2.44	7.11					[53]
Ca	Au	0.35	0.711		567		1116	0.508				9.17	4.61	8.56	1	1	2	0.61	8.56					[54]
Ca	Cu	0.125	0.627									8.11	1.16	8.11	1	0.16	0	0	8.11					[53]
Ca	Cu	0.30	0.627	1.81								8.11	3.48	8.11	1	1	1.48	0	8.11					[57]
Ca	Cu	0.35	0.627		438	441	1033	0.424	0.427	3	0.300	8.19	4.27	7.92	1	1	2	0.27	7.92					[54, 53]
Ca	Cu	0.50	0.627									8.87	6.44	6.44	1	1	2	2.44	6.44					[53]
Ca	Cu	0.625	0.627									9.55	8.47	5.08	1	1	2	4.47	5.08					[53]
Ca	Ga	0.16	0.667									8.53	1.62	8.53	1	0.62	0	0	8.53					[52]
Ca	Ga	0.35	0.667		562		991	0.567				8.65	4.43	8.22	1	1	2	0.43	8.22					[54]
Ca	Mg	0.225	0.796									9.97	2.89	9.97	1	1	0.89	0	9.97					[53]
Ca	Mg	0.27	0.796									9.97	3.69	9.97	1	1	1.69	0	9.97					[52]
Ca	Mg	0.30	0.796	1.45								10.0	4.20	9.80	1	1	2	0.2	9.80					[57]
Ca	Mg	0.35	0.796		411	414	987	0.417	0.419	3	0.296	10.2	4.95	9.19	1	1	2	0.95	9.19					[54, 53]
Ca	Mg	0.40	0.796	1.47								10.3	5.72	8.57	1	1	2	1.72	8.57					[56]
Ca	Mg	0.425	0.796									10.4	6.11	8.26	1	1	2	2.11	8.26					[53]
Ca	Pd	0.35	0.706									9.11	4.59	8.52	1	1	2	0.59	8.52					[54]
Ca	Zn	0.175	0.697									8.85	1.88	8.85	1	0.88	0	0	8.85					[53]
Ca	Zn	0.27	0.697									8.85	3.27	8.85	1	1	1.27	0	8.85					[52]
Ca	Zn	0.35	0.697		389	407	687	0.566	0.592	18	0.378	9.00	4.55	8.45	1	1	2	0.55	8.45					[53]
Ca	Zn	0.50	0.697									9.60	6.80	6.80	1	1	2	2.80	6.80					[53]
Ce	Au	0.20	0.786									9.85	2.46	9.85	1	1	0.46	0	9.85					[58]
Co	B	0.11	0.704									8.94	1.10	8.94	1	0.10	0	0	8.94					[59]
Co	B	0.12	0.704									8.94	1.22	8.94	1	0.22	0	0	8.94					[59]

Co	B	0.16	0.704	8.225							8.94	1.70	8.94	1	0.70	0	0	8.94					[59, 60]
Co	B	0.170	0.704	8.34							8.94	1.83	8.94	1	0.83	0	0	8.94					[61]
Co	B	0.18	0.704			656	1403		0.468		8.94	1.96	8.94	1	0.96	0	0	8.94					[62]
Co	B	0.18	0.704	8.205		603	1403		0.430		8.94	1.96	8.94	1	0.96	0	0	8.94					[63, 60]
Co	B	0.185	0.704	8.29		603	1383		0.436		8.94	2.03	8.94	1	1	0.03	0	8.94					[64]
Co	B	0.20	0.704			659	1393		0.473		8.94	2.23	8.94	1	1	0.23	0	8.94					[62]
Co	B	0.20	0.704	8.11							8.94	2.23	8.94	1	1	0.23	0	8.94					[64]
Co	B	0.20	0.704	8.185							8.94	2.23	8.94	1	1	0.23	0	8.94					[59, 60]
Co	B	0.22	0.704			660	1433		0.461		8.94	2.52	8.94	1	1	0.52	0	8.94					[62]
Co	B	0.22	0.704	8.12		638	1433		0.445		8.94	2.52	8.94	1	1	0.52	0	8.94					[63, 60]
Co	B	0.23	0.704	8.16							8.94	2.67	8.94	1	1	0.67	0	8.94					[61]
Co	B	0.24	0.704			660	1468		0.450		8.94	2.82	8.94	1	1	0.82	0	8.94					[62]
Co	B	0.24	0.704	8.055							8.94	2.82	8.94	1	1	0.82	0	8.94					[59, 60]
Co	B	0.25	0.704	8.02							8.94	2.98	8.94	1	1	0.98	0	8.94					[64]
Co	B	0.26	0.704			671	1503		0.446		8.94	3.14	8.94	1	1	1.14	0	8.94					[62]
Co	B	0.26	0.704			690	1503		0.459		8.94	3.14	8.94	1	1	1.14	0	8.94					[63]
Co	B	0.28	0.704			696	1538		0.453		8.94	3.47	8.94	1	1	1.47	0	8.94					[62]
Co	B	0.28	0.704	7.93							8.94	3.47	8.94	1	1	1.47	0	8.94					[59, 60]
Co	B	0.30	0.704	7.73							8.94	3.83	8.94	1	1	1.83	0	8.94					[64]
Co	B	0.30	0.704	7.86							8.94	3.83	8.94	1	1	1.83	0	8.94					[63, 60]
Co	B	0.31	0.704	7.815							8.94	4.01	8.93	1	1	2	0.01	8.93					[60]
Co	B	0.32	0.704								8.97	4.15	8.82	1	1	2	0.15	8.82					[59]
Co	B	0.33	0.704								9.01	4.29	8.72	1	1	2	0.29	8.72					[59]
Co	B	0.34	0.704								9.05	4.44	8.61	1	1	2	0.44	8.61					[65]
Co	B	0.35	0.704	7.59							9.08	4.58	8.50	1	1	2	0.58	8.50					[64]
Co	B	0.36	0.704			704	1523		0.462		9.12	4.72	8.40	1	1	2	0.72	8.40					[66, 63]
Co	B	0.38	0.704			725	1573		0.461		9.20	5.01	8.18	1	1	2	1.01	8.18					[66, 63]
Co	B	0.400	0.704	7.44		647	1623		0.399		9.27	5.31	7.96	1	1	2	1.31	7.96					[66, 63, 64]
Co	P	0.19	0.816	7.97							10.2	2.39	10.2	1	1	0.39	0	10.2					[67, 68]
Co	P	0.20	0.816								10.2	2.55	10.2	1	1	0.55	0	10.2	0	8.9	2.23	10.1	[39]
Co	P	0.203	0.816	7.94							10.2	2.60	10.2	1	1	0.60	0	10.2					[67]
Co	P	0.22	0.816	7.89							10.2	2.88	10.2	1	1	0.88	0	10.2					[67]

Co	P	0.236	0.816	7.9								10.2	3.15	10.2	1	1	1.15	0	10.2						[67]
Co	Ti	0.21	1.136									15.3	4.05	15.2	1	1	2	0.05	15.2						[69]
Co	Ti	0.22	1.136			777	1463		0.531			15.3	4.24	15.0	1	1	2	0.24	15.0						[69]
Co	Ti	0.23	1.136									15.2	4.42	14.8	1	1	2	0.42	14.8						[69]
Co	Zr	0.09	1.264			779	1543		0.505			17.3	1.71	17.3	1	0.71	0	0	17.2						[70]
Co	Zr	0.10	1.264			776	1505		0.516			17.3	1.92	17.3	1	0.92	0	0	17.2						[70]
Co	Zr	0.10	1.264			833	1505		0.553			17.3	1.92	17.3	1	0.92	0	0	17.2						[71, 72]
Co	Zr	0.10	1.264			804	1505		0.534			17.3	1.92	17.3	1	0.92	0	0	17.2						[73]
Co	Zr	0.10	1.264			764	1505		0.508			17.3	1.92	17.3	1	0.92	0	0	17.2						[74]
Co	Zr	0.11	1.264			768	1506		0.510			17.3	2.13	17.3	1	1	0.13	0	17.2						[70]
Co	Zr	0.12	1.264									17.3	2.35	17.3	1	1	0.35	0	17.2						[72]
Co	Zr	0.40	1.264									16.0	8.01	12.0	1	1	2	4.01	12.0						[75]
Cu	Hf	0.30	1.254									16.5	6.14	14.3	1	1	2	2.14	14.3						[76]
Cu	Hf	0.35	1.254		781	832	1259	0.621	0.661	51	0.408	16.2	7.07	13.1	1	1	2	3.07	13.1						[77]
Cu	Hf	0.40	1.254		773	827	1290	0.599	0.641	54	0.401	15.9	7.98	12.0	1	1	2	3.98	12.0						[78, 76]
Cu	Te	0.42	1.111									14.5	7.76	10.7	1	1	2	3.76	10.7						[79]
Cu	Ti	0.25	1.127									15.1	4.76	14.3	1	1	2	0.76	14.3						[80]
Cu	Ti	0.27	1.127									15.0	5.13	13.9	1	1	2	1.13	13.9						[80, 81]
Cu	Ti	0.30	1.127			692	1143		0.605			14.9	5.68	13.3	1	1	2	1.68	13.2						[80, 82, 83, 81]
Cu	Ti	0.340	1.127			697	1173		0.594			14.8	6.40	12.4	1	1	2	2.40	12.4						[83]
Cu	Ti	0.350	1.127									14.8	6.58	12.2	1	1	2	2.58	12.2						[82]
Cu	Ti	0.40	1.127	6.69								14.7	7.47	11.2	1	1	2	3.47	11.2						[80, 84, 81]
Cu	Ti	0.42	1.127			701	1228		0.571			14.6	7.82	10.8	1	1	2	3.82	10.8						[83]
Cu	Ti	0.43	1.127									14.6	8.00	10.6	1	1	2	4	10.6						[85]
Cu	Ti	0.45	1.127									14.6	8.35	10.2	1	1	2	4.35	10.2						[80]
Cu	Y	0.167	1.421									19.8	3.97	19.8	1	1	1.97	0	19.8	0	14	2.8	10.4		[39, 86]
Cu	Zr	0.10	1.254			880	1263		0.697			17.1	1.90	17.1	1	0.90	0	0	17.1						[87]
Cu	Zr	0.12	1.254			885	1285		0.688			17.1	2.33	17.1	1	1	0.33	0	17.1						[87]
Cu	Zr	0.25	1.254									16.8	5.19	15.6	1	1	2	1.19	15.6						[82]
Cu	Zr	0.28	1.254		780	804	1358	0.574	0.592	24	0.376	16.6	5.76	14.8	1	1	2	1.76	14.8						[88]
Cu	Zr	0.30	1.254			788	1333		0.591			16.5	6.14	14.3	1	1	2	2.14	14.3						[87, 76]
Cu	Zr	0.34	1.254		762	785	1263	0.603	0.622	23	0.388	16.3	6.89	13.4	1	1	2	2.89	13.4						[89, 90]

Cu	Zr	0.35	1.254		781	798	1248	0.626	0.639	17	0.393	16.2	7.07	13.1	1	1	2	3.07	13.1					[87, 91]
Cu	Zr	0.35	1.254		745	792	1279	0.582	0.619	47	0.391	16.2	7.07	13.1	1	1	2	3.07	13.1					[88]
Cu	Zr	0.355	1.254		747	769	1243	0.601	0.618	22	0.386	16.2	7.16	13.0	1	1	2	3.16	13.0					[92]
Cu	Zr	0.36	1.254	7.54	787	833	1233	0.638	0.676	46	0.412	16.2	7.25	12.9	1	1	2	3.25	12.9					[84, 90]
Cu	Zr	0.36	1.254	7.62								16.2	7.25	12.9	1	1	2	3.25	12.9					[11]
Cu	Zr	0.38	1.254		728	793	1158	0.629	0.685	65	0.421	16.0	7.62	12.4	1	1	2	3.62	12.4					[87]
Cu	Zr	0.382	1.254		767	823	1158	0.662	0.711	56	0.428	16.0	7.65	12.4	1	1	2	3.65	12.4					[90]
Cu	Zr	0.40	1.254		740	760	1198	0.618	0.634	20	0.392	15.9	7.98	12.0	1	1	2	3.98	12.0					[93, 50, 76]
Cu	Zr	0.40	1.254		714	764	1198	0.596	0.638	50	0.400	15.9	7.98	12.0	1	1	2	3.98	12.0					[88]
Cu	Zr	0.40	1.254		763	812	1198	0.637	0.677	49	0.414	15.9	7.98	12.0	1	1	2	3.98	12.0					[91]
Cu	Zr	0.40	1.254		733	791	1198	0.612	0.660	58	0.410	15.9	7.98	12.0	1	1	2	3.98	12.0					[78]
Cu	Zr	0.40	1.254		755	811	1198	0.630	0.677	56	0.415	15.9	7.98	12.0	1	1	2	3.98	12.0					[90]
Dy	Al	0.40	0.806									10.4	5.76	8.64	1	1	2	1.76	8.64					[94]
Dy	Al	0.45	0.806									10.5	6.54	8.00	1	1	2	2.54	8.00					[94]
Dy	Al	0.50	0.806									10.7	7.34	7.34	1	1	2	3.34	7.34					[94]
Dy	Al	0.55	0.806									10.8	8.16	6.68	1	1	2	4.16	6.68					[94]
Dy	Au	0.20	0.817									10.2	2.55	10.2	1	1	0.55	0	10.2					[58]
Dy	Cu	0.30	0.720			540	1063		0.508			9.11	3.90	9.11	1	1	1.90	0	9.11					[87]
Dy	Ni	0.30	0.720									9.11	3.90	9.11	1	1	1.90	0	9.11	1.29	7.16	3.07	10.4	[95]
Dy	Ni	0.30	0.720									9.11	3.90	9.11	1	1	1.90	0	9.11	3	10.8	4.63	12.4	[95]
Dy	Ni	0.56	0.720									10.1	7.89	6.20	1	1	2	3.89	6.20	3.1	5.2	6.62	6.9	[95]
Er	Au	0.20	0.817									10.21	2.55	10.2	1	1	0.55	0	10.2					[58]
Er	Cu	0.30	0.720			566	1153		0.491			9.11	3.90	9.11	1	1	1.90	0	9.11					[87]
Er	Fe	0.32	0.714									9.10	4.19	8.90	1	1	2	0.19	8.90					[86]
Eu	Au	0.20	0.730									9.22	2.30	9.22	1	1	0.30	0	9.22					[58]
Fe	B	0.09	0.704									8.94	0.88	8.94	0.88	0	0	0	8.94					[96]
Fe	B	0.11	0.704									8.94	1.10	8.94	1	0.10	0	0	8.94					[96]
Fe	B	0.12	0.704	7.44		595	1573		0.378			8.94	1.22	8.94	1	0.22	0	0	8.94					[96]
Fe	B	0.12	0.704			560	1573		0.356			8.94	1.22	8.94	1	0.22	0	0	8.94					[97]
Fe	B	0.13	0.704			611	1548		0.395			8.94	1.34	8.94	1	0.34	0	0	8.94					[96]
Fe	B	0.13	0.704	7.51		770	1548		0.497			8.94	1.34	8.94	1	0.34	0	0	8.94					[63, 67]
Fe	B	0.13	0.704			585	1548		0.378			8.94	1.34	8.94	1	0.34	0	0	8.94					[97]

Fe	B	0.14	0.704			623	1523		0.409			8.94	1.45	8.94	1	0.45	0	0	8.94						[96]
Fe	B	0.14	0.704	7.5		770	1523		0.506			8.94	1.45	8.94	1	0.45	0	0	8.94						[67]
Fe	B	0.14	0.704			600	1523		0.394			8.94	1.45	8.94	1	0.45	0	0	8.94						[97]
Fe	B	0.15	0.704			641	1493		0.429			8.94	1.58	8.94	1	0.58	0	0	8.94						[96]
Fe	B	0.15	0.704			750	1493		0.502			8.94	1.58	8.94	1	0.58	0	0	8.94						[96, 67]
Fe	B	0.16	0.704			653	1478		0.442			8.94	1.70	8.94	1	0.70	0	0	8.94						[96]
Fe	B	0.16	0.704	7.51		740	1478		0.501			8.94	1.70	8.94	1	0.70	0	0	8.94						[96, 67]
Fe	B	0.16	0.704	7.38		643	1478		0.435			8.94	1.70	8.94	1	0.70	0	0	8.94						[97, 61]
Fe	B	0.17	0.704			666	1447		0.460			8.94	1.83	8.94	1	0.83	0	0	8.94						[96]
Fe	B	0.17	0.704	7.47		740	1447		0.511			8.94	1.83	8.94	1	0.83	0	0	8.94						[67]
Fe	B	0.17	0.704			710	1447		0.491			8.94	1.83	8.94	1	0.83	0	0	8.94						[50]
Fe	B	0.18	0.704			678	1468		0.462			8.94	1.96	8.94	1	0.96	0	0	8.94						[96]
Fe	B	0.18	0.704	7.48		738	1468		0.503			8.94	1.96	8.94	1	0.96	0	0	8.94						[63, 67]
Fe	B	0.18	0.704			657	1468		0.448			8.94	1.96	8.94	1	0.96	0	0	8.94						[97]
Fe	B	0.19	0.704			687	1493		0.460			8.94	2.10	8.94	1	1	0.10	0	8.94						[96]
Fe	B	0.19	0.704	7.5		740	1493		0.496			8.94	2.10	8.94	1	1	0.10	0	8.94						[67]
Fe	B	0.19	0.704			698	1493		0.468			8.94	2.10	8.94	1	1	0.10	0	8.94						[62]
Fe	B	0.20	0.704			694	1523		0.456			8.94	2.23	8.94	1	1	0.23	0	8.94	0	8.64	2.16	12.4		[96, 39]
Fe	B	0.20	0.704	7.4		700	1523		0.460			8.94	2.23	8.94	1	1	0.23	0	8.94						[98, 84, 99]
Fe	B	0.20	0.704	7.45		738	1523		0.485			8.94	2.23	8.94	1	1	0.23	0	8.94						[67]
Fe	B	0.20	0.704			650	1523		0.427			8.94	2.23	8.94	1	1	0.23	0	8.94						[97, 61]
Fe	B	0.21	0.704			701	1538		0.456			8.94	2.38	8.94	1	1	0.38	0	8.94						[96]
Fe	B	0.21	0.704	7.41		728	1538		0.473			8.94	2.38	8.94	1	1	0.38	0	8.94						[67]
Fe	B	0.21	0.704			703	1493		0.471			8.94	2.38	8.94	1	1	0.38	0	8.94						[62]
Fe	B	0.22	0.704	7.38		720	1558		0.462			8.94	2.52	8.94	1	1	0.52	0	8.94						[63, 67]
Fe	B	0.22	0.704			665	1558		0.427			8.94	2.52	8.94	1	1	0.52	0	8.94						[97]
Fe	B	0.23	0.704	7.34		730	1583		0.461			8.94	2.67	8.94	1	1	0.67	0	8.94						[67]
Fe	B	0.24	0.704	7.3		732	1593		0.460			8.94	2.82	8.94	1	1	0.82	0	8.94						[67]
Fe	B	0.24	0.704			677	1593		0.425			8.94	2.82	8.94	1	1	0.82	0	8.94						[97]
Fe	B	0.25	0.704	7.27								8.94	2.98	8.94	1	1	0.98	0	8.94						[99, 67]
Fe	B	0.25	0.704	7.22								8.94	2.98	8.94	1	1	0.98	0	8.94						[61]
Fe	B	0.26	0.704	7.215		734	1618		0.454			8.94	3.14	8.94	1	1	1.14	0	8.94						[67]

Fe	B	0.26	0.704			685	1618		0.423			8.94	3.14	8.94	1	1	1.14	0	8.94						97
Fe	B	0.27	0.704	7.18								8.94	3.30	8.94	1	1	1.30	0	8.94						67
Fe	B	0.28	0.704	7.09								8.94	3.47	8.94	1	1	1.47	0	8.94						97
Fe	C	0.155	0.616									7.99	1.47	7.99	1	0.47	0	0	7.99						14
Fe	Hf	0.09	1.264									17.3	1.71	17.3	1	0.71	0	0	17.2						14
Fe	P	0.145	0.816	7.285								10.2	1.73	10.2	1	0.73	0	0	10.2						60
Fe	P	0.145	0.816	7.25								10.2	1.73	10.2	1	0.73	0	0	10.2						67
Fe	P	0.15	0.816									10.2	1.80	10.2	1	0.80	0	0	10.2						100
Fe	P	0.16	0.816	7.27								10.2	1.94	10.2	1	0.94	0	0	10.2						60
Fe	P	0.16	0.816	7.2								10.2	1.94	10.2	1	0.94	0	0	10.2						67
Fe	P	0.170	0.816	7.26		640	1321		0.484			10.2	2.09	10.2	1	1	0.09	0	10.2						98, 60, 100
Fe	P	0.18	0.816	7.225								10.2	2.24	10.2	1	1	0.24	0	10.2						60, 100
Fe	P	0.182	0.816	7.14								10.2	2.27	10.2	1	1	0.27	0	10.2						67
Fe	P	0.19	0.816	7.175								10.2	2.39	10.2	1	1	0.39	0	10.2						60
Fe	P	0.20	0.816	7.118								10.2	2.55	10.2	1	1	0.55	0	10.2						60, 100
Fe	P	0.20	0.816	7.1								10.2	2.55	10.2	1	1	0.55	0	10.2						67
Fe	P	0.216	0.816	7.03								10.2	2.81	10.2	1	1	0.81	0	10.2						67
Fe	P	0.24	0.816									10.2	3.22	10.2	1	1	1.22	0	10.2						100
Fe	P	0.25	0.816									10.2	3.40	10.2	1	1	1.40	0	10.2	3.5	8.1	2.6	10.4		100
Fe	P	0.26	0.816									10.2	3.58	10.2	1	1	1.58	0	10.2						100
Fe	Sc	0.10	1.296									17.8	1.97	17.8	1	0.97	0	0	17.8						101
Fe	Si	0.25	0.880									11.0	3.65	11.0	1	1	1.65	0	11.0						99
Fe	Th	0.28	1.424			813	1523		0.534			18.7	6.34	16.3	1	1	2	2.34	16.3						102
Fe	Th	0.30	1.424			808	1458		0.554			18.5	6.74	15.7	1	1	2	2.74	15.7						103
Fe	Th	0.31	1.424			745	1383		0.539			18.4	6.93	15.4	1	1	2	2.93	15.4						102
Fe	Th	0.33	1.424			745	1383		0.539			18.2	7.32	14.9	1	1	2	3.32	14.9						103, 102
Fe	Zr	0.08	1.264									17.3	1.50	17.3	1	0.50	0	0	17.2						104
Fe	Zr	0.09	1.264			774	1653		0.468			17.3	1.71	17.3	1	0.71	0	0	17.2						105, 70
Fe	Zr	0.10	1.264			775	1610		0.481			17.3	1.92	17.3	1	0.92	0	0	17.2						104, 70
Fe	Zr	0.10	1.264			791	1610		0.491			17.3	1.92	17.3	1	0.92	0	0	17.2						73, 106, 74
Fe	Zr	0.11	1.264			770	1673		0.460			17.3	2.13	17.3	1	1	0.13	0	17.2						70
Fe	Zr	0.12	1.264									17.3	2.35	17.3	1	1	0.35	0	17.2						104

Gd	Ag	0.30	0.818								10.3	4.28	9.99	1	1	2	0.28	9.99				107, 108
Gd	Ag	0.46	0.818								10.7	6.76	7.94	1	1	2	2.76	7.94				107
Gd	Al	0.22	0.801			591	1173		0.504		10.0	2.83	10.0	1	1	0.83	0	10.0				107, 109, 108
Gd	Al	0.40	0.801								10.4	5.74	8.61	1	1	2	1.74	8.61				94
Gd	Al	0.45	0.801								10.5	6.52	7.97	1	1	2	2.52	7.97				94
Gd	Al	0.50	0.801								10.6	7.32	7.32	1	1	2	3.32	7.32				94
Gd	Al	0.55	0.801								10.8	8.14	6.66	1	1	2	4.14	6.66				94
Gd	Au	0.20	0.813								10.2	2.54	10.2	1	1	0.54	0	10.2				58, 107, 108
Gd	Au	0.25	0.813								10.2	3.39	10.2	1	1	1.39	0	10.2				110
Gd	C	0.20	0.438								6.22	1.55	6.22	1	0.55	0	0	6.22				108
Gd	Co	0.31	0.710			550	1033		0.532		9.01	4.03	8.98	1	1	2	0.03	8.98				109
Gd	Co	0.40	0.710								9.34	5.34	8.01	1	1	2	1.34	8.01				111
Gd	Co	0.45	0.710			590	1153		0.512		9.54	6.09	7.45	1	1	2	2.09	7.45				109, 111
Gd	Co	0.50	0.710			600	1273		0.471		9.74	6.87	6.87	1	1	2	2.87	6.87				109, 111
Gd	Co	0.55	0.710			575	1353		0.425		9.96	7.68	6.28	1	1	2	3.68	6.28				109
Gd	Cu	0.24	0.716			473	1073		0.441		9.07	2.86	9.07	1	1	0.86	0	9.07				109
Gd	Cu	0.30	0.716			470	948		0.496		9.07	3.89	9.07	1	1	1.89	0	9.07				107, 109, 108
Gd	Cu	0.34	0.716			473	1025		0.461		9.19	4.48	8.70	1	1	2	0.48	8.70				109
Gd	Cu	0.58	0.716								10.1	8.20	5.94	1	1	2	4.20	5.94				87
Gd	Fe	0.32	0.710								9.05	4.18	8.87	1	1	2	0.18	8.87				109
Gd	Fe	0.40	0.710			413	1223		0.338		9.34	5.34	8.01	1	1	2	1.34	8.01				109
Gd	Fe	0.50	0.710								9.74	6.87	6.87	1	1	2	2.87	6.87				109
Gd	Ga	0.21	0.761			558	1153		0.484		9.57	2.54	9.57	1	1	0.54	0	9.57				107, 109, 108
Gd	Ga	0.25	0.761								9.57	3.19	9.57	1	1	1.19	0	9.57				109
Gd	Mn	0.40	0.750			520	1153		0.451		9.79	5.51	8.27	1	1	2	1.51	8.27				109
Gd	Ni	0.31	0.716			553	953		0.580		9.08	4.05	9.02	1	1	2	0.05	9.02				109, 108
Gd	Ni	0.32	0.716								9.11	4.20	8.92	1	1	2	0.20	8.92				107
Gd	Ni	0.40	0.716			538	903		0.596		9.41	5.36	8.04	1	1	2	1.36	8.04				109
Gd	Pd	0.24	0.807			569	1058		0.538		10.1	3.19	10.1	1	1	1.19	0	10.1				107, 109, 108
Gd	Pt	0.17	0.790			628	1393		0.451		9.90	2.03	9.90	1	1	0.03	0	9.90				109
Gd	Rh	0.18	0.750			563	1218		0.462		9.44	2.07	9.44	1	1	0.07	0	9.44				107, 109, 108
Gd	Ru	0.15	0.761			573	1190		0.482		9.57	1.69	9.57	1	0.69	0	0	9.57				109

Gd	Ru	0.30	0.761			728	1288		0.565			9.59	4.08	9.51	1	1	2	0.08	9.51					[109]
Gd	Ru	0.40	0.761			765	1528		0.501			9.91	5.56	8.35	1	1	2	1.56	8.35					[109]
Hf	Au	0.30	0.905			1000	1793		0.558			12.1	4.84	11.3	1	1	2	0.84	11.3					[112]
Hf	Co	0.22	0.791			758	1833		0.414			9.91	2.80	9.91	1	1	0.80	0	9.91					[113]
Hf	Co	0.33	0.791									10.0	4.63	9.40	1	1	2	0.63	9.40					[114]
Hf	Co	0.40	0.791			823	1913		0.430			10.2	5.70	8.54	1	1	2	1.70	8.54					[113]
Hf	Cu	0.29	0.797									9.99	4.06	9.94	1	1	2	0.06	9.94					[76]
Hf	Cu	0.30	0.797			739	1333		0.554			10.0	4.21	9.82	1	1	2	0.21	9.82					[87, 76]
Hf	Cu	0.40	0.797									10.3	5.72	8.58	1	1	2	1.72	8.58					[76]
Hf	Cu	0.50	0.797									10.6	7.30	7.30	1	1	2	3.30	7.30					[76]
Hf	Cu	0.55	0.797		771	830	1295	0.595	0.641	59	0.402	10.8	8.12	6.65	1	1	2	4.12	6.65					[78]
Hf	Cu	0.56	0.797			831	1523		0.546			10.8	8.29	6.51	1	1	2	4.29	6.51					[87]
Hf	Cu	0.57	0.797									10.8	8.45	6.38	1	1	2	4.45	6.38					[85]
Hf	Ge	0.13	0.722									9.13	1.36	9.13	1	0.36	0	0	9.13					[115, 116]
Hf	Ge	0.15	0.722									9.13	1.61	9.13	1	0.61	0	0	9.13					[115, 116]
Hf	Ni	0.20	0.797			738	1533		0.481			9.98	2.50	9.98	1	1	0.50	0	9.98					[113]
Hf	Ni	0.25	0.797			753	1613		0.467			9.98	3.33	9.98	1	1	1.33	0	9.98					[113]
Hf	Ni	0.30	0.797									10.0	4.21	9.82	1	1	2	0.21	9.82					[76]
Hf	Ni	0.33	0.797									10.1	4.65	9.45	1	1	2	0.65	9.45					[114]
Hf	Ni	0.38	0.797			808	1753		0.461			10.3	5.41	8.83	1	1	2	1.41	8.83					[113]
Hf	Ni	0.40	0.797									10.3	5.72	8.58	1	1	2	1.72	8.58					[76]
Hf	Ni	0.50	0.797									10.6	7.30	7.30	1	1	2	3.30	7.30					[76]
Hf	Si	0.13	0.696									8.85	1.32	8.85	1	0.32	0	0	8.85					[115, 116]
Hf	Si	0.15	0.696									8.85	1.56	8.85	1	0.56	0	0	8.85					[115, 116]
Hf	Si	0.17	0.696									8.85	1.81	8.85	1	0.81	0	0	8.85					[115, 116]
Ho	Au	0.20	0.808									10.1	2.53	10.1	1	1	0.53	0	10.1					[58]
Ho	Co	0.43	0.706									9.41	5.75	7.66	1	1	2	1.75	7.66					[117]
La	Ag	0.25	0.770									9.67	3.22	9.67	1	1	1.22	0	9.67					[118]
La	Ag	0.26	0.770									9.67	3.40	9.67	1	1	1.40	0	9.67					[119]
La	Ag	0.30	0.770			363	913		0.398			9.69	4.11	9.59	1	1	2	0.11	9.59					[119]
La	Ag	0.40	0.770									10.0	5.60	8.40	1	1	2	1.60	8.40					[119]
La	Ag	0.56	0.770			363	1098		0.331			10.6	8.15	6.40	1	1	2	4.15	6.40					[119]

La	Al	0.13	0.754								9.49	1.42	9.49	1	0.42	0	0	9.49				45
La	Al	0.18	0.754								9.49	2.08	9.49	1	1	0.08	0	9.49				120
La	Al	0.20	0.754								9.49	2.37	9.49	1	1	0.37	0	9.49				120, 46
La	Al	0.22	0.754			500	848		0.590		9.49	2.68	9.49	1	1	0.68	0	9.49				120, 45
La	Al	0.25	0.754								9.49	3.16	9.49	1	1	1.16	0	9.49				120
La	Al	0.27	0.754								9.49	3.51	9.49	1	1	1.51	0	9.49				120
La	Al	0.30	0.754			520	955		0.545		9.50	4.05	9.45	1	1	2	0.05	9.45				120, 46
La	Al	0.32	0.754								9.56	4.34	9.22	1	1	2	0.34	9.22				120
La	Al	0.34	0.754			540	1023		0.528		9.63	4.63	9.00	1	1	2	0.63	9.00				120, 45
La	Al	0.36	0.754			560	1058		0.529		9.70	4.93	8.77	1	1	2	0.93	8.77				45
La	Al	0.40	0.754			580	1113		0.521		9.83	5.53	8.30	1	1	2	1.53	8.30				45, 46
La	Al	0.50	0.754			620	1413		0.439		10.2	7.09	7.09	1	1	2	3.09	7.09				45, 46
La	Al	0.55	0.754								10.4	7.90	6.47	1	1	2	3.90	6.47				45
La	Au	0.18	0.765								9.61	2.11	9.61	1	1	0.11	0	9.61				120, 121
La	Au	0.20	0.765								9.61	2.40	9.61	1	1	0.40	0	9.61				120, 121
La	Au	0.22	0.765								9.61	2.71	9.61	1	1	0.71	0	9.61				121
La	Au	0.24	0.765								9.61	3.03	9.61	1	1	1.03	0	9.61				120, 122, 121
La	Au	0.25	0.765								9.61	3.20	9.61	1	1	1.20	0	9.61				120
La	Au	0.26	0.765								9.61	3.38	9.61	1	1	1.38	0	9.61				121
La	Au	0.27	0.765								9.61	3.55	9.61	1	1	1.55	0	9.61				120
La	Cu	0.27	0.674								8.61	3.18	8.61	1	1	1.18	0	8.61				123
La	Cu	0.30	0.674			395	773		0.511		8.61	3.69	8.61	1	1	1.69	0	8.61				87, 46
La	Cu	0.37	0.674								8.81	4.74	8.07	1	1	2	0.74	8.07				123
La	Cu	0.375	0.674								8.83	4.81	8.02	1	1	2	0.81	8.02				123
La	Ga	0.16	0.717	6.07							9.07	1.73	9.07	1	0.73	0	0	9.07				124
La	Ga	0.18	0.717	6.24							9.07	1.99	9.07	1	0.99	0	0	9.07				124
La	Ga	0.20	0.717	6.25							9.07	2.27	9.07	1	1	0.27	0	9.07				124
La	Ga	0.22	0.717	6.28							9.07	2.56	9.07	1	1	0.56	0	9.07				124
La	Ga	0.24	0.717	6.22							9.07	2.87	9.07	1	1	0.87	0	9.07				124
La	Ga	0.26	0.717	6.28							9.07	3.19	9.07	1	1	1.19	0	9.07				124
La	Ga	0.28	0.717	6.42							9.07	3.53	9.07	1	1	1.53	0	9.07				124
La	Ge	0.17	0.610								7.93	1.62	7.93	1	0.62	0	0	7.93				120

La	Ge	0.20	0.610									7.93	1.98	7.93	1	0.98	0	0	7.93						120
La	Ge	0.22	0.610									7.93	2.24	7.93	1	1	0.24	0	7.93						120
La	Ni	0.20	0.674									8.61	2.15	8.61	1	1	0.15	0	8.61						45
La	Ni	0.30	0.674			465	1433		0.324			8.61	3.69	8.61	1	1	1.69	0	8.61						45
La	Ni	0.40	0.674			495	1033		0.479			8.93	5.17	7.76	1	1	2	1.17	7.76						87, 76
La	Ni	0.48	0.674			515	958		0.538			9.28	6.37	6.90	1	1	2	2.37	6.90						45
Mg	Cu	0.20	0.788			405	813		0.498			9.87	2.47	9.87	1	1	0.47	0	9.87						45, 123
Mg	Cu	0.30	0.788	3.11		420	833		0.504			9.90	4.17	9.73	1	1	2	0.17	9.73						123, 125, 126
Mg	Cu	0.40	0.788			473	823		0.575			10.2	5.68	8.52	1	1	2	1.68	8.52						123, 125
Mg	Ga	0.187	0.838									10.5	2.41	10.5	1	1	0.41	0	10.4						127
Mg	Ni	0.10	0.788									9.87	1.10	9.87	1	0.10	0	0	9.87						128
Mg	Ni	0.15	0.788									9.87	1.74	9.87	1	0.74	0	0	9.87						128
Mg	Ni	0.20	0.788			438	973		0.450			9.87	2.47	9.87	1	1	0.47	0	9.87						128, 123, 125
Mg	Y	0.15	1.119									15.0	2.65	15.0	1	1	0.65	0	15.0						129
Mg	Y	0.16	1.119									15.0	2.86	15.0	1	1	0.86	0	15.0						123
Mg	Zn	0.25	0.875									10.9	3.63	10.9	1	1	1.63	0	10.9						130, 53
Mg	Zn	0.281	0.875									10.9	4.19	10.7	1	1	2	0.19	10.7						131
Mg	Zn	0.292	0.875									10.9	4.36	10.6	1	1	2	0.36	10.6						131
Mg	Zn	0.30	0.875	2.92								11.0	4.49	10.5	1	1	2	0.49	10.5						130, 126
Mg	Zn	0.321	0.875									11.0	4.81	10.2	1	1	2	0.81	10.2						131
Mg	Zn	0.35	0.875		359	379	616	0.583	0.615	20	0.389	11.0	5.27	9.78	1	1	2	1.27	9.78						132, 130, 53
Mg	Zn	0.40	0.875									11.1	6.06	9.08	1	1	2	2.06	9.08						130
Mn	Si	0.23	0.833									10.4	3.11	10.4	1	1	1.11	0	10.4						14
Mn	Zr	0.100	1.197									16.2	1.80	16.2	1	0.80	0	0	16.2						133
Mo	Zr	0.40	1.137									14.8	7.51	11.3	1	1	2	3.51	11.3						134
Mo	Zr	0.45	1.137									14.6	8.39	10.3	1	1	2	4.39	10.3						134
Mo	Zr	0.466	1.137									14.6	8.67	9.93	1	1	2	4.67	9.93						134
Nb	Ir	0.45	0.951			1133	2373		0.477			12.8	7.58	9.26	1	1	2	3.58	9.26						135
Nb	Ir	0.50	0.951									12.9	8.44	8.44	1	1	2	4.44	8.44						135
Nb	Ni	0.40	0.881	8.86								12.0	6.40	9.60	1	1	2	2.40	9.60	3.8	8.2	5.5	9		122, 39, 86
Nb	Ni	0.50	0.881	8.91								12.2	8.10	8.10	1	1	2	4.10	8.10	5	7.4	7.4	7.5		39, 86
Nb	Rh	0.40	0.923									12.5	6.59	9.89	1	1	2	2.59	9.89						135

Nb	Rh	0.42	0.923									12.5	6.93	9.58	1	1	2	2.93	9.58						122
Nb	Rh	0.45	0.923			973	1773		0.549			12.6	7.45	9.10	1	1	2	3.45	9.10						135
Nb	Rh	0.515	0.923									12.6	8.57	8.07	1	1	2	4.57	8.07						135
Nb	Si	0.17	0.769									9.66	1.98	9.66	1	0.98	0	0	9.66						136
Nb	Si	0.18	0.769									9.66	2.12	9.66	1	1	0.12	0	9.66						136
Nb	Si	0.19	0.769									9.66	2.27	9.66	1	1	0.27	0	9.66						136
Nb	Si	0.20	0.769			953	2273		0.419			9.66	2.42	9.66	1	1	0.42	0	9.66						136
Nb	Si	0.21	0.769									9.66	2.57	9.66	1	1	0.57	0	9.66						136
Nb	Si	0.22	0.769									9.66	2.72	9.66	1	1	0.72	0	9.66						134
Nd	Au	0.20	0.786									9.85	2.46	9.85	1	1	0.46	0	9.85						58
Nd	Fe	0.49	0.687									9.46	6.60	6.86	1	1	2	2.60	6.86						137
Nd	Ni	0.30	0.692									8.81	3.77	8.81	1	1	1.77	0	8.81						123
Nd	Ni	0.40	0.692									9.14	5.26	7.89	1	1	2	1.26	7.89						123
Ni	B	0.18	0.698	8.36		533	1383		0.385			8.87	1.95	8.87	1	0.95	0	0	8.87						63, 61
Ni	B	0.19	0.698									8.87	2.08	8.87	1	1	0.08	0	8.87	0	9.3	2.18	10.8		39
Ni	B	0.20	0.698									8.87	2.22	8.87	1	1	0.22	0	8.87	0	5.8	1.45	10.8		39, 86
Ni	B	0.28	0.698									8.87	3.45	8.87	1	1	1.45	0	8.87						138
Ni	B	0.30	0.698			585	1393		0.420			8.87	3.80	8.87	1	1	1.80	0	8.87						63, 139
Ni	B	0.33	0.698									8.94	4.27	8.67	1	1	2	0.27	8.67	0.9	9	4.43	9.4		39, 86
Ni	B	0.34	0.698			658	1398		0.471			8.98	4.41	8.57	1	1	2	0.41	8.57						66, 63, 138, 139, 65
Ni	B	0.36	0.698			662	1393		0.475			9.06	4.70	8.36	1	1	2	0.70	8.36	1.1	8.7	4.9	9.2		66, 139, 39
Ni	B	0.38	0.698			659	1353		0.487			9.13	4.99	8.14	1	1	2	0.99	8.14						66, 63, 138
Ni	B	0.40	0.698			663	1291		0.514			9.21	5.28	7.93	1	1	2	1.28	7.93						66, 63
Ni	B	0.42	0.698			655	1304		0.502			9.29	5.58	7.71	1	1	2	1.58	7.71						66, 63, 138
Ni	Hf	0.11	1.254			728	1523		0.478			17.1	2.11	17.1	1	1	0.11	0	17.1						113
Ni	Hf	0.30	1.254									16.5	6.14	14.3	1	1	2	2.14	14.3						76
Ni	Hf	0.36	1.254			923	1493		0.618			16.2	7.25	12.9	1	1	2	3.25	12.9						113
Ni	Hf	0.40	1.254									15.9	7.98	12.0	1	1	2	3.98	12.0						76
Ni	Nb	0.37	1.135	8.95								14.8	6.97	11.9	1	1	2	2.97	11.9	5.6	10	5.9	6.6		39, 86
Ni	Nb	0.38	1.135		892	930	1473	0.606	0.631	38	0.393	14.8	7.15	11.7	1	1	2	3.15	11.7	5.5	9.3	5.7	6.1		39, 140
Ni	Nb	0.40	1.135			910	1484		0.613			14.8	7.50	11.3	1	1	2	3.50	11.3						50, 141
Ni	Nb	0.40	1.135			933	1473		0.633			14.8	7.50	11.3	1	1	2	3.50	11.3						142

Ni	Nb	0.44	1.135	8.92								14.7	8.21	10.5	1	1	2	4.21	10.4	6.5	8.4	6.6	5.5	39, 86
Ni	P	0.112	0.810	8.31								10.1	1.28	10.1	1	0.28	0	0	10.1					67
Ni	P	0.152	0.810	8.16								10.1	1.81	10.1	1	0.81	0	0	10.1					67
Ni	P	0.18	0.810									10.1	2.22	10.1	1	1	0.22	0	10.1					143, 144
Ni	P	0.185	0.810	8								10.1	2.30	10.1	1	1	0.30	0	10.1					67
Ni	P	0.19	0.810									10.1	2.37	10.1	1	1	0.37	0	10.1					144
Ni	P	0.20	0.810	7.9		635	1173		0.541			10.1	2.53	10.1	1	1	0.53	0	10.1	0	9.3	2.33	9.4	84, 145, 68, 39, 144
Ni	P	0.20	0.810			600	1173		0.512			10.1	2.53	10.1	1	1	0.53	0	10.1					50
Ni	P	0.21	0.810	7.94								10.1	2.69	10.1	1	1	0.69	0	10.1					67
Ni	P	0.222	0.810	7.8								10.1	2.89	10.1	1	1	0.89	0	10.1					67
Ni	P	0.24	0.810	7.8								10.1	3.20	10.1	1	1	1.20	0	10.1					67
Ni	P	0.263	0.810	7.73								10.1	3.61	10.1	1	1	1.61	0	10.1					67
Ni	Ta	0.10	1.151									15.5	1.72	15.5	1	0.72	0	0	15.5					146
Ni	Ta	0.20	1.151									15.5	3.88	15.5	1	1	1.88	0	15.5					146
Ni	Ta	0.30	1.151			928	1778		0.522			15.2	5.77	13.5	1	1	2	1.77	13.5					146
Ni	Ta	0.35	1.151									15.1	6.67	12.4	1	1	2	2.67	12.4					146
Ni	Ta	0.40	1.151			1023	1673		0.611			14.9	7.57	11.4	1	1	2	3.57	11.4					146
Ni	Ta	0.45	1.151									14.8	8.45	10.3	1	1	2	4.45	10.3	5.3	6.2	7.6	6.4	147
Ni	Ti	0.40	1.127									14.7	7.47	11.2	1	1	2	3.47	11.2					148
Ni	Zr	0.10	1.254			616	1518		0.406			17.1	1.90	17.1	1	0.90	0	0	17.1					70
Ni	Zr	0.10	1.254			736	1518		0.485			17.1	1.90	17.1	1	0.90	0	0	17.1					71
Ni	Zr	0.11	1.254			614	1493		0.411			17.1	2.11	17.1	1	1	0.11	0	17.1					70
Ni	Zr	0.30	1.254									16.5	6.14	14.3	1	1	2	2.14	14.3					75
Ni	Zr	0.32	1.254									16.4	6.52	13.9	1	1	2	2.52	13.8					45
Ni	Zr	0.33	1.254									16.3	6.70	13.6	1	1	2	2.70	13.6	6.6	10.8	5.3	6.4	39
Ni	Zr	0.34	1.254		859	876	1393	0.617	0.629	17	0.389	16.3	6.89	13.4	1	1	2	2.89	13.4					91
Ni	Zr	0.35	1.254		827	863	1353	0.611	0.638	36	0.396	16.2	7.07	13.1	1	1	2	3.07	13.1					149
Ni	Zr	0.35	1.254			850	1353		0.628			16.2	7.07	13.1	1	1	2	3.07	13.1					150
Ni	Zr	0.36	1.254		834	856	1343	0.621	0.637	22	0.393	16.2	7.25	12.9	1	1	2	3.25	12.9	5	8.89	5	6	39, 91
Ni	Zr	0.363	1.254									16.1	7.31	12.8	1	1	2	3.31	12.8	5.8	8.77	5	6	39, 86
Ni	Zr	0.37	1.254			839	1363		0.616			16.1	7.44	12.7	1	1	2	3.44	12.7					148, 71
Ni	Zr	0.39	1.254			808	1400		0.577			16.0	7.80	12.2	1	1	2	3.80	12.2					91

Ni	Zr	0.40	1.254			791	1418		0.558			15.9	7.98	12.0	1	1	2	3.98	12.0					71, 76
Ni	Zr	0.40	1.254			835	1418		0.589			15.9	7.98	12.0	1	1	2	3.98	12.0					150
Np	Co	0.14	0.714									9.05	1.47	9.05	1	0.47	0	0	9.05					151
Np	Fe	0.14	0.714									9.05	1.47	9.05	1	0.47	0	0	9.05					151
Np	Ga	0.30	0.766									9.64	4.09	9.55	1	1	2	0.09	9.55					151
Np	Ga	0.40	0.766									9.96	5.58	8.38	1	1	2	1.58	8.38					151
Pb	Au	0.25	0.822									10.3	3.42	10.3	1	1	1.42	0	10.3					49
Pd	As	0.16	0.810									10.1	1.93	10.1	1	0.93	0	0	10.1					123
Pd	As	0.17	0.810									10.1	2.07	10.1	1	1	0.07	0	10.1					123
Pd	As	0.18	0.810									10.1	2.22	10.1	1	1	0.22	0	10.1					123
Pd	As	0.190	0.810									10.1	2.38	10.1	1	1	0.38	0	10.1					123
Pd	As	0.20	0.810									10.1	2.53	10.1	1	1	0.53	0	10.1					123
Pd	Ge	0.18	0.803	11.06		603	1083		0.557			10.0	2.20	10.0	1	1	0.20	0	10.0					152
Pd	Ge	0.198	0.803	11.12		622	1083		0.574			10.0	2.48	10.0	1	1	0.48	0	10.0					152
Pd	Ge	0.20	0.803									10.0	2.51	10.0	1	1	0.51	0	10.0					82
Pd	Ge	0.21	0.803									10.0	2.67	10.0	1	1	0.67	0	10.0					153
Pd	Ge	0.22	0.803									10.0	2.83	10.0	1	1	0.83	0	10.0					68
Pd	Ge	0.221	0.803	11.07		603	1173		0.514			10.0	2.85	10.0	1	1	0.85	0	10.0					152
Pd	Ge	0.248	0.803	11.1		523	1333		0.392			10.0	3.31	10.0	1	1	1.31	0	10.0					152
Pd	Ge	0.30	0.803									10.1	4.23	9.86	1	1	2	0.23	9.86					82
Pd	P	0.17	0.718									9.09	1.86	9.09	1	0.86	0	0	9.09					123
Pd	P	0.19	0.718									9.09	2.13	9.09	1	1	0.13	0	9.09					154
Pd	Sb	0.20	1.092									14.6	3.66	14.6	1	1	1.66	0	14.6					82
Pd	Sb	0.30	1.092									14.5	5.55	12.9	1	1	2	1.55	12.9					82
Pd	Se	0.30	0.831									10.4	4.33	10.1	1	1	2	0.33	10.1					155
Pd	Se	0.33	0.831									10.5	4.78	9.71	1	1	2	0.78	9.71					155
Pd	Si	0.15	0.775			633	1213		0.522			9.72	1.72	9.72	1	0.72	0	0	9.72					156, 157
Pd	Si	0.16	0.775		635	640	1108	0.573	0.578	5	0.367	9.72	1.85	9.72	1	0.85	0	0	9.72					156, 68
Pd	Si	0.165	0.775		635	642	1105	0.575	0.581	7	0.369	9.72	1.92	9.72	1	0.92	0	0	9.72					158
Pd	Si	0.17	0.775		632	645	1092	0.579	0.591	13	0.374	9.72	1.99	9.72	1	0.99	0	0	9.72					50, 157
Pd	Si	0.18	0.775	10.25	648	658	1113	0.582	0.591	10	0.374	9.72	2.13	9.72	1	1	0.13	0	9.72					156, 159
Pd	Si	0.18	0.775		630	687	1088	0.579	0.631	57	0.400	9.72	2.13	9.72	1	1	0.13	0	9.72					158, 89 160

Pd	Si	0.18	0.775		642	661	1113	0.577	0.594	19	0.377	9.72	2.13	9.72	1	1	0.13	0	9.72					74
Pd	Si	0.19	0.775		634	695	1128	0.562	0.616	61	0.394	9.72	2.43	9.72	1	1	0.28	0	9.72					160
Pd	Si	0.20	0.775	10.3	655	667	1220	0.537	0.547	12	0.356	9.72	2.43	9.72	1	1	0.43	0	9.72	0	6.6	1.65	10.6	156, 84, 157, 82, 89, 39
Pd	Si	0.20	0.775		641	700	1228	0.522	0.570	59	0.375	9.72	2.43	9.72	1	1	0.43	0	9.72					93, 160
Pd	Si	0.21	0.775			640	1253		0.511			9.72	2.58	9.72	1	1	0.58	0	9.72					156, 153
Pd	Si	0.23	0.775			673	1349		0.499			9.72	2.90	9.72	1	1	0.90	0	9.72					157
Pd	Si	0.25	0.775									9.72	3.24	9.72	1	1	1.24	0	9.72					141
Pd	Si	0.30	0.775									9.75	4.12	9.62	1	1	2	0.12	9.62					82
Pr	Au	0.20	0.781									9.80	2.45	9.80	1	1	0.45	0	9.80					58
Pt	Ge	0.17	0.820									10.3	2.10	10.3	1	1	0.10	0	10.2					14
Pt	Ge	0.20	0.820									10.3	2.56	10.3	1	1	0.56	0	10.2	0	5.6	1.4	10.3	82, 39
Pt	Ge	0.30	0.820									10.3	4.29	10.0	1	1	2	0.29	10.0					82
Pt	P	0.20	0.734			483	861		0.561			9.26	2.32	9.26	1	1	0.32	0	9.26					50
Pt	P	0.25	0.734	15.8								9.26	3.09	9.26	1	1	1.09	0	9.26					161
Pt	Sb	0.20	1.115									15.0	3.75	15.0	1	1	1.75	0	15.0					82
Pt	Sb	0.30	1.115									14.8	5.63	13.1	1	1	2	1.63	13.1					82
Pt	Sb	0.34	1.115			480	905		0.530			14.7	6.35	12.3	1	1	2	2.35	12.3					50
Pt	Si	0.20	0.791									9.91	2.48	9.91	1	1	0.48	0	9.91					82
Pt	Si	0.23	0.791									9.91	2.96	9.91	1	1	0.96	0	9.91					14
Pt	Si	0.30	0.791									9.95	4.18	9.76	1	1	2	0.18	9.76					82
Pu	Co	0.20	0.714									9.05	2.26	9.05	1	1	0.26	0	9.05					151
Pu	Cu	0.14	0.720									9.11	1.48	9.11	1	0.48	0	0	9.11					151
Pu	Cu	0.20	0.720									9.11	2.28	9.11	1	1	0.28	0	9.11					151
Pu	Fe	0.15	0.714									9.05	1.60	9.05	1	0.60	0	0	9.05					151
Pu	Fe	0.20	0.714									9.05	2.26	9.05	1	1	0.26	0	9.05					151
Pu	Ni	0.12	0.720									9.11	1.24	9.11	1	0.24	0	0	9.11					151
Pu	Ni	0.30	0.720									9.11	3.90	9.11	1	1	1.90	0	9.11					151
Pu	Ru	0.20	0.766									9.62	2.41	9.62	1	1	0.41	0	9.62					151
Rh	Si	0.22	0.833									10.4	2.93	10.4	1	1	0.93	0	10.4					14
Sc	Fe	0.25	0.772									9.69	3.23	9.69	1	1	1.23	0	9.69					101
Sm	Au	0.20	0.773									9.70	2.43	9.70	1	1	0.43	0	9.70					58
Sn	Fe	0.45	0.806			390	1753		0.222			10.6	6.55	8.00	1	1	2	2.55	8.00					162

Sn	Fe	0.50	0.806			435	1778		0.245			10.7	7.35	7.35	1	1	2	3.35	7.35						162
Sr	Al	0.18	0.665		455		863	0.527				8.51	1.87	8.51	1	0.87	0	0	8.51						52
Sr	Al	0.30	0.665		530		953	0.556				8.51	3.65	8.51	1	1	1.65	0	8.51						52
Sr	Al	0.35	0.665		490		993	0.493				8.63	4.42	8.21	1	1	2	0.42	8.21						53
Sr	Ga	0.18	0.632		445		793	0.561				8.16	1.79	8.16	1	0.79	0	0	8.16						52
Sr	Mg	0.30	0.755		390		699	0.558				9.51	4.05	9.46	1	1	2	0.05	9.46						52
Sr	Mg	0.35	0.755		383		756	0.507				9.67	4.78	8.89	1	1	2	0.78	8.89						53
Sr	Zn	0.25	0.660		380		738	0.515				8.46	2.82	8.46	1	1	0.82	0	8.46						52
Ta	Ir	0.450	0.938			1283	2228		0.576			12.7	7.52	9.19	1	1	2	3.52	9.19						135
Ta	Ir	0.50	0.938									12.8	8.38	8.38	1	1	2	4.38	8.38						135
Ta	Ni	0.50	0.869									12.1	8.04	8.04	1	1	2	4.04	8.04	4.9	6	6	8.2		163
Ta	Rh	0.45	0.910			1118	2013		0.555			12.4	7.39	9.03	1	1	2	3.39	9.03						135
Tb	Au	0.20	0.813									10.2	2.54	10.2	1	1	0.54	0	10.2						58
Tb	Au	0.25	0.813									10.2	3.39	10.2	1	1	1.39	0	10.2						110
Tb	Cu	0.35	0.716									9.22	4.63	8.59	1	1	2	0.63	8.59						164
Tb	Fe	0.28	0.710									9.00	3.50	9.00	1	1	1.50	0	9.00						165
Te	Al	0.23	1.007									13.4	4.01	13.4	1	1	2	0.01	13.4						166
Te	Cu	0.32	0.900									12.1	5.15	10.9	1	1	2	1.15	10.9						79
Te	Ge	0.15	0.814									10.2	1.80	10.2	1	0.80	0	0	10.2						166
Te	Ge	0.20	0.814									10.2	2.54	10.2	1	1	0.54	0	10.2						166
Te	Tl	0.15	1.229									16.7	2.95	16.7	1	1	0.95	0	16.7						167
Te	Tl	0.20	1.229									16.7	4.13	16.5	1	1	2	0.13	16.5						167
Te	Tl	0.25	1.229									16.4	5.10	15.4	1	1	2	1.10	15.3						167
Te	Tl	0.27	1.229									16.3	5.48	14.8	1	1	2	1.48	14.8						167
Te	Tl	0.29	1.229									16.2	5.86	14.4	1	1	2	1.86	14.4						167
Te	Tl	0.30	1.229									16.2	6.05	14.1	1	1	2	2.05	14.1						167
Te	Tl	0.33	1.229									16.0	6.61	13.4	1	1	2	2.61	13.4						167
Te	Tl	0.36	1.229									15.9	7.16	12.7	1	1	2	3.16	12.7						167
Te	Tl	0.38	1.229									15.8	7.52	12.3	1	1	2	3.52	12.3						167
Te	Tl	0.40	1.229									15.7	7.88	11.8	1	1	2	3.88	11.8						167
Th	Fe	0.20	0.702			647	1553		0.417			8.92	2.23	8.92	1	1	0.23	0	8.92						103, 102
Th	Fe	0.25	0.702			645	1418		0.455			8.92	2.97	8.92	1	1	0.97	0	8.92						103

Th	Fe	0.30	0.702			638	1213		0.526			8.92	3.82	8.92	1	1	1.82	0	8.92					103, 102
Th	Fe	0.33	0.702			631	1205		0.524			8.99	4.29	8.70	1	1	2	0.29	8.70					103
Th	Fe	0.35	0.702			643	1198		0.537			9.06	4.57	8.49	1	1	2	0.57	8.49					103
Th	Fe	0.40	0.702			654	1173		0.558			9.25	5.30	7.95	1	1	2	1.30	7.95					103, 102
Th	Fe	0.45	0.702			691	1233		0.560			9.45	6.05	7.40	1	1	2	2.05	7.40					103, 102
Th	Fe	0.48	0.702			698	1173		0.595			9.58	6.52	7.06	1	1	2	2.52	7.06					103, 102
Th	Fe	0.50	0.702									9.66	6.83	6.83	1	1	2	2.83	6.83					102
Th	Fe	0.55	0.702			745	1383		0.539			9.88	7.64	6.25	1	1	2	3.64	6.25					102
Th	Fe	0.60	0.702			745	1383		0.539			10.1	8.47	5.64	1	1	2	4.47	5.64					103, 102
Ti	Be	0.375	0.789	3.83		668	1353		0.493			10.1	5.22	8.90	1	1	2	1.22	8.90					75, 168
Ti	Be	0.38	0.789	3.8								10.1	5.30	8.84	1	1	2	1.30	8.84	2.9	6.9	3.6	8	169
Ti	Be	0.38	0.789									10.2	5.38	8.77	1	1	2	1.38	8.77					168
Ti	Be	0.39	0.789									10.2	5.53	8.65	1	1	2	1.53	8.65					168
Ti	Be	0.40	0.789	3.77		669	1401		0.478			10.2	5.68	8.53	1	1	2	1.68	8.53					75, 168, 170
Ti	Be	0.41	0.789	3.72		670	1411		0.475			10.2	5.84	8.40	1	1	2	1.84	8.40					75, 170
Ti	Be	0.42	0.789									10.3	5.99	8.28	1	1	2	1.99	8.28					170
Ti	Be	0.43	0.789									10.3	6.15	8.15	1	1	2	2.15	8.15					170
Ti	Cu	0.30	0.887									11.1	4.53	10.6	1	1	2	0.53	10.6					81
Ti	Cu	0.35	0.887			639	1281		0.499			11.2	5.31	9.87	1	1	2	1.31	9.87					80, 83
Ti	Cu	0.39	0.887			657	1257		0.523			12.1	6.26	9.80	1	1	2	2.26	9.80					83
Ti	Cu	0.40	0.887									12.1	6.43	9.65	1	1	2	2.43	9.65					80, 81
Ti	Cu	0.43	0.887			680	1233		0.552			12.1	6.94	9.20	1	1	2	2.94	9.20					83
Ti	Cu	0.45	0.887									12.2	7.28	8.90	1	1	2	3.28	8.90					80
Ti	Cu	0.50	0.887	6.25		680	1257		0.541			12.3	8.14	8.14	1	1	2	4.14	8.14	4.5	6	6	6.4	80, 84, 171, 83, 39, 81
Ti	Ni	0.25	0.887									11.0	3.68	11.0	1	1	1.68	0	11.0					171
Ti	Ni	0.26	0.887									11.0	3.88	11.0	1	1	1.88	0	11.0					172
Ti	Ni	0.30	0.887			720	1247		0.577			11.1	4.53	10.6	1	1	2	0.53	10.6					80, 171, 173, 75
Ti	Ni	0.33	0.887			723	1256		0.576			11.2	5.00	10.2	1	1	2	1	10.1					148, 80, 172, 173
Ti	Ni	0.35	0.887			760	1328		0.572			11.2	5.31	9.87	1	1	2	1.31	9.87					171, 81
Ti	Ni	0.40	0.887			762	1472		0.518			12.1	6.43	9.65	1	1	2	2.43	9.65	2.3	7.9	5.27	8.1	80, 171, 173, 39
Ti	Ni	0.45	0.887									12.2	7.28	8.90	1	1	2	3.28	8.90					80, 75
Ti	Pt	0.33	0.979									13.1	5.63	11.4	1	1	2	1.63	11.4					81

Ti	Si	0.13	0.775			702	1620		0.433			9.72	1.45	9.72	1	0.45	0	0	9.72						174
Ti	Si	0.15	0.775			702	1677		0.419			9.72	1.72	9.72	1	0.72	0	0	9.72						115, 174
Ti	Si	0.16	0.775									9.72	1.85	9.72	1	0.85	0	0	9.72	0	9.4	1.79	11.5		39, 86
Ti	Si	0.20	0.775			867	1903		0.456			9.72	2.43	9.72	1	1	0.43	0	9.72						115, 171, 75, 168, 81
Tm	Au	0.20	0.817									10.2	2.55	10.2	1	1	0.55	0	10.2						58
U	Co	0.24	0.791									9.91	3.13	9.91	1	1	1.13	0	9.91						151
U	Co	0.27	0.791			554	1080		0.513			9.91	3.67	9.91	1	1	1.67	0	9.91						175
U	Co	0.40	0.791									10.2	5.70	8.54	1	1	2	1.70	8.54						151
U	Cr	0.20	0.823									10.3	2.57	10.3	1	1	0.57	0	10.3						151
U	Cr	0.27	0.823			684	1240		0.552			10.3	3.80	10.3	1	1	1.80	0	10.3						175
U	Cr	0.40	0.823									10.6	5.83	8.75	1	1	2	1.83	8.75						151
U	Fe	0.14	0.791									9.91	1.61	9.91	1	0.61	0	0	9.91						151
U	Fe	0.143	0.791									9.91	1.65	9.91	1	0.65	0	0	9.91						176
U	Fe	0.33	0.791			566	1006		0.562			10.0	4.63	9.40	1	1	2	0.63	9.40						175
U	Fe	0.40	0.791			560	1173		0.477			10.2	5.70	8.54	1	1	2	1.70	8.54						151, 175
U	Ir	0.30	0.861			670	1370		0.489			10.8	4.43	10.4	1	1	2	0.43	10.3						151
U	Mn	0.30	0.835			605	1115		0.542			10.5	4.34	10.1	1	1	2	0.34	10.1						175
U	Mn	0.353	0.835			593	1186		0.500			10.6	5.16	9.45	1	1	2	1.16	9.45						175
U	Ni	0.24	0.797									9.98	3.15	9.98	1	1	1.15	0	9.98						151
U	Ni	0.33	0.797			599	1013		0.591			10.1	4.65	9.45	1	1	2	0.65	9.45						175
U	Ni	0.40	0.797									10.3	5.72	8.58	1	1	2	1.72	8.58						151
U	Os	0.30	0.854			790	1273		0.621			10.7	4.41	10.3	1	1	2	0.41	10.3						151
U	Pd	0.30	0.899									12.0	4.81	11.2	1	1	2	0.81	11.2						151
U	Pd	0.40	0.899									12.2	6.48	9.72	1	1	2	2.48	9.72						151
U	V	0.20	0.848									10.6	2.64	10.6	1	1	0.64	0	10.6						151
U	V	0.40	0.848									10.9	5.94	8.91	1	1	2	1.94	8.91						151
Y	Cu	0.33	0.704			535	1043		0.513			9.01	4.29	8.72	1	1	2	0.29	8.72	2.9	8.4	4.14	10.7		87, 39
Y	Cu	0.400	0.704	6.06		517	1127		0.459			9.27	5.31	7.96	1	1	2	1.31	7.96						177, 178
Y	Cu	0.570	0.704			522	1108		0.471			9.99	7.97	6.01	1	1	2	3.97	6.01	2.9	8.4	11.1	10.7		87
Y	Ni	0.33	0.704									9.01	4.29	8.72	1	1	2	0.29	8.72	1.9	9.3	4.58	9.5		39, 86
Zn	Ca	0.375	1.436									17.9	8.20	13.7	1	1	2	4.20	13.7						53
Zr	Al	0.26	0.892									11.1	3.90	11.1	1	1	1.90	0	11.1						14

Zr	Au	0.30	0.905									12.1	4.84	11.3	1	1	2	0.84	11.3						179
Zr	Be	0.30	0.709	5.72	613	648	1393	0.440	0.465	35	0.323	8.99	3.85	8.99	1	1	1.85	0	8.99						75, 170
Zr	Be	0.30	0.709	5.72	600		1393	0.431				8.99	3.85	8.99	1	1	1.85	0	8.99						180
Zr	Be	0.33	0.709									9.05	4.24	8.81	1	1	2	0.24	8.81						181
Zr	Be	0.325	0.709	5.65	614		1238	0.496				9.14	4.60	8.54	1	1	2	0.60	8.54						180
Zr	Be	0.35	0.709	5.48	618	647	1238	0.499	0.523	29	0.349	9.14	4.60	8.54	1	1	2	0.60	8.54						75, 170
Zr	Be	0.40	0.709	5.46	623	673	1343	0.464	0.501	50	0.342	9.33	5.33	8.00	1	1	2	1.33	8.00						75, 170
Zr	Be	0.40	0.709	5.48	625		1393	0.449				9.33	5.33	8.00	1	1	2	1.33	8.00						180
Zr	Be	0.43	0.709									9.45	5.78	7.66	1	1	2	1.78	7.66	2	7.1	5.35	6.2		32
Zr	Be	0.45	0.709	5.18	646	681	1413	0.457	0.482	35	0.331	9.52	6.09	7.44	1	1	2	2.09	7.44						75, 170
Zr	Be	0.50	0.709	5.08	672	682	1473	0.456	0.463	10	0.318	9.73	6.87	6.87	1	1	2	2.87	6.87						75, 170
Zr	Co	0.20	0.791	6.8		580	1388		0.418			9.91	2.48	9.91	1	1	0.48	0	9.91						182, 183, 184
Zr	Co	0.22	0.791			643	1254		0.513			9.91	2.80	9.91	1	1	0.80	0	9.91						71, 91
Zr	Co	0.27	0.791									9.91	3.67	9.91	1	1	1.67	0	9.91						75
Zr	Co	0.30	0.791	7								9.95	4.18	9.76	1	1	2	0.18	9.76						184
Zr	Co	0.30	0.791	6.68		700	1394		0.502			9.95	4.18	9.76	1	1	2	0.18	9.76						71, 184, 185
Zr	Co	0.33	0.791	7.12								10.0	4.63	9.40	1	1	2	0.63	9.40						182, 184
Zr	Co	0.35	0.791	7.2								10.1	4.93	9.16	1	1	2	0.93	9.16						184
Zr	Co	0.36	0.791			740	1394		0.531			10.1	5.08	9.04	1	1	2	1.08	9.04						71
Zr	Co	0.40	0.791	7.35		767	1523		0.504			10.2	5.70	8.54	1	1	2	1.70	8.54						182, 184, 91
Zr	Co	0.45	0.791	7.4								10.4	6.48	7.91	1	1	2	2.48	7.91						184
Zr	Co	0.47	0.791	7.63								10.5	6.79	7.66	1	1	2	2.79	7.66						184
Zr	Co	0.50	0.791									10.6	7.27	7.27	1	1	2	3.27	7.27						148
Zr	Co	0.52	0.791	7.7								10.6	7.60	7.01	1	1	2	3.60	7.01						184
Zr	Co	0.53	0.791			785	1585		0.495			10.6	7.76	6.88	1	1	2	3.76	6.88						71
Zr	Cu	0.20	0.797									9.98	2.50	9.98	1	1	0.50	0	9.98						88
Zr	Cu	0.25	0.797		571	618	1363	0.419	0.454	47	0.320	9.98	3.33	9.98	1	1	1.33	0	9.98						87
Zr	Cu	0.28	0.797		600	666	1268	0.473	0.525	66	0.356	9.98	3.88	9.98	1	1	1.88	0	9.98						87
Zr	Cu	0.30	0.797									10.0	4.21	9.82	1	1	2	0.21	9.82						76
Zr	Cu	0.335	0.797		631	690	1273	0.496	0.542	59	0.362	10.1	4.73	9.39	1	1	2	0.73	9.39						88
Zr	Cu	0.40	0.797		677		1248	0.542				10.3	5.72	8.58	1	1	2	1.72	8.58						93, 82, 76
Zr	Cu	0.40	0.797		646	707	1248	0.518	0.567	61	0.373	10.3	5.72	8.58	1	1	2	1.72	8.58						88

Zr	Cu	0.40	0.797		654	718	1343	0.487	0.534	64	0.359	10.3	5.72	8.58	1	1	2	1.72	8.58					87
Zr	Cu	0.45	0.797		661	729	1203	0.549	0.606	68	0.391	10.5	6.51	7.95	1	1	2	2.51	7.95					87
Zr	Cu	0.45	0.797		669	719	1206	0.555	0.596	50	0.383	10.5	6.51	7.95	1	1	2	2.51	7.95					78
Zr	Cu	0.46	0.797		696	746	1201	0.580	0.621	50	0.393	10.5	6.66	7.82	1	1	2	2.66	7.82					141
Zr	Cu	0.48	0.797		689	749	1207	0.571	0.620	59	0.395	10.6	6.98	7.56	1	1	2	2.98	7.56					87
Zr	Cu	0.50	0.797	7.33	707	749	1208	0.585	0.620	42	0.391	10.6	7.30	7.30	1	1	2	3.30	7.30					84, 11, 89, 76, 91
Zr	Cu	0.50	0.797		680	730	1214	0.560	0.602	50	0.386	10.6	7.30	7.30	1	1	2	3.30	7.30					88 186
Zr	Cu	0.50	0.797		711	774	1214	0.586	0.638	63	0.402	10.6	7.30	7.30	1	1	2	3.30	7.30					87
Zr	Cu	0.55	0.797		698	748	1183	0.590	0.632	50	0.398	10.8	8.12	6.65	1	1	2	4.12	6.65					88
Zr	Cu	0.56	0.797		728	792	1163	0.626	0.681	64	0.419	10.8	8.29	6.51	1	1	2	4.29	6.51					93, 87
Zr	Cu	0.56	0.797	7.42								10.8	8.29	6.51	1	1	2	4.29	6.51					11
Zr	Cu	0.57	0.797									10.8	8.45	6.38	1	1	2	4.45	6.38	5.4	5	6.7	5.9	85, 187, 82
Zr	Fe	0.20	0.791									9.91	2.48	9.91	1	1	0.48	0	9.91					182
Zr	Fe	0.24	0.791									9.91	3.13	9.91	1	1	1.13	0	9.91					188, 105, 106
Zr	Fe	0.25	0.791									9.91	3.30	9.91	1	1	1.30	0	9.91					182, 75, 101
Zr	Fe	0.28	0.791									9.91	3.85	9.91	1	1	1.85	0	9.91					105
Zr	Fe	0.30	0.791	6.45								9.95	4.18	9.76	1	1	2	0.18	9.76					185
Zr	Fe	0.33	0.791			682	1553		0.439			10.0	4.63	9.40	1	1	2	0.63	9.40					91
Zr	Fe	0.35	0.791									10.1	4.93	9.16	1	1	2	0.93	9.16					106, 75
Zr	Fe	0.40	0.791									10.2	5.70	8.54	1	1	2	1.70	8.54					106
Zr	Ge	0.13	0.722									9.13	1.36	9.13	1	0.36	0	0	9.13					115
Zr	Ge	0.15	0.722									9.13	1.61	9.13	1	0.61	0	0	9.13					115
Zr	Ge	0.17	0.722									9.13	1.87	9.13	1	0.87	0	0	9.13					115
Zr	Mn	0.45	0.835									10.8	6.68	8.16	1	1	2	2.68	8.16					75
Zr	Mn	0.50	0.835									11.0	7.49	7.49	1	1	2	3.49	7.49					75
Zr	Mo	0.40	0.88									11.1	6.08	9.11	1	1	2	2.08	9.11					75
Zr	Mo	0.533	0.88									12.3	8.67	7.60	1	1	2	4.67	7.60					75
Zr	Ni	0.18	0.797									9.98	2.19	9.98	1	1	0.19	0	9.98					45
Zr	Ni	0.20	0.797			660	1423		0.464			9.98	2.50	9.98	1	1	0.50	0	9.98					182, 150, 82
Zr	Ni	0.22	0.797			611	1343		0.455			9.98	2.82	9.98	1	1	0.82	0	9.98					71
Zr	Ni	0.24	0.797			638	1233		0.517			9.98	3.15	9.98	1	1	1.15	0	9.98					71, 75
Zr	Ni	0.25	0.797									9.98	3.33	9.98	1	1	1.33	0	9.98					182

Zr	Ni	0.28	0.797		642	664	1313	0.489	0.506	22	0.340	9.98	3.88	9.98	1	1	1.88	0	9.98					91
Zr	Ni	0.30	0.797	6.71		660	1338		0.493			10.0	4.21	9.82	1	1	2	0.21	9.82					150, 185, 76
Zr	Ni	0.33	0.797									10.1	4.65	9.45	1	1	2	0.65	9.45					148, 182
Zr	Ni	0.333	0.797									10.1	4.70	9.41	1	1	2	0.70	9.41	1.3	8.4	4.2	11.6	189, 86
Zr	Ni	0.35	0.797									10.2	4.96	9.21	1	1	2	0.96	9.21	3.3	8.6	4.8	11	189
Zr	Ni	0.36	0.797			730	1293		0.565			10.2	5.11	9.08	1	1	2	1.11	9.08	2.3	7.9	3.9	9.1	71, 189
Zr	Ni	0.36	0.797									10.2	5.11	9.08	1	1	2	1.11	9.08	3.3	8.56	4.81	11	190
Zr	Ni	0.37	0.797		700	720	1313	0.533	0.548	20	0.358	10.2	5.26	8.96	1	1	2	1.26	8.96					91
Zr	Ni	0.40	0.797		713	735	1413	0.505	0.520	22	0.346	10.3	5.72	8.58	1	1	2	1.72	8.58					150, 82, 76, 91
Zr	Ni	0.50	0.797			795	1523		0.522			10.6	7.30	7.30	1	1	2	3.30	7.30	3.3	6.7	6.7	7.8	148, 150, 39, 76
Zr	Pd	0.20	0.899									11.2	2.79	11.2	1	1	0.79	0	11.2					82
Zr	Pd	0.25	0.899									11.2	3.73	11.2	1	1	1.73	0	11.2					75
Zr	Pd	0.30	0.899	7.53								12.0	4.81	11.2	1	1	2	0.81	11.2					179, 122, 185
Zr	Pd	0.30	0.899	7.71	680	690	1343	0.506	0.514	10	0.341	12.0	4.81	11.2	1	1	2	0.81	11.2	3.6	5.37	2.3	11.5	50, 35
Zr	Pd	0.33	0.899	7.9								12.1	5.31	10.8	1	1	2	1.31	10.8					148, 191
Zr	Pd	0.35	0.899	8.02								12.1	5.64	10.5	1	1	2	1.64	10.5					191, 82
Zr	Pd	0.45	0.899									12.3	7.33	8.96	1	1	2	3.33	8.96					75
Zr	Pt	0.20	0.880									11.0	2.74	11.0	1	1	0.74	0	10.9					179, 35
Zr	Rh	0.17	0.835									10.4	2.14	10.4	1	1	0.14	0	10.4					75
Zr	Rh	0.18	0.835									10.4	2.29	10.4	1	1	0.29	0	10.4					192
Zr	Rh	0.27	0.835									10.4	3.86	10.4	1	1	1.86	0	10.4					192
Zr	Rh	0.28	0.835									10.4	4.04	10.4	1	1	2	0.04	10.4					75
Zr	Si	0.12	0.696			804	1936		0.416			8.85	1.21	8.85	1	0.21	0	0	8.85					193
Zr	Si	0.13	0.696			772	1984		0.389			8.85	1.32	8.85	1	0.32	0	0	8.85					115, 193
Zr	Si	0.14	0.696			757	2019		0.375			8.85	1.44	8.85	1	0.44	0	0	8.85					193
Zr	Si	0.15	0.696	6.327		759	2047		0.371			8.85	1.56	8.85	1	0.56	0	0	8.85					115, 193, 194
Zr	Si	0.16	0.696			735	2081		0.353			8.85	1.69	8.85	1	0.69	0	0	8.85					193
Zr	Si	0.17	0.696			720	2095		0.344			8.85	1.81	8.85	1	0.81	0	0	8.85					193
Zr	Si	0.18	0.696			725	2130		0.340			8.85	1.94	8.85	1	0.94	0	0	8.85					115, 193
Zr	Si	0.19	0.696			724	2151		0.336			8.85	2.08	8.85	1	1	0.08	0	8.85					115, 193
Zr	Si	0.20	0.696			720	2172		0.332			8.85	2.21	8.85	1	1	0.21	0	8.85					115, 193
Zr	Si	0.22	0.696			737	2198		0.335			8.85	2.50	8.85	1	1	0.50	0	8.85					115, 193

Zr	Si	0.24	0.696			768	2297		0.334			8.85	2.79	8.85	1	1	0.79	0	8.85					193	

Table A2. Constitutions, thicknesses, characteristic temperatures and structural parameters of most stable glasses.

Ω	α	F_α	R	Thickness, mm	T_g, K	T_x, K	T_l, K	T_{rg}	T_x / T_l	ΔT_x, K	γ	$\hat{S}_\alpha$	$\overline{S}_\alpha$	$\overline{S}_\alpha$	$S(\alpha_\alpha)$	$S(\alpha_\beta)$	$S(\alpha_\gamma)$	$S(\alpha_\Omega)$	$\overline{S}_\alpha / \hat{S}_\Omega$	Citations
Ca	Al	0.336	0.701	1	528	540	873	0.605	0.619	12	0.385	9.00	4.37	8.63	1	1	2	0.37	0.04	55
Ca	Al	0.35	0.701		563	585	818	0.688	0.715	22	0.424	9.05	4.57	8.49	1	1	2	0.57	0.06	52, 53
Ca	Zn	0.35	0.697		389	407	687	0.566	0.592	18	0.378	9.00	4.55	8.45	1	1	2	0.55	0.06	53
Cu	Hf	0.35	1.254	2	781	832	1259	0.621	0.661	51	0.408	16.20	7.07	13.13	1	1	2	3.07	0.19	77
Cu	Hf	0.40	1.254	1	773	827	1290	0.599	0.641	54	0.401	15.94	7.98	11.96	1	1	2	3.98	0.25	78, 76
Cu	Zr	0.28	1.254		780	804	1358	0.574	0.592	24	0.376	16.58	5.76	14.82	1	1	2	1.76	0.11	88
Cu	Zr	0.34	1.254		762	785	1263	0.603	0.622	23	0.388	16.25	6.89	13.37	1	1	2	2.89	0.18	89, 90
Cu	Zr	0.35	1.254		763±18	795±3	1264±16	0.604±0.022	0.629±0.010	32±15	0.392±0.001	16.20	7.07	13.13	1	1	2	3.07	0.19	88, 87, 91
Cu	Zr	0.355	1.254	2	747	769	1243	0.601	0.618	22	0.386	16.17	7.16	13.01	1	1	2	3.16	0.2	92
Cu	Zr	0.36	1.254	1.6±0.4	787	833	1233	0.638	0.676	46	0.412	16.15	7.25	12.89	1	1	2	3.25	0.2	84, 11, 90
Cu	Zr	0.38	1.254		728	793	1158	0.629	0.685	65	0.421	16.04	7.62	12.43	1	1	2	3.62	0.23	87
Cu	Zr	0.382	1.254		767	823	1158	0.662	0.711	56	0.428	16.03	7.65	12.38	1	1	2	3.65	0.23	90
Cu	Zr	0.40	1.254	1	739±25	786±26	1198	0.616±0.220	0.656±0.022	39±19	0.404±0.012	15.94	7.98	11.96	1	1	2	3.98	0.25	93, 88, 50, 78, 90, 76, 91 195
Hf	Cu	0.55	0.797	1.5	771	830	1295	0.595	0.641	59	0.402	10.77	8.12	6.65	1	1	2	4.12	0.38	78
Mg	Zn	0.35	0.875		359	379	616	0.583	0.615	20	0.389	11.04	5.27	9.78	1	1	2	1.27	0.11	132, 130, 53
Ni	Nb	0.38	1.135	2	892	930	1473	0.606	0.631	38	0.393	14.81	7.15	11.66	1	1	2	3.15	0.21	39, 140
Ni	Nb	0.40	1.135	1		922±12	1479±6		0.623±0.010			14.76	7.50	11.25	1	1	2	3.5	0.24	50, 142, 141
Ni	Zr	0.34	1.254		859	876	1393	0.617	0.629	17	0.389	16.25	6.89	13.37	1	1	2	2.89	0.18	91
Ni	Zr	0.35	1.254		827	857±7	1353	0.611	0.633±0.005	36	0.396	16.20	7.07	13.13	1	1	2	3.07	0.19	150, 149
Ni	Zr	0.36	1.254		834	856	1343	0.621	0.637	22	0.393	16.15	7.25	12.89	1	1	2	3.25	0.2	39, 91
Pd	Si	0.17	0.775		632	645	1092	0.579	0.591	13	0.374	9.72	1.99	9.72	1	0.99	0	0	0	50, 157
Pd	Si	0.18	0.775	7	639±9	673±15	1101±13	0.579±0.003	0.611±0.020	34±24	0.387±0.013	9.72	2.13	9.72	1	1	0.13	0	0	156, 158, 74, 159, 89 160
Pd	Si	0.19	0.775	8	634	695	1128	0.562	0.616	61	0.394	9.72	2.28	9.72	1	1	0.28	0	0	160
Pd	Si	0.20	0.775	8	648±7	684±17	1224±4	0.530±0.008	0.559±0.012	36±24	0.366±0.010	9.72	2.43	9.72	1	1	0.43	0	0	156, 84, 157, 82, 89, 39 160

Zr	Be	0.30	0.709		607±7	648	1393	0.435±0.005	0.465	35	0.323	8.99	3.85	8.99	1	1	1.85	0	0	180, 75, 170
Zr	Be	0.35	0.709		616±2	647	1238	0.498±0.002	0.523	29	0.349	9.14	4.60	8.54	1	1	2	0.6	0.07	180, 75, 170
Zr	Be	0.40	0.709		624±1	673	1368±25	0.456±0.008	0.501	50	0.342	9.33	5.33	8.00	1	1	2	1.33	0.14	180, 75, 170
Zr	Be	0.45	0.709		646	681	1413	0.457	0.482	35	0.331	9.52	6.09	7.44	1	1	2	2.09	0.22	75, 170
Zr	Be	0.50	0.709		672	682	1473	0.456	0.463	10	0.318	9.73	6.87	6.87	1	1	2	2.87	0.29	75, 170
Zr	Cu	0.25	0.797		571	618	1363	0.419	0.454	47	0.320	9.98	3.33	9.98	1	1	1.33	0	0	87
Zr	Cu	0.28	0.797		600	666	1268	0.473	0.525	66	0.356	9.98	3.88	9.98	1	1	1.88	0	0	87
Zr	Cu	0.335	0.797		631	690	1273	0.496	0.542	59	0.362	10.12	4.73	9.39	1	1	2	0.73	0.07	88
Zr	Cu	0.40	0.797		662±16	712±6	1296±48	0.515±0.028	0.551±0.017	63±2	0.366±0.007	10.31	5.72	8.58	1	1	2	1.72	0.17	93, 88, 87, 82, 76
Zr	Cu	0.45	0.797	1.5	665±4	724±5	1205±2	0.552±0.003	0.601±0.005	59±9	0.387±0.004	10.46	6.51	7.95	1	1	2	2.51	0.24	87, 78 195
Zr	Cu	0.46	0.797	2	696	746	1201	0.580	0.621	50	0.393	10.49	6.66	7.82	1	1	2	2.66	0.25	141
Zr	Cu	0.48	0.797		689	749	1207	0.571	0.620	59	0.395	10.55	6.98	7.56	1	1	2	2.98	0.28	87
Zr	Cu	0.50	0.797	1.2	696±16	752±22	1211±3	0.573±0.013	0.620±0.018	52±11	0.394±0.008	10.61	7.30	7.30	1	1	2	3.3	0.31	88, 87, 84, 11, 89, 76, 91
Zr	Cu	0.55	0.797		698	748	1183	0.590	0.632	50	0.398	10.77	8.12	6.65	1	1	2	4.12	0.38	88
Zr	Cu	0.56	0.797	1	728	792	1163	0.626	0.681	64	0.419	10.80	8.29	6.51	1	1	2	4.29	0.4	93, 87, 11
Zr	Ni	0.28	0.797		642	664	1313	0.489	0.506	22	0.340	9.98	3.88	9.98	1	1	1.88	0	0	91
Zr	Ni	0.37	0.797		700	720	1313	0.533	0.548	20	0.358	10.22	5.26	8.96	1	1	2	1.26	0.12	91
Zr	Ni	0.40	0.797		713	735	1413	0.505	0.520	22	0.346	10.31	5.72	8.58	1	1	2	1.72	0.17	150, 82, 76, 91
Zr	Pd	0.30	0.899		680	690	1343	0.506	0.514	10	0.341	12.04	4.81	11.23	1	1	2	0.81	0.07	50, 35